



Calhoun: The NPS Institutional Archive
DSpace Repository

Theses and Dissertations

1. Thesis and Dissertation Collection, all items

1982

A comparison of two initialization methods in data assimilation

Barker, Edward Harrison

<http://hdl.handle.net/10945/20102>

This publication is a work of the U.S. Government as defined in Title 17, United States Code, Section 101. Copyright protection is not available for this work in the United States.

Downloaded from NPS Archive: Calhoun



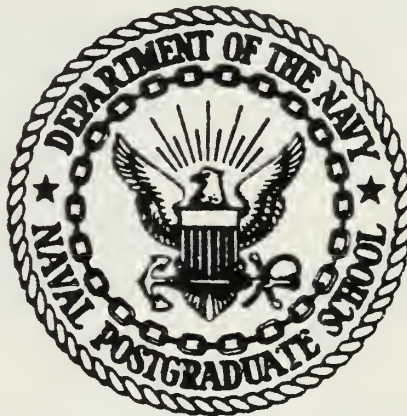
Calhoun is the Naval Postgraduate School's public access digital repository for research materials and institutional publications created by the NPS community. Calhoun is named for Professor of Mathematics Guy K. Calhoun, NPS's first appointed -- and published -- scholarly author.

Dudley Knox Library / Naval Postgraduate School
411 Dyer Road / 1 University Circle
Monterey, California USA 93943

<http://www.nps.edu/library>

NAVAL POSTGRADUATE SCHOOL

Monterey, California



THESIS

A COMPARISON OF TWO INITIALIZATION
METHODS IN DATA ASSIMILATION

by

Edward H. Barker

June 1982

Thesis Advisor:

G. J. Haltiner

Approved for public release; distribution unlimited

T205417

UNCLASSIFIED

SECURITY CLASSIFICATION OF THIS PAGE (When Data Entered)

REPORT DOCUMENTATION PAGE		READ INSTRUCTIONS BEFORE COMPLETING FORM
1. REPORT NUMBER	2. GOVT ACCESSION NO.	3. RECIPIENT'S CATALOG NUMBER
4. TITLE (and Subtitle) A Comparison of Two Initialization Methods in Data Assimilation		5. TYPE OF REPORT & PERIOD COVERED Doctor of Philosophy Thesis, June 1982
7. AUTHOR(s) Edward H. Barker		6. PERFORMING ORG. REPORT NUMBER
9. PERFORMING ORGANIZATION NAME AND ADDRESS Naval Postgraduate School Monterey, California 93940		8. CONTRACT OR GRANT NUMBER(s)
11. CONTROLLING OFFICE NAME AND ADDRESS Naval Postgraduate School Monterey, California 93940		10. PROGRAM ELEMENT, PROJECT, TASK AREA & WORK UNIT NUMBERS
12. REPORT DATE June 1982		13. NUMBER OF PAGES 160
14. MONITORING AGENCY NAME & ADDRESS (if different from Controlling Office)		15. SECURITY CLASS. (of this report) UNCLASSIFIED
16. DISTRIBUTION STATEMENT (of this Report) Approved for public release; distribution unlimited.		15a. DECLASSIFICATION/DOWNGRADING SCHEDULE
17. DISTRIBUTION STATEMENT (of the abstract entered in Block 20, if different from Report)		
18. SUPPLEMENTARY NOTES		
19. KEY WORDS (Continue on reverse side if necessary and identify by block number) Numerical Weather Prediction Data Assimilation Initialization Objective Analysis		
20. ABSTRACT (Continue on reverse side if necessary and identify by block number) Two different initialization methods were developed and tested in global data assimilation experiments covering a five-day period. One method was based on the nonlinear normal mode initialization, and the other was based on the balance equation. Both techniques were developed using the calculus of variations methodology. In both methods, the initial divergence was computed from the forecast first-guess fields, except it was partially		

20. Abstract (continued)

modified in the nonlinear normal mode method to improve the balance.

The assimilation system used to test the initialization methods was developed for the global forecast model at the Fleet Numerical Oceanography Center. This model was adapted from the general circulation model developed at the University of California at Los Angeles. A comparison of the gravity wave noise from the two methods is given for versions of the model with and without heating. Other comparisons are given for divergence, precipitation rates, wave structure and cyclogenesis. The two methods are similar in their performance in data assimilation. The balance equation method is more flexible in weight specification and, consequently, the forecasts verify with observations closer than the normal mode method.

Approved for public release; distribution unlimited

A Comparison of Two Initialization Methods
in Data Assimilation

by

Edward H. Barker

B.S., University of Wyoming, 1965

M.S., San Jose State University, 1972

Submitted in partial fulfillment of the
requirements for the degree of

DOCTOR OF PHILOSOPHY

from the

NAVAL POSTGRADUATE SCHOOL

June 1982

ABSTRACT

Two different initialization methods were developed and tested in global data assimilation experiments covering a five-day period. One method was based on the nonlinear normal mode initialization, and the other was based on the balance equation. Both techniques were developed using the calculus of variations methodology. In both methods, the initial divergence was computed from the forecast first-guess fields, except it was partially modified in the nonlinear normal mode method to improve the balance.

The assimilation system used to test the initialization methods was developed for the global forecast model at the Fleet Numerical Oceanography Center. This model was adapted from the general circulation model developed at the University of California at Los Angeles. A comparison of the gravity wave noise from the two methods is given for versions of the model with and without heating. Other comparisons are given for divergence, precipitation rates, wave structure and cyclogenesis. The two methods are similar in their performance in data assimilation. The balance equation method is more flexible in weight specification and, consequently the forecasts verify with observations closer than the normal mode method.

TABLE OF CONTENTS

I.	INTRODUCTION -----	15
II.	THE DATA ASSIMILATION SYSTEM -----	22
III.	NONLINEAR NORMAL MODE INITIALIZATION -----	24
	A. VERTICAL MODES -----	24
	B. HORIZONTAL MODES -----	31
	C. NONLINEAR BALANCING -----	47
	D. VARIATIONAL BALANCING -----	49
	E. TESTS OF THE NORMAL MODE METHOD -----	56
IV.	THE BALANCE EQUATION INITIALIZATION -----	65
	A. THE VARIATIONAL FORMULATIONS -----	65
	B. VERTICAL FILTERING WITH EMPIRICAL ORTHOGONAL FUNCTIONS -----	68
	C. WEIGHT STRUCTURE -----	72
V.	COMPUTATIONAL RESULTS -----	76
	A. EXPERIMENT DESCRIPTION -----	76
	B. DIFFERENCES BETWEEN BALANCED AND ANALYZED VARIABLES -----	77
	C. ELIMINATION OF GRAVITY WAVE NOISE -----	82
	D. VERTICAL MOTION, PRECIPITATION AND CYCLOGENESIS -----	92
	E. FORECAST VERIFICATION -----	113
VI.	SUMMARY AND CONCLUSIONS-----	126

APPENDIX A: DATA ANALYSIS WITH SIMULTANEOUS FILTERING	- 132
APPENDIX B: LINEARIZED HYDROSTATIC, THERMODYNAMIC AND CONTINUITY EQUATIONS	----- 142
APPENDIX C: EMPIRICAL ORTHOGONAL FUNCTIONS	----- 148
LIST OF REFERENCES	----- 151
INITIAL DISTRIBUTION LIST	----- 158

LIST OF TABLES

1. Equivalent depth (eigenvalues) of the vertical modes of the Arakawa and Lamb (1977) model. ----- 29
2. Frequencies of Rossby modes for $D = 10$ km, $k=1$ from computations of Temperton and Williamson (1981) (T&W), Dickenson and Williamson (1972) (D&W) and for the model used in this study (B). The horizontal grid intervals are specified in degrees. ----- 45
3. Similar to Table 2 except for frequencies of eastward gravity modes for $D = 10$ km, $k=1$. ----- 46

LIST OF FIGURES

1. Vertical modes for model with six levels, a rest-state temperature of 300°C and a top at 50 mb. ---- 27
2. Same as Fig. 1 except for a rest-state temperature of (209, 214, 233, 254, 270, 281) $^{\circ}\text{K}$. ----- 28
3. Structure of selected rotational modes for the model used in this study, which may be compared directly with those of Dickenson and Williamson (1972). ----- 43
4. Similar to Fig. 3 except for selected gravitational modes. ----- 44
5. Manifold schematic of the update and balance procedure used in the data assimilation. Point 0 represents the forecast before the update. The path between 0 and 1 represents the linear balance step. The path between 1 and 2 represents the nonlinear balance step. ----- 55
6. Update analysis (solid line) and its rotational component (dashed line). Subscript 3 designates level 3. ----- 57
7. Analyzed corrections and their gravitational components (dashed line) for third level from the top of the model. The residual of the temperature and surface pressure not resolved onto either the gravitational or rotational manifold is shown by the dark dashed line near the abscissa of (c) and (d). ----- 58
8. The RMS differences between the analyzed and initialized variables for different weighting on the mass analysis, W_{ϕ} . The averages are for the entire globe and all levels. The dashed straight line shows the RMS differences between the analysis and the forecast first-guess. ----- 60
9. Updated 500 mb vorticity when (a) weight on mass is zero, (b) weight on mass is 1000 poleward of 30° . The unprocessed analysis is dashed and the contour interval is $25 \cdot 10^{-6} \text{ sec}^{-1}$. ----- 62

10.	Updated 500 mb geopotential when (a) weight on mass is zero, (b) weight on mass is 1000 poleward of 30°. The unprocessed analysis is dashed and the contour interval is 60 m. -----	63
11.	The first six empirical orthogonal functions derived from a ten-level analysis of geopotential. -----	70
12.	Adjustments made to the temperature in order to balance wind at 60°E, 30°N on 27 Mar 1982. No vertical coupling (dashed line) and vertically coupled using empirical orthogonal functions (solid line). -----	73
13.	RMS differences between the first guess and analysis (solid line), and RMS differences between balanced values and analysis (dashed lines) where BE1 is represented by long dashes and BE2 is represented by short dashes. The subscript 4 designates level 4, and the global RMS values are given above the respective plots. -----	79
14.	Divergence (a) and vorticity (b) at 500 mb in the region of New Zealand. The values after balance are depicted with a solid line and the analyzed values are depicted with a dashed line. Contour interval is $10 \cdot 10^{-6} \text{ sec}^{-1}$ for divergence and $25 \cdot 10^{-6} \text{ sec}^{-1}$ for vorticity. The time is 00Z GMT 11 Nov 1979. -----	80
15.	Similar to Fig. 13 except for the normal mode methods. NM1 (long dashes) and NM2 (short dashes). -----	83
16.	Global RMS average of surface pressure tendency from a forecast initialized with no divergence (solid line) and a forecast initialized with the balance equation (dashed line). -----	85
17.	Global RMS average of surface pressure tendency from a forecast initialized with linear normal mode balance (solid line) and nonlinear normal mode balance (dashed line). -----	86
18.	RMS of surface pressure tendency for the normal mode initialization (dashed line) and for the balance equation (solid line) when latent heating is not included in the forecast model. ----	88

19. RMS average of surface pressure tendency in forecasts initialized with the balance equation method. The adiabatic forecast is represented by a dashed line and the forecast including latent heat effects is represented by a solid line. ----- 89
20. Similar to Fig. 19 except for the nonlinear normal mode technique. ----- 90
21. RMS of surface pressure tendency for the nonlinear normal mode initialization (dashed line) and for the balance equation (solid line) when latent heating is included in the forecast. ----- 91
22. Precipitation rate forecasts (cm hr^{-1}) from 12 GMT 11 Nov 1979 and 00 GMT 12 Nov 1979 data. Both forecasts were initialized without divergence. The averages during the first six hours are shown in (a) and (c) and the averages during the second six hours are shown in (b) and (d). The contour interval is 2 cm hr^{-1} and the interval between 4 and 6 is cross-hatched. ---- 93
23. The first-guess divergence (dashed line) and normal mode computed divergence (solid lines) at 500 mb valid at 00 GMT 20 Nov 1979. The contour interval is 10^{-5} sec^{-1} . ----- 95
24. Forecast first-guess divergence (a, c, e) and divergence computed using the normal mode method, NM2 (b, d, f), for three successive 12-hourly updates beginning at 12 GMT 17 Nov 1979. Contour interval is 10^{-5} sec^{-1} . The interval between $-1 \cdot 10^{-5} \text{ sec}^{-1}$ and $-2 \cdot 10^{-5} \text{ sec}^{-1}$ is cross-hatched and the interval between 10^{-5} sec^{-1} and $2 \cdot 10^{-5} \text{ sec}^{-1}$ is cross-hatched twice. ----- 96
25. Precipitation rates during the first six hours from forecasts initiated from: (a) no balance, (b) BE1, (c) BE2, (d) NM1 and (e) NM2. The contour interval is 2 cm hr^{-1} and the interval between the 6 and 8 isolines is cross-hatched. The time is 00 GMT 16 Nov 1979. ----- 98

26. Precipitation rate during the first six hours from forecasts initialized with BE1 (a), BE2 (c), NM1 (e) and NM2 (g), and precipitation rate during the second six hours for BE1 (b), BE2 (d), NM1 (f) and NM2 (h). The contour interval and cross-hatching are as in Fig. 25. The starting time is 00 GMT 11 Nov 1979. ----- 101
27. Twelve hour forecasts of 500 mb geopotential (a, c, e) and sea-level pressure (b, d, f) during the assimilation run using the BE1 initialization method. Contour interval for geopotential is 60 m and for sea-level pressure is 4 mb. The 4920 to 4980 m interval is cross-hatched in the 500 mb maps. The 996 to 1000 mb and 980-984 mb intervals are cross-hatched in the sea-level pressure maps. ----- 103
28. Precipitation rate during the first six hours (a, c, e) and second six hours (b, d, f) of the forecasts from the BE1 initialization. Contour interval is 2 cm hr^{-1} and the contour interval between 2 and 4 cm hr^{-1} is cross-hatched. ----- 104
29. Similar to Fig. 27 except for the BE2 method. ----- 105
30. Similar to Fig. 28 except for the BE2 method. ----- 106
31. Similar to Fig. 27 except for the NM1 method. ----- 107
32. Similar to Fig. 28 except for the NM1 method. ----- 108
33. Similar to Fig. 27 except for the NM2 method. ----- 109
34. Similar to Fig. 28 except for the NM2 method. ----- 110
35. Sea-level pressure analysis for 19 Nov 00 GMT produced by the BE1 (a), BE2 (b), NM1 (c) and NM2 (d) assimilation runs. ----- 111
36. Latitudinal variation of RMS (a) pressure height and (b) wind differences between observations and 12-hr forecasts without balance (stars) and with NM1 initialization (circles). ----- 114
37. Sequence of 12-hr forecasts of 500 mb height from assimilation runs using BE1 (a), BE2 (b), NM1 (c) and NM2 (d) initialization methods. The contour intervals 4860-4920 m and 5760-5820 m are cross-hatched. ----- 116

38.	RMS differences between radiosonde observations of pressure height and 12-hr forecasts for the assimilation runs comparing BE2 (a), NM1 (b) and NM2 (c) with BE1 initialization methods. Each data point represents the error in the assimilation model just prior to the update. Abscissa labels are hours after start of the assimilation run. -----	118
39.	Similar to Fig. 38 except for radiosonde wind observations. -----	119
40.	Similar to Fig. 38 except for surface ship observations converted to geopotential height. ----	120
41.	Similar to Fig. 38 except for satellite derived geopotentials. -----	122
42.	Similar to Fig. 38 except for satellite wind observations. -----	123
43.	Similar to Fig. 38 except for aircraft wind observations. -----	124

ACKNOWLEDGMENT

The author expresses his appreciation to Professors G. J. Haltiner, Y. S. Sasaki and R. T. Williams for their helpful guidance in all aspects of this research. Professor Haltiner's assistance and patience made it possible to test many more methods than would have been possible otherwise. Professor Sasaki's enduring friendship and teaching was particularly helpful in the adoption of the calculus of variations methods. Professor Williams helped in the understanding of many concepts, and his interest and encouragement were very helpful.

This study could not have been conducted without the numerous contributions of Dr. T. E. Rosmond. Besides developing the UCLA general circulation model so that it could be run on real cases, he provided many helpful suggestions.

Sincere appreciation is extended to Professor R. L. Elsberry for his very careful review of the manuscript.

The typing was expertly done by Ms. Winona Carlisle and the figure layouts were done by Mr. Stephen Bishop.

The computer resources were professionally provided by the Fleet Numerical Oceanography Center and the work was supported by the Naval Environmental Prediction Research Facility.

Deepest gratitude is extended to Karen, Randy and Amy Jo Barker. Their unselfish support provided the time necessary to do this work.

I. INTRODUCTION

Numerical methods have been useful in the prediction of atmospheric flow patterns since the pioneering work of Charney et al. (1950) on the ENIAC computer. In that first experiment, and in operational models that soon followed, pressure height analyses were used as initial conditions for the prediction equations. At that time, the numerical models excluded gravity waves, and no special processing of the initial conditions were necessary. However, when the primitive equation (PE) models came into widespread use, the independent variables consisted of mass (pressure, temperature and geopotential height) and motion (wind, vorticity and divergence) variables. Rather than analyze separately the wind field, it was computed from the geopotential height analyses with a diagnostic field relationship such as the balance equation (see Charney, 1955). Since PE models permit gravity waves as well as Rossby waves, unbalanced initial conditions may become badly distorted during the integration. Such imbalances occur when the motion and mass variables are not dynamically matched, as is typically the case due to the inaccuracies and the spatial distribution of the observations. Therefore, although winds are analyzed along with the pressure heights, some method is required to remove the gravity wave noise.

With the advent of large quantities of asynoptic data (data observed at random times, such as from satellites and aircraft) came the concept of data assimilation, in which the numerical model plays a crucial role of carrying information between observation times (Charney, Halem and Jastrow, 1969; Hayden, 1973; Bengtsson and Gustavsson, 1971, 1972; and Williamson and Kasahara, 1971). The primary motivation for data assimilation has been to update the numerical model frequently enough that it would represent the state of the atmosphere at all times. In this way, the asynoptic data could be used in the analysis more effectively, and thereby improve forecasts. However, several difficult problems became apparent from the initial, somewhat naive, methods of updating a model. The most difficult problem has been the inability to assimilate all types of data. The mass observations are particularly difficult (Kistler and McPherson, 1975; Daley and Puri, 1980; Puri, 1981) because the geostrophic adjustment mechanism of the model tends to disperse unbalanced mass information through the gravity waves. Another problem, particularly noticeable in the tropics, is that the model may become severely unbalanced. This may set up spurious oscillations on a global scale that are very difficult to damp with time filters. For example, the pressure field in the tropics may tend to slosh with periods of 12 to 18 hours and amplitudes in

excess of 10 mb. It then becomes extremely difficult to get the model state to approach asymptotically that of the atmosphere.

Balancing the analyzed data, which removes the gravity wave noise, avoids the problems mentioned above. Because the wind data may be located in regions without mass data and vice versa, the balancing method should be flexible. Although much of the gravity wave noise that interferes with data assimilation can be controlled with some sort of filter applied during the integration, most operational centers constrain the initial data so that winds and mass are balanced.

The two basic categories of the balancing procedure are the dynamic and the static. The dynamic method involves continuously inserting data until the model fields are adjusted to the new information. Integration may be performed in a forward-backward fashion as discussed by Nitta and Hovermale (1969), Temperton (1976), and Haltiner and McCollough (1975), or it may be performed in only one direction as discussed by Miyakoda et al. (1976) and Hoke and Anthes (1976). The main difficulty with the dynamic method is inefficiency; it requires the equivalent of a 24-hour forecast, and it does not seem to work well for mass data (Williamson and Temperton, 1981). Static methods, on the other hand, are widely used in operational centers

(Daley, 1981). In the static method, a diagnostic relationship is imposed on the analyzed heights and winds. The acceptance of the mass data in the model depends on the constraints imposed during the balancing (Daley, 1978) or whether the analysis of mass variables also produces corrections to the motion variables (Philips, 1982b).

Several static initialization methods are available. One method utilizes the multivariate optimum interpolation to make mass corrections consistent with motion corrections (Lorenc, 1981; Schlatter, 1975), and then the remaining gravity noise is removed with some sort of balancing. Unfortunately, this multivariate analysis method links the mass and motion through the geostrophic approximation, and therefore produces a bias around well-developed systems (Williamson, Daley and Schlatter, 1981). Another method requires that the mass and motion variables be analyzed independently, and then the calculus of variations initialization of Sasaki (1958) either adjusts the mass variables to the motion variables, or vice versa, depending on the expected accuracy in the mass variables relative to the winds. The main difficulty with this method is that there is no convergence guarantee for the iterative methods required to solve these problems (Tribbia, 1981; 1982).

The constraints imposed on the initial data to remove gravity waves are most commonly the nonlinear normal mode methods of Machenhauer (1977) and Baer and Tribbia (1977). In these methods, the nonlinear component of the balance is computed assuming little or no tendency of the gravity mode coefficients. No other initialization method is capable of suppressing the initial imbalance in a forecast so effectively. Additionally, the nonlinear normal mode methods have the advantages that they provide conditions that are compatible with the numerical scheme of the model, generate realistic vertical motion in the extratropics, and produce balanced flow in the regions with terrain (Daley, 1981).

In a theoretical study, Leith (1980) used a quasigeostrophic model to show that the nonlinear normal mode methods are nearly the same as constraining the initial conditions to the balance and omega equations. Therefore, it seems reasonable to expect that the balance equation might still be competitive with the normal mode methods, particularly since the balance equation constraint is relatively easy to impose.

There remains the problem of generating an appropriate divergence to go with the nondivergent winds produced by the balance equation. Tarbell et al. (1981) used a modified omega equation which improved the precipitation forecasts of a mesoscale model during the initial hours. Considering

that the omega equation, and even the nonlinear normal mode method do not generate divergence patterns in the tropics that are compatible with the latent heat release (Bengtsson, 1981), the divergence from the forecast first-guess may be the best estimate for divergence.

In this study, we examine the adequacy of the forecast first-guess divergence. Because this divergence is generated by the model, it is compatible. Thus, the interruption to the cumulus convection in the tropics is minimized during assimilation. Another goal of this study is to determine whether the classical balance equation method of Charney (1955) used in the variational method of Sasaki (1958) is competitive with the more elegant, yet cumbersome, nonlinear normal mode method. Since one of the main benefits of the nonlinear normal mode method is the divergence it generates, comparison of the balance equation and normal mode method is, in many respects, a test of the accuracy of the forecast first-guess divergence.

In the following, a brief description of the data assimilation system used in this study is given. Besides the initialization methods, this system includes an objective analysis method for wind and pressure height observations and the global finite difference model described by Arakawa and Lamb (1977). The initialization methods, which are the primary topics of this report, are

presented in detail. Both methods are presented in a calculus of variations framework. The normal mode method uses Machenhauer's (1977) initialization as a constraint, whereas the other method uses the balance equation as a constraint. Finally, several data assimilation experiments are described that illustrate some of the characteristics of the different initialization methods, particularly with regard to precipitation rates and divergence during the early forecast hours.

II. THE DATA ASSIMILATION SYSTEM

In the data assimilation method used in this study, the prediction model is periodically updated at 12-h intervals. Each update requires several steps. First, the 12-h forecast is interpolated to the analysis coordinates, which are pressure surfaces on a 2.5° by 2.5° grid. This forecast becomes the first-guess field. The objective analyses of wind and pressure height are done with a three-dimensional successive corrections method (See Appendix A) on the standard pressure surfaces (50, 100, 150, 200, 250, 300, 400, 500, 700, 850 and 925 mb). However, the surface pressure analysis is produced from the calculus of variations method of Holl and Mendenhall (1972). At this time, the initialization is conducted. The balance equation initialization is done on pressure surfaces prior to the interpolation to model coordinates, whereas the normal mode initialization is done in model coordinates. These initialization methods are described in the next two chapters. Finally, a 12-h forecast is made in preparation for the next update.

The other variables in the model, such as boundary layer depth and moisture, are not updated with new data. Rather, they are carried forward from the forecast first guess.

The numerical model used to assimilate the data was developed at the University of California at Los Angeles (UCLA) to study the general circulation of the atmosphere (Arakawa and Mintz, 1975; Arakawa and Lamb, 1977). In this model, the resolution of the mass variables (surface pressure and temperature) is 4° latitude by 5° longitude and six levels from 50 mb to the surface. The zonal wind is defined one-half grid interval to the east and the meridional wind is defined one-half grid interval to the south (Scheme C in Arakawa and Mintz, 1975). The heating parameterization includes the Arakawa and Schubert (1974) parameterization interacting with a bulk parameter boundary layer (Randall, 1976; Lord, 1978).

The time differencing is a combination of five leap-frog steps for each Matsuno backward step, while the heating is computed during a single forward step preceding each Matsuno step.

In the next section, the model's normal modes are computed, and more detail is given on the dynamical forecast scheme.

III. NONLINEAR NORMAL MODE INITIALIZATION

Before nonlinear normal mode initialization can be applied, the normal modes of the linearized model equations are required. These are obtained below by separation of variables of the linearized equations. Unfortunately, the normal mode methods match the motion variables more closely than the mass variables (Daley, 1981). To establish control over this mass rejection mechanism, the normal mode method is converted to a variational one similar to that of Daley (1978) and Tribbia (1982).

A. VERTICAL MODES

The linearized governing equations may be written with the vertical component in vector form as

$$\frac{\partial}{\partial t} \underline{W} + f \mathbf{k} \times \underline{W} + \nabla (R \bar{T} \ln p_s + \phi) = Q \underline{W}, \quad (3.1)$$

$$\frac{\partial}{\partial t} \underline{T} + \underline{\pi} (\nabla \cdot \underline{W}) = Q_T, \quad (3.2)$$

$$\frac{\partial}{\partial t} \ln p_s + \underline{\pi}^T (\nabla \cdot \underline{V}) = Q_p, \quad \text{and} \quad (3.3)$$

$$\phi = \phi_s + \underline{G} \underline{T}$$

Here \underline{W} is the vector form of wind, T is temperature and \bar{T} is the rest state temperature. p_s is surface pressure, ϕ is geopotential, $\nabla \cdot \underline{W}$ is divergence and ϕ_s is terrain

geopotential. τ , $\underline{\pi}$ and \underline{G} are linearized operators defined in Appendix B. \underline{Q}_V , \underline{Q}_T and \underline{Q}_p are the nonlinear components of their respective equations.

Following Temperton and Williamson (1981), the temperature and surface pressure may be described by a single variable by using

$$gh = \underline{\phi} + R \bar{T} \ln p_s \quad (3.5)$$

Operating on (3.2) with \underline{G} , multiplying (3.3) by $R \bar{T}$, and then adding the resulting two equations gives a single equation for mass,

$$g \frac{\partial}{\partial t} \underline{h} + \underline{G} \underline{\tau} (\nabla \cdot \underline{W}) + R \bar{T} [\underline{\pi}^T] (\nabla \cdot \underline{W}) = \underline{G} \underline{Q}_T + \underline{Q}_p R \bar{T} \quad (3.6)$$

which may be rewritten as

$$g \frac{\partial}{\partial t} \underline{h} + \underline{C} (\nabla \cdot \underline{W}) = g \underline{Q}_h \quad (3.7)$$

where

$$\underline{C} = \underline{G} \underline{\tau} + R \bar{T} \underline{\pi}^T \quad (3.8)$$

and

$$\underline{Q}_h = \underline{G} \underline{Q}_T + R \underline{Q}_p \bar{T} \quad (3.9)$$

The equation set (3.7) is vertically coupled, but by separation of variables, it can be transformed into a set that is not coupled. This is done through the identity

$$\underline{E}^{-1} \underline{C} \underline{E} = g \underline{D} \quad (3.10)$$

where matrix E and diagonal matrix D contain the eigenvectors and eigenvalues of C , respectively. Transforming h and W , or

$$\bar{W} = E^{-1} W \quad \text{and} \quad (3.11)$$

$$\bar{h} = E^{-1} h, \quad (3.12)$$

produces the following uncoupled equation set:

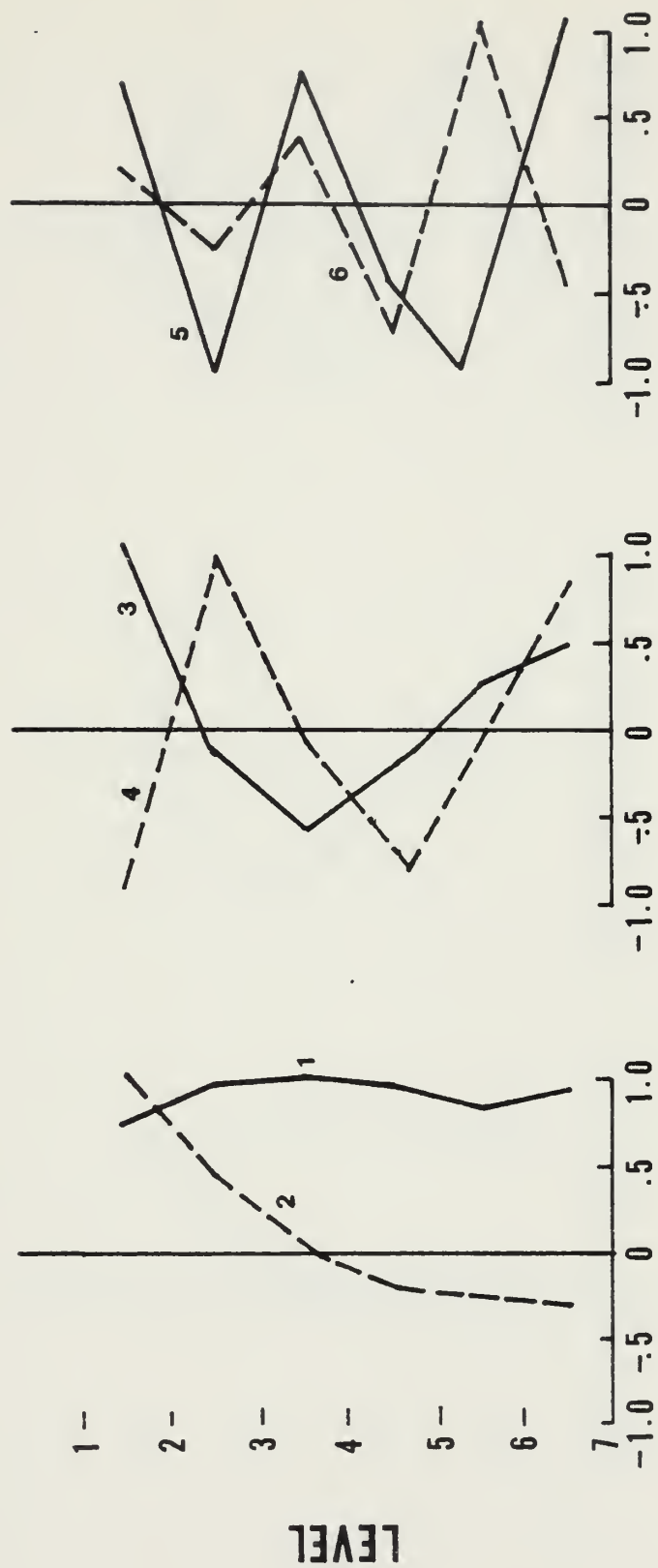
$$\frac{\partial}{\partial t} \bar{W} + f l k \cdot \nabla \bar{W} + g(\bar{h}) = \bar{Q}_W \quad \text{and} \quad (3.13)$$

$$\frac{\partial}{\partial t} \bar{h} + D(\nabla \cdot \bar{W}) = \bar{Q}_h \quad (3.14)$$

where \bar{Q}_W and \bar{Q}_h are transforms of Q_W and Q_h , respectively.

The independent variables in (3.13) and (3.14) are the coefficients of the vertical modes, i.e., the eigenvectors E . Naturally, there are as many modes as there are levels \bar{z} in the model.

The eigenvectors, \bar{E} , are shown in Figures 1 and 2 for \bar{T} equal to a constant (300°K) and for \bar{T} equal to (209, 214, 233, 254, 270, 281)°K. The corresponding eigenvalues (equivalent depths) are given in Table 1. Notice that while the profiles do not significantly change shape for the different temperature profiles, their eigenvalues are considerably different. Also, the vertical modes of the Arakawa and Lamb (1977) model shown here are noticeably different from those given by Temperton and Williamson (1981) for the same values of T . Specifically, the peaks in



AMPLITUDE

Fig. 1. Vertical modes for model with six levels, a rest-state temperature of 300°C and a top at 50 mb.

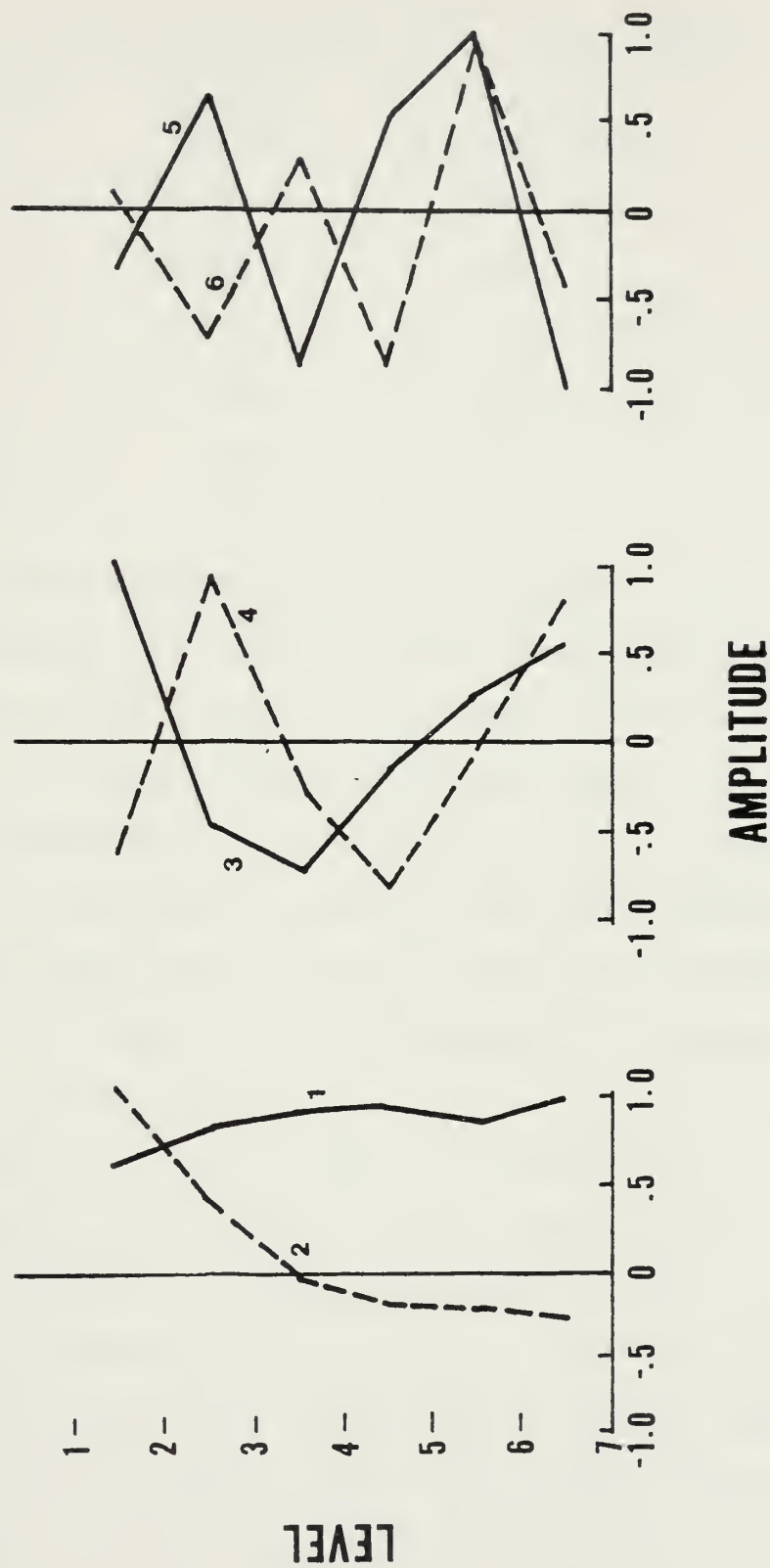


Fig. 2. Same as Fig. 1 except for a rest-state temperature of (209, 214, 233, 254, 270, 281)°K.

Table 1. Equivalent depths (eigenvalues) of the vertical modes of the Arakawa and Lamb (1977) model.

Level	T Constant 300°K	T Average of 1 March 1965
1	9,291 m	7,874 m
2	1,689	784
3	387	171
4	126	55
5	45	18
6	10	3

the profiles near the model top are not present in the gravest modes given in Figures 1 and 2. Since these modes are insensitive to the values of rest state temperature, they need not be updated for each new data set.

The equivalent depths are sensitive to the location of the model top. For example, changing the model top from 50 mb to 0 mb increases the equivalent depths of the external mode from 7874 m to 9660 m. The consequence of keeping the model top at 50 mb is that all the vertical eigenvalues or equivalent depths are smaller than if the top was placed at, say, 10 or 20 mb. This becomes a factor when the nonlinear balance is performed, as will be discussed later.

After \bar{h} is balanced, the inverse of (3.5) is required to solve for P_s and \bar{T} . This is done following the approach of Temperton and Williamson (1981) and Andersen (1977), where $\nabla \cdot \mathbf{w}$ may be eliminated between (3.3) and (3.7) to give

$$\frac{\partial}{\partial t} (\ln p_s) + \tilde{\Pi}^T (-\tilde{C}^{-1}) g \frac{\partial h}{\partial t} = \text{NLT}. \quad (3.15)$$

The nonlinear components are grouped in the term NLT. From linear theory, it is possible to relate h adjustments to p_s adjustments, or

$$\Delta \ln p_s = \tilde{\Pi}^T (-\tilde{C}^{-1}) g \Delta h, \quad (3.16)$$

where the adjustment balances the analyzed fields.

In a similar manner, elimination of $\nabla \cdot W$ between (3.2) and (3.7) produces

$$\Delta \tilde{T} = \tilde{\tau} [\tilde{C}^{-1}] g \Delta h \quad (3.17)$$

Using definition (3.5), it is easily shown that (3.16) and (3.17) are consistent methods for determining $\Delta \ln p_s$ and ΔT from Δh .

A two-grid interval wave was found to exist in the solution of (3.17). To eliminate this problem, a variational method was used which minimizes $\Delta \tilde{T}$, thereby removing the two-grid length waves. In this method, $\Delta \phi$ is computed from (3.5) and then $\Delta \tilde{T}$ is determined from the minimization of

$$\sum_{L=1}^N (\Delta T_L)^2 + \beta (\Delta \phi_L)^2 + 2\lambda_T (\Delta \phi_L - \sum_{k=1}^N G_{Lk} \Delta T_k) \Delta \sigma_L. \quad (3.18)$$

The details of this solution are found in Barker (1981c). This method reduced the size of the root mean square (RMS) corrections to about one half of those obtained using (3.17).

In this section, the vertical coupling of the linearized equations (3.1)-(3.4) was eliminated through separation of variables. Following a similar procedure, the horizontal coupling can also be removed, as shown in the next section.

B. HORIZONTAL MODES

The equations (3.13) and (3.14) in linearized finite difference form for each vertical mode are

$$\delta_t \bar{u}_{i+1/2,j} - f_j \overline{\lambda, \theta}_{i+1/2,j} + \frac{g(\delta_\lambda \bar{h})_{i+1/2,j}}{a \sigma_j \Delta \lambda} = \bar{Q}_{u_{i+1/2,j}}, \quad (3.19)$$

$$\delta_t \bar{v}_{i,j-1/2} + \frac{(f_\sigma \bar{u})_{i,j-1/2}}{\sigma_{j-1/2}} + \frac{g(\delta_\theta \bar{h})_{i,j+1/2}}{a \Delta \theta} = \bar{Q}_{v_{i,j-1/2}} \quad (3.20)$$

and

$$\delta_t \bar{h}_{i,j} + D \left(\frac{(\delta_\theta \bar{v})_{i,j}}{a \Delta \theta} + \frac{(\delta_\lambda \bar{u})_{i,j}}{\sigma_j a \Delta \lambda} \right) = \bar{Q}_{h_{i,j}}. \quad (3.21)$$

The mode index, m , is assumed for D and each variable.

The finite difference operators are

$$(\delta_x T)_k \equiv T_{k+1/2} + T_{k-1/2},$$

$$\overline{(T)}_k^x \equiv \frac{T_{k+1/2} + T_{k-1/2}}{2}$$

and

$$\overline{(T)}_k^{x,y} = \overline{\overline{(T)}_k^x}^y.$$

The other variables are defined as follows: a is the earth's radius, $\Delta\lambda$ is the longitudinal grid interval, $\Delta\theta$ is latitudinal grid interval, \bar{u} and \bar{v} are the east and north components of wind, respectively, i and j are the longitudinal and latitudinal indexes, respectively, and σ is $\cos\theta$.

The linearized equations (3.19)-(3.21) are derived from the model equations in the flux form given by Arakawa and Lamb (1977). However, linearization of these equations removes their flux form, and the only terms absolutely unique to the model are the Coriolis terms, which differ from other models in the way that f is averaged. As it turns out, special definitions for the Coriolis terms are desirable in order to keep the matrix operator of (3.19)-(3.21) symmetric, which simplifies the corresponding eigenvector matrix so that it can be inverted with a transpose operation. This decreases the computer storage and time requirements needed to transpose the variables into normal mode coefficients to one half that required for non-symmetric operators. Fortunately, the small errors introduced by these modifications do not affect the normal mode balancing (Temperton and Williamson, 1979). To achieve symmetry, the Coriolis term in (3.19) is replaced by

$$\frac{f_j^- \sigma_{j-1/2} \overline{(\bar{v})}_{i+1/2, j-1/2}^\lambda + f_j^+ \sigma_{j+1/2} \overline{(\bar{v})}_{i+1/2, j+1/2}^\lambda}{2 \sigma_j}$$

and the Coriolis term in (3.20) is replaced by

$$\frac{f_j^- \overline{(\bar{u})}_{i,j}^\theta + f_{j-1}^+ \overline{(\bar{u})}_{i,j-1}^\theta}{2}$$

where

$$f_j^+ = \frac{2/3 f_{j+1/2} + 1/3 f_{j-1/2}}{\cos(\frac{\Delta\theta}{2})}$$

and

$$f_j^- = \frac{1/3 f_{j+1/2} + 2/3 f_{j-1/2}}{\cos(\frac{\Delta\theta}{2})}.$$

These definitions correspond to a potential enstrophy conserving finite difference scheme as derived by Temperton and Williamson (1979).

From this point, the procedure closely follows that of Dickenson and Williamson (1972) except that the finite differences are written for scheme C (see Arakawa and Lamb, 1977; Temperton and Williamson, 1981). The dynamical state vector is defined as

$$\tilde{\gamma}(\lambda_i, \theta_j, m) = \begin{pmatrix} \bar{u}(\lambda_i, \theta_j, m) \\ \bar{v}(\lambda_i, \theta_j, m) \\ \bar{h}(\lambda_i, \theta_j, m) \end{pmatrix}. \quad (3.22)$$

By assuming a wave solution in the form

$$\tilde{\gamma}(\lambda_i, \theta_j, m) = \sum_{k=0}^{I-1} \tilde{\gamma}(k, \theta_j, m) e^{ik\lambda_i} \quad (3.23)$$

and consequently,

$$\tilde{\gamma}(k, \theta_j, m) = \frac{1}{I} \sum_{i=1}^I \tilde{\gamma}(\lambda_i, \theta_j, m) e^{-ik\lambda_i}, \quad (3.24)$$

(3.19)-(3.21) become

$$\begin{aligned} \frac{\partial}{\partial t} \tilde{u}_j m'(k) - \frac{1}{\sigma_j} \frac{r(k)}{2} [f_j^- \sigma_{j-1/2} \tilde{v}_{j-1/2} + f_j^+ \sigma_{j+1/2} \tilde{v}_{j+1/2}] + \\ g \frac{ik'}{a\sigma_j} \tilde{h}_j s_f = \tilde{Q}_u, \end{aligned} \quad (3.25)$$

$$\begin{aligned} \frac{\partial}{\partial t} \tilde{v}_{j-1/2} + \frac{r(k)}{2} [f_j^- \tilde{u}_j + f_{j-1}^+ \tilde{u}_{j-1}] m'(k) + \\ \frac{g}{a\Delta\theta} [\tilde{h}_j - \tilde{h}_{j-1}] = \tilde{Q}_v \quad \text{and} \end{aligned} \quad (3.26)$$

$$\begin{aligned} \frac{\partial}{\partial t} \tilde{h}_j + \frac{D_m}{a\sigma_j} [ik' \tilde{u}_j s_f + \frac{1}{\Delta\theta} (\tilde{v}_{j+1/2} \sigma_{j-1/2} - \\ \tilde{v}_{j-1/2} \sigma_{j-1/2})] = \tilde{Q}_h. \end{aligned} \quad (3.27)$$

where

$$m'(k) = \cos\left(\frac{\Delta\lambda}{2}\right) - i \sin\left(\frac{\Delta\lambda}{2}\right),$$

$k' = \sin\left(\frac{k\Delta\lambda}{2}\right) / \left(\frac{\Delta\lambda}{2}\right)$, $r(k) = \cos\left(\frac{k\Delta\lambda}{2}\right)$, and S_f is the filtering applied near the poles to keep the gravity-wave terms computationally stable (Arakawa and Lamb, 1977).

The symmetric operator

$$S_m = \begin{pmatrix} m'(k) & 0 & 0 \\ 0 & -i & 0 \\ 0 & 0 & (g/D_m)^{1/2} \end{pmatrix}$$

is used to redefine

$$\tilde{\gamma}, \text{ i.e., } \tilde{\gamma}' = \sum_m \tilde{\gamma} \quad (3.28)$$

so that

$$\begin{aligned} -i\sigma_j \frac{\partial}{\partial t}(\tilde{u}_j') - \frac{r(k)}{2} \{f_j^- \sigma_{j-1/2} \tilde{v}_{j-1/2}' + f_j^+ \sigma_{j+1/2} \tilde{v}_{j+1/2}'\} + \\ \frac{C_m}{a} k' \tilde{h}_j' S_f = \tilde{Q}_u' \end{aligned} \quad (3.29)$$

$$\begin{aligned} -i\sigma_{j-1/2} \frac{\partial}{\partial t}(\tilde{v}_{j-1/2}') - \sigma_{j-1/2} \frac{r(k)}{2} [f_j^- \tilde{u}_j' + f_{j-1}^+ \tilde{u}_{j-1}'] - \\ \sigma_{j-1/2} \frac{C_m}{a\Delta\theta} [\tilde{h}_j' - \tilde{h}_{j-1}'] = \tilde{Q}_h' \end{aligned} \quad (3.30)$$

$$\begin{aligned} -i\sigma_j \frac{\partial}{\partial t}(\tilde{h}_j') + \frac{C_m}{a} k' \tilde{u}_j' S_f + \frac{C_m}{a\Delta\theta} [\tilde{v}_{j+1/2}' \sigma_{j+1/2} - \\ \tilde{v}_{j-1/2}' \sigma_{j-1/2}] = \tilde{Q}_h' \end{aligned} \quad (3.31)$$

or in matrix form,

$$-i \underline{\underline{Q}} \frac{\partial}{\partial t} \tilde{\gamma}' + \underline{\underline{L}} \tilde{\gamma}' = -i \underline{\underline{Q}} \tilde{H}' \quad (3.32)$$

$$\underline{Q} = \begin{bmatrix} Q_1 & & 0 \\ & Q_2 & \\ 0 & \dots & Q_N \end{bmatrix}, \quad \text{where}$$

$$Q_j = \begin{bmatrix} \sigma_j & 0 & 0 \\ 0 & \sigma_{j-1/2} & 0 \\ 0 & 0 & \sigma_j \end{bmatrix}, \quad \text{and}$$

$$\underline{L} = \begin{bmatrix} B_1 & C_1 & 0 & \dots \\ A_2 & B_2 & C_2 & 0 \dots \\ \dots & 0 & A_N & B_N \end{bmatrix}$$

For the general case when j is not near the north pole or the equator

$$A_j = \begin{bmatrix} 0 & -\frac{r(k)}{2} f_j^- \sigma_{j-1/2} + \frac{C_m}{a} k' S_f & \\ -\sigma_{j-1/2} \frac{r(k)}{2} f_j^- & 0 & -\sigma_{j-1/2} \frac{C_m}{a \Delta \theta} \\ \frac{C_m}{a} k' S_f & -\frac{C_m}{a \Delta \theta} \sigma_{j-1/2} & 0 \end{bmatrix},$$

$$B_j = \begin{bmatrix} 0 & -\frac{r(k)}{2} f_j^+ \sigma_{j+1/2} & 0 \\ 0 & 0 & 0 \\ 0 & \frac{C_m}{a\Delta\theta} \sigma_{j+1/2} & 0 \end{bmatrix},$$

and

$$C_j = \begin{bmatrix} 0 & 0 & 0 \\ -\sigma_{j-1/2} \frac{r(k)}{2} f_{j-1}^+ & 0 & \sigma_{j-1/2} \frac{C_m}{a\Delta\theta} \\ 0 & 0 & 0 \end{bmatrix}.$$

To produce continuous Coriolis forcing near the poles, a computational u is defined. At the North Pole,

$$[u]_N = 0, \text{ where}$$

the $[]$ represents a zonal average.

Continuity requires that

$$(u_{i+1/2,N} - u_{i-1/2,N}) \frac{S_f}{\Delta\lambda} - v_{i,N-1/2} \frac{\sigma_{N-1/2}}{(\Delta\theta/2)} = [v]_{N-1/2} \frac{\sigma_{N-1/2}}{(\Delta\theta/2)}. \quad (3.33)$$

It is important to notice that except for wave number zero ($k \neq 0$),

$$[v]_{N-1/2} = 0.$$

Consequently, \underline{L} is one row and column larger when K is zero than it is otherwise. Transforming the variables using (3.23) gives

$$\tilde{u}_N = \alpha \tilde{v}_{N-1/2} \quad (3.34)$$

where $\alpha = 2\sigma_{N-1/2} / (S_f k' \Delta\theta)$.

The \tilde{v} - equation becomes

$$-i \sigma_{N-1/2} \frac{\partial}{\partial t} \tilde{v}_{N-1/2}' - \frac{r(k)}{2} \sigma_{N-1/2} [f_N^- \alpha \tilde{v}_{N-1/2}' + f_{N-1}^+ \tilde{u}_{N-1}'] - \frac{\sigma_{N-1/2}}{a\Delta\theta} C_m [\tilde{h}_N' - \tilde{h}_{N-1}'] = \tilde{Q}_v' \quad (3.35)$$

The continuity equation at the pole is

$$\frac{\partial h_N}{\partial t} = D_n \oint v_N ds / \text{Area},$$

where $\text{Area} = I(a\Delta\theta \sigma_{N-1/2})/4$

and

$$\oint v_N ds = \sum_{i=1}^I v_N a\Delta\theta \sigma_{N-1/2}.$$

\tilde{h}_N is zero except for wave number zero, so that

$$-i \frac{1}{4} \sigma_{N-1/2} \frac{\partial}{\partial t} \tilde{h}_N' - C_m \frac{\tilde{v}_{N-1/2}'}{a\Delta\theta} \sigma_{N-1/2} = \tilde{Q}_h' \quad (3.36)$$

Therefore (3.35) and (3.36) give

$$A_N = \begin{bmatrix} 0 & -\frac{C_m \sigma_{N-1/2}}{a\Delta\theta} \\ \frac{C_m \sigma_{N-1/2}}{a\Delta\theta} & 0 \end{bmatrix}$$

$$C_N = \begin{bmatrix} -\frac{r(k)}{2} \sigma_{N-1/2} & f_{N-1}^+ & 0 & \frac{\sigma_{N-1/2}}{a\Delta\theta} C_m \\ 0 & 0 & 0 & 0 \end{bmatrix}$$

and

$$B_{N-1} = C_N^T.$$

A grid with a four degree meridional interval puts the equator at a v-point. Using $v_{1/2}$ as the equator point, the equations can be written for the symmetric and antisymmetric components. For the symmetric component, $u_1 = u_0$, $h_1 = h_0$ and $v_{1/2} = 0$. The h- and u-equations are

$$-i \sigma_1 \frac{\partial}{\partial t} \tilde{u}_1' - \frac{r(k)}{2} [f_1^+ \sigma_{1+1/2} \tilde{v}_{1+1/2}'] + \frac{C_m}{a} k' \tilde{h}_1' S_f = \tilde{Q}_u' \quad \text{and} \quad (3.37)$$

$$-i \sigma_1 \frac{\partial}{\partial t} \tilde{h}_1' + \frac{C_m}{a} k' \tilde{u}_1' S_f + \frac{C_m}{a \Delta \theta} \sigma_{1+1/2} \tilde{v}_{1+1/2}' = \tilde{Q}_h', \quad (3.38)$$

so that

$$A_1 = \begin{bmatrix} 0 & \frac{C_m}{a} k' S_f \\ \frac{C_m}{a} k' S_f & 0 \end{bmatrix},$$

$$B_1 = \begin{bmatrix} 0 & -\frac{r(k)}{2} f_1^+ \sigma_{1+1/2} & 0 \\ 0 & \sigma_{1+1/2} \frac{C_m}{a \Delta \theta} & 0 \end{bmatrix},$$

$$Q_1 = \begin{bmatrix} \sigma_1 & 0 \\ 0 & \sigma_1 \end{bmatrix}$$

and $C_2 = B_1^T$.

For the antisymmetric component, $u_1 = -u_0$, $h_1 = -h_0$ and $v_{1/2}$ is not identically zero. The equations are

$$\begin{aligned}
& - i \sigma_1 \frac{\partial}{\partial t} \tilde{u}_1' - \frac{r(k)}{2} \{ f_1^- \sigma_{1/2} \tilde{v}_{1/2}' + f_1^+ \sigma_{1+1/2} \tilde{v}_{1+1/2}' \} + \\
& \frac{C_m}{a} k' \tilde{h}_1' S_f = \tilde{Q}_u' , \quad (3.39)
\end{aligned}$$

$$\begin{aligned}
& - i \sigma_{1/2} \frac{\partial}{\partial t} \tilde{v}_{1/2}' - \sigma_{1/2} \frac{r(k)}{2} \{ f_1^- \tilde{u}_1' - f_1^- (-\tilde{u}_1') \} - \\
& \sigma_{1/2} \frac{C_m}{a \Delta \theta} (\tilde{h}_1' + \tilde{h}_1') = \tilde{Q}_v' \quad \text{and} \quad (3.40)
\end{aligned}$$

$$\begin{aligned}
& - i \sigma_1 \frac{\partial}{\partial t} \tilde{h}_1' + \frac{C_m}{a} k' \tilde{u}_1' S_f + \\
& \quad (3.41)
\end{aligned}$$

$$\frac{C_m}{a \Delta \theta} \{ \tilde{v}_{1+1/2}' \sigma_{1+1/2} - \tilde{v}_{1/2}' \sigma_{1/2} \} = \tilde{Q}_h' ,$$

or

$$A_1 = \begin{bmatrix} 0 & - \frac{r(k)}{2} f_1^- \sigma_{1/2} & \frac{C_m}{a} k' S_f \\ - \sigma_{1/2} \frac{r(k)}{2} f_1^- & 0 & - \sigma_{1/2} \frac{C_m}{a \Delta \theta} \\ \frac{C_m}{a} k' S_f & - \sigma_{1/2} \frac{C_m}{a \Delta \theta} & 0 \end{bmatrix} ,$$

$$B_1 = \begin{bmatrix} 0 & - \frac{r(k)}{2} f_1^+ \sigma_{1+1/2} & 0 \\ 0 & 0 & 0 \\ 0 & \frac{C_m}{a \Delta \theta} \sigma_{1+1/2} & 0 \end{bmatrix} \quad \text{and}$$

$$Q_1 = \begin{bmatrix} \sigma_1 & 0 & 0 \\ 0 & \sigma_{1/2/2} & 0 \\ 0 & 0 & \sigma_1 \end{bmatrix}.$$

Changing the model resolution will generally require that these equations also be changed, depending on how the variables are staggered relative to the equator.

To complete the computation of the horizontal modes, the matrix equation (3.32) is rescaled using

$$\hat{\underline{\underline{Y}}} = \underline{\underline{Q}}^{1/2} \tilde{\underline{\underline{Y}}}', \quad \hat{\underline{\underline{H}}} = \underline{\underline{Q}}^{1/2} \tilde{\underline{\underline{H}}}'$$

and

$$\hat{\underline{\underline{L}}} = \underline{\underline{Q}}^{-1/2} \underline{\underline{L}} \underline{\underline{Q}}^{-1/2}.$$

This allows (3.32) to be written

$$-i \underline{\underline{Q}}^{1/2} \frac{\partial}{\partial t} \hat{\underline{\underline{Y}}} + \underline{\underline{Q}}^{1/2} \hat{\underline{\underline{L}}} \hat{\underline{\underline{Y}}} = -i \underline{\underline{Q}}^{1/2} \hat{\underline{\underline{H}}},$$

or

$$-i \frac{\partial}{\partial t} \hat{\underline{\underline{Y}}} + \hat{\underline{\underline{L}}} \hat{\underline{\underline{Y}}} = -i \hat{\underline{\underline{H}}}. \quad (3.42)$$

If $\hat{\underline{\underline{Y}}}$ contains the eigenvectors or normal modes of $\hat{\underline{\underline{L}}}$, then this equation becomes

$$-i \frac{\partial}{\partial t} [\hat{\underline{\underline{Y}}}^{-1} \hat{\underline{\underline{Y}}}] + \hat{\underline{\underline{Y}}}^{-1} \hat{\underline{\underline{L}}} \hat{\underline{\underline{Y}}} (\hat{\underline{\underline{Y}}}^{-1} \hat{\underline{\underline{Y}}}) = -i \hat{\underline{\underline{Y}}}^{-1} \hat{\underline{\underline{H}}}. \quad (3.43)$$

The identity

$$\hat{\underline{\underline{\Lambda}}} = \hat{\underline{\underline{Y}}}^{-1} \hat{\underline{\underline{L}}} \hat{\underline{\underline{Y}}}, \quad (3.44)$$

where $\hat{\underline{\underline{\Lambda}}}$ is a diagonal matrix containing the eigenvalues of $\hat{\underline{\underline{L}}}$, makes it possible to rewrite (3.43) as

$$\frac{\partial}{\partial t} \underline{\underline{C}} = -i \hat{\underline{\underline{\Lambda}}} \underline{\underline{C}} + \underline{\underline{r}}. \quad (3.45)$$

This is the wave equation of the expansion coefficients, \underline{C} , that we have been seeking. The elements of \underline{C} are functions of the vertical, zonal and meridional mode numbers m , k and l , respectively. These coefficients are the amplitudes of the various modes required to represent a particular atmospheric state, i.e.,

$$\underline{C} = \hat{\underline{Y}}^{-1} \hat{\underline{Y}} . \quad (3.46)$$

The nonlinear term is now \underline{r} , and the mode frequencies are $\underline{\Lambda}$. For each m and k , there are $3N$ equations for \underline{C} ; $2N$ are gravity waves and N are rotational waves. N , in this case, is the number of degrees of freedom in the meridional direction.

The structure of the modes from (3.43) is given in Figures .3 and 4. They are nearly identical to the modes published by Dickenson and Williamson (1972). The scaling is different, but this is of no consequence, as the modes are put in orthonormal form before they are used. The frequencies of the various modes corresponding to those given by Dickenson and Williamson (1972) and Temperton and Williamson (1981) are given in Tables 2 and 3. Resolution differences account for most of the variability of the frequencies, which can be seen from the computations of Dickenson and Williamson (1972) for two different resolutions. Their 5° unstaggered grid results are similar to the

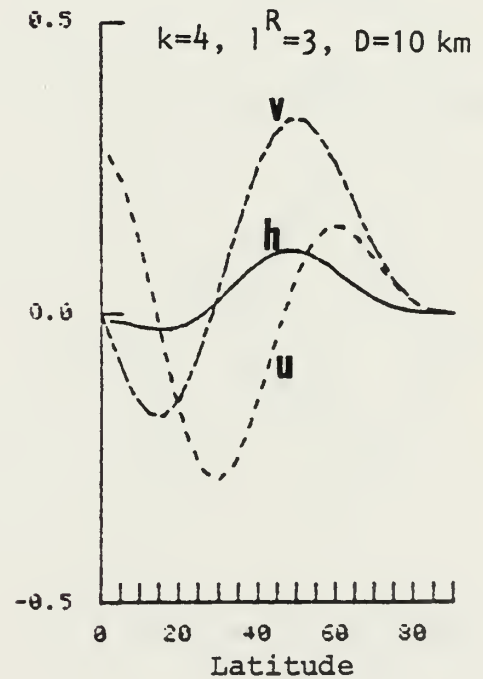
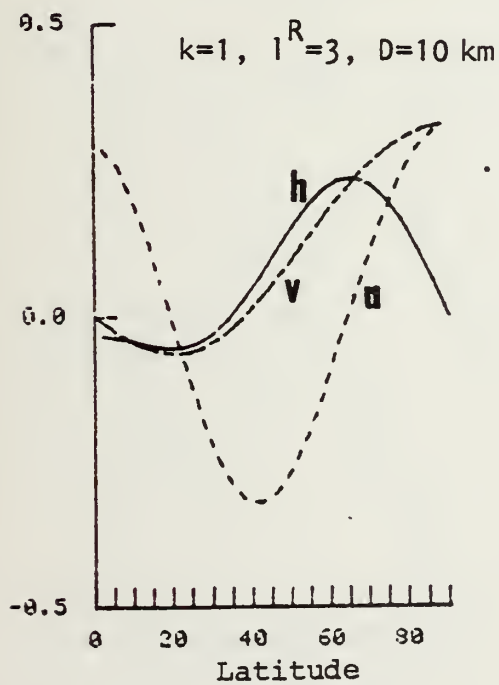
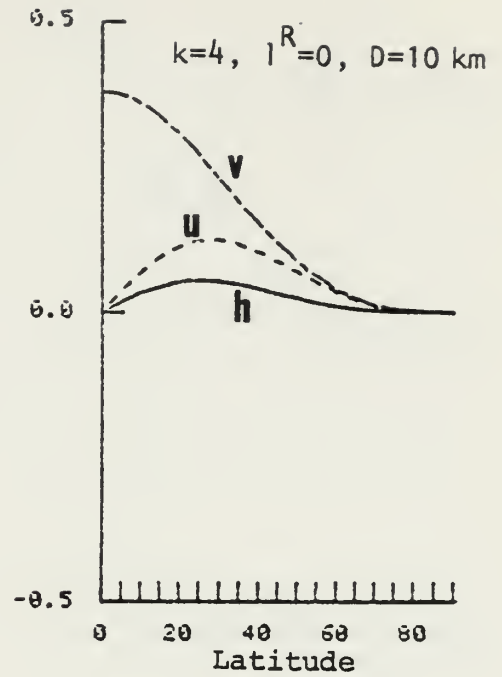
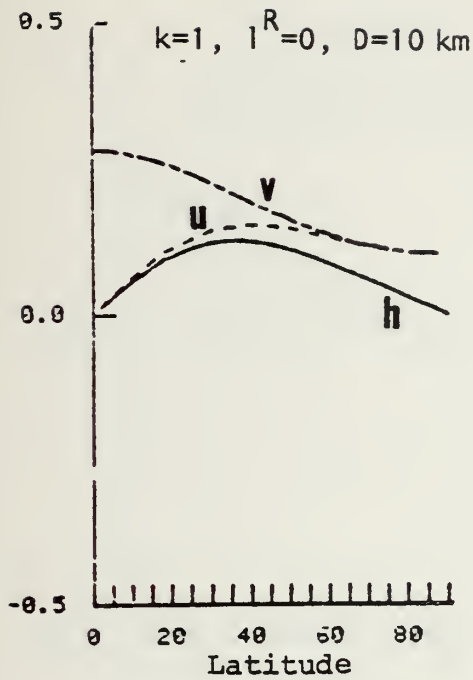


Fig. 3. Structure of selected rotational modes for the model used in this study, which may be compared directly with those of Dickenson and Williamson (1972).

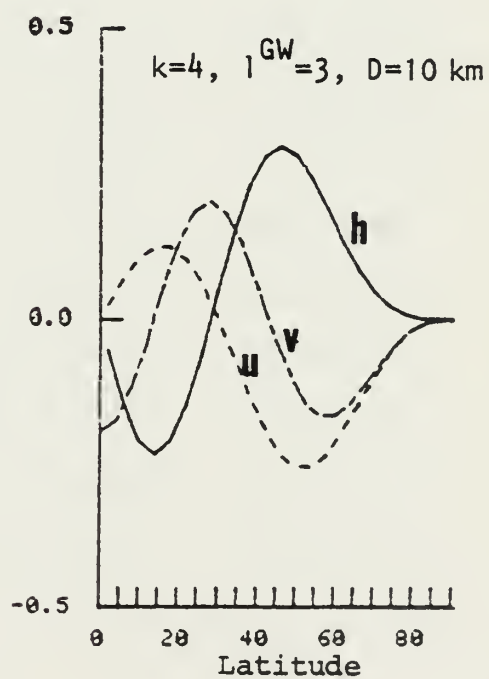
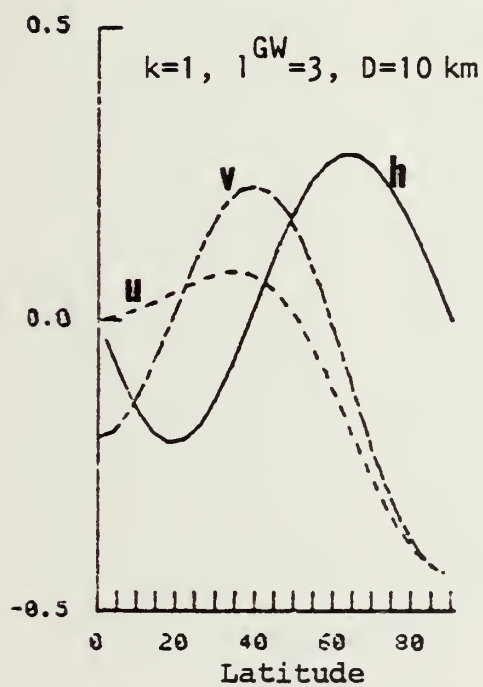
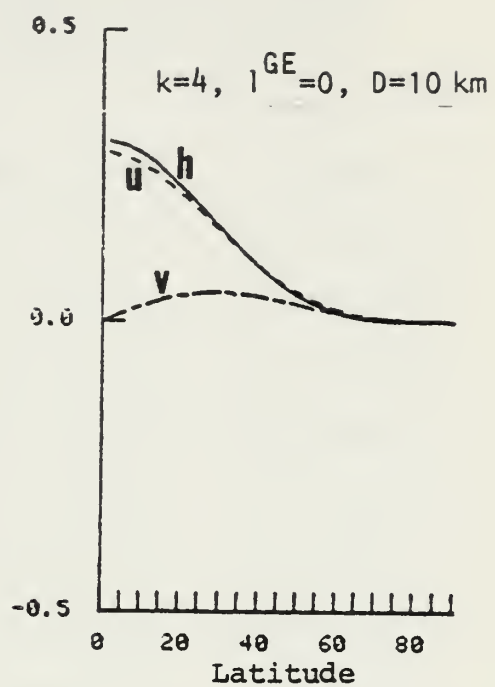
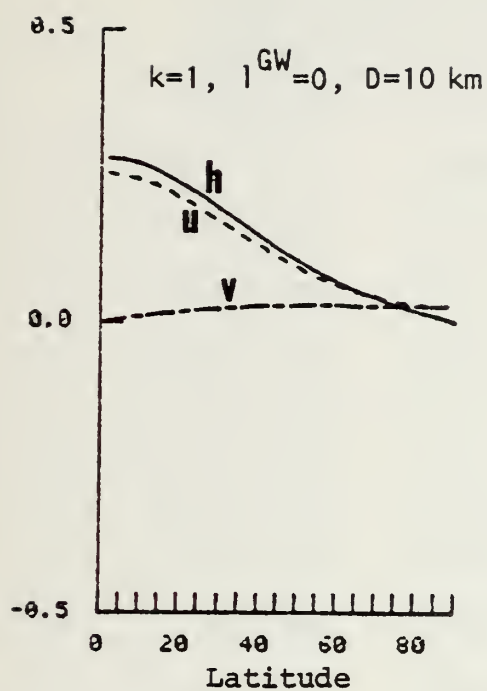


Fig. 4. Similar to Fig. 3 except for selected gravitational modes.

Table 2. Frequencies of Rossby modes for $D = 10$ km, $k=1$ from computations of Temperton and Williamson (1981) (T&W), Dickenson and Williamson (1972) (D&W), and for the model used in this study, B. The horizontal grid intervals are specified in degrees.

1	T&W, 10°	D&W, 5°	D&W, 2.5°	B $4^\circ \times 5^\circ$
0	6.11 E-05	6.12 E-05	6.14 E-05	6.14 E-05
1	1.44 E-05	1.43 E-05	1.45 E-05	1.45 E-05
2	8.64 E-06	8.60 E-06	8.73 E-06	8.74 E-06
3	5.72 E-06	5.73 E-06	5.87 E-06	5.88 E-06
4	3.98 E-06	4.02 E-06	4.17 E-06	4.17 E-06
5	2.87 E-06	2.93 E-06	3.08 E-06	3.09 E-06
6	2.14 E-06	2.20 E-06	2.36 E-06	2.36 E-06
7	1.63 E-06	1.69 E-06	1.86 E-06	1.86 E-06
8	1.27 E-06	1.32 E-06	1.49 E-06	1.49 E-06
9	1.01 E-06	1.04 E-06	1.22 E-06	1.22 E-06
10	8.10 E-07	3.18 E-06	1.02 E-06	1.02 E-06
11	6.62 E-07	6.43 E-06	8.58 E-07	8.57 E-07
12	5.52 E-07	4.99 E-07	7.30 E-07	7.30 E-07
13	4.70 E-07	3.77 E-07	6.27 E-07	6.28 E-07
14	4.11 E-07	2.71 E-07	5.43 E-07	5.45 E-07
15	3.75 E-07	1.75 E-07	4.73 E-07	4.76 E-07
16	3.13 E-07	8.60 E-08	4.14 E-07	4.18 E-07

Table 3. Similar to Table 2 except for frequencies of eastward gravity modes for $D = 10$ km, $k=1$.

1	T&W, 10^0	D&W, 5^0	D&W, 2.5^0	B $4^0 \times 5^0$
0	-5.44 E-05	-5.38 E-05	-5.38 E-05	-5.38 E-05
1	-1.31 E-04	-1.30 E-04	-1.30 E-04	-1.30 E-04
2	-1.87 E-04	-1.85 E-04	-1.86 E-04	-1.87 E-04
3	-2.35 E-04	-2.33 E-04	-2.36 E-04	-2.36 E-04
4	-2.79 E-04	-2.78 E-04	-2.83 E-04	-2.84 E-04
5	-3.22 E-04	-3.20 E-04	-3.29 E-04	-3.31 E-04
6	-3.63 E-04	-3.61 E-04	-3.75 E-04	-3.78 E-04
7	-4.01 E-04	-4.00 E-04	-4.21 E-04	-4.25 E-04
8	-4.36 E-04	-4.34 E-04	-4.66 E-04	-4.71 E-04
9	-4.69 E-04	-4.67 E-04	-5.10 E-04	-5.18 E-04
10	-4.98 E-04	-4.96 E-04	-5.54 E-04	-5.64 E-04
11	-5.23 E-04	-5.21 E-04	-5.97 E-04	-6.09 E-04
12	-5.44 E-04	-5.42 E-04	-6.38 E-04	-6.54 E-04
13	-5.61 E-04	-5.59 E-04	-6.79 E-04	-6.99 E-04
14	-5.72 E-04	-5.68 E-04	-7.19 E-04	-7.43 E-04
15	-5.94 E-04	-5.75 E-04	-7.57 E-04	-7.86 E-04
16	-5.94 E-04	-5.91 E-04	-7.94 E-04	-8.29 E-04

Temperton and Williamson (1981) 10^0 staggered grid values, whereas their 2.5^0 nonstaggered grid results are similar to those computed from the above equations for a $4^0 \times 5^0$ staggered grid. As Temperton and Williamson (1981) point out, the staggered grid produces modes comparable to those of a nonstaggered grid with half the resolution.

C. NONLINEAR BALANCING

Machenhauer (1977) discovered that the nonlinear terms have a much slower time variation than their respective gravity modes. Under this first order approximation, the equation for the gravity modes from (3.45),

$$\frac{\partial}{\partial t} C(k, \ell, m) = -ivC(k, \ell, m) + r(k, \ell, m) \quad (3.47)$$

has the solution (3.48)

$$C(k, \ell, m, t) = \frac{r(k, \ell, m)}{iv(k, \ell, m)} + [C(k, \ell, m, \phi) - \frac{r(k, \ell, m)}{iv}]e^{-ivt}$$

Therefore, removal of the fast modes requires that the second term on the right-hand side of (3.48) be zero, i.e.,

$$C_B(k, \ell, m, \phi) = r(k, \ell, m)/(iv). \quad (3.49)$$

The subscript B signifies the balance condition.

Rather than define the nonlinear terms, it is easier to use the model to make this computation. This is done by running the model for one time step and determining the tendency of the gravity mode coefficients. The nonlinear term is the total minus the linear tendency, or

$$r(k, \ell, m) = \frac{C(k, \ell, m, \Delta t) - C(k, \ell, m, 0)}{\Delta t} + i v_c C(k, \ell, m, t). \quad (3.50)$$

v_c is the computational frequency for the forward timestep, which may be determined from the analytic frequency by

$$v_c = \arctan v \Delta t / \Delta t + \frac{i}{2 \Delta t} \text{Log} [1 + (v \Delta t)^2] \quad (3.51)$$

using standard methods. Using v_c for v in (3.49) and then substituting (3.50) gives the corrections to the fast modes required to balance, or

$$\Delta C_B = -i(C(k, \ell, m, \Delta t) - C(k, \ell, m, 0)) / (\Delta t v_c(k, \ell, m)) \quad (3.52)$$

Leith (1981) used the quasi-geostrophic relations to show that this balance is equivalent to using a slightly modified version of the balance equation along with the omega equation. Phillips (1981) points out, however, that more than one iteration with (3.52) introduces new terms not consistent with quasi-geostrophic balancing, and therefore,

should be avoided. The Baer-Tribbia (1977) method, however, does allow more iterations, and will be tested in future versions of the normal mode balance.

Additionally, Machenhauer's method (3.52) does not work except for those gravity modes with periods equal to or less than any of the rotational modes (Ballish, 1981; Phillips, 1981). For the version of model used here, this restriction limited the modes that could be balanced to all of the external and first internal, and a few of the second internal, modes.

D. VARIATIONAL BALANCING

One of the difficulties with the nonlinear normal mode method is that the rotational modes are primarily determined from the vorticity of the analyzed wind fields (Daley, 1981; Daley and Puri, 1981). This becomes a problem over vast regions of the globe in which the principal observations are remotely sensed temperature profiles from satellites. Therefore, to describe these regions adequately, the initialization must be able to assimilate mass observations. A possible method for incorporating mass observations is to convert the normal mode balance into a variational framework (Daley, 1978). Tribbia's (1982) spectral shallow water approach was adapted for this purpose, except here the method is developed for a multilevel finite difference model.

The normal modes introduced by (3.43) may be written

$$\hat{Y}_k^\ell(\lambda_i, \theta_j) = \begin{bmatrix} \hat{U}(\ell, \theta_j) \\ \hat{V}(\ell, \theta_j) \\ \hat{\Phi}(\ell, \theta_j) \end{bmatrix} \exp(-ik\lambda_i)/I^{1/2} \quad (3.53)$$

but instead of (3.46), the coefficients of the rotational modes are determined from a specially designed inner product

$$C(k, \ell) = \langle \hat{\tilde{Y}} \cdot \hat{\tilde{Y}}^*(k, \ell) \rangle \quad (3.54)$$

where

$$\begin{aligned} \langle \hat{\tilde{Y}} \cdot \hat{\tilde{Y}}(k, \ell) \rangle &= \sum_{i=1}^I \sum_{j=1}^J \{ W_u(\theta_j, \lambda_{i+1/2}) [\hat{u}(\theta_j, \lambda_{i+1/2}) \hat{U}(\ell, \theta_j) \sigma(\theta_j) \\ &+ W_u(\theta_{j-1/2}, \lambda_i) [\hat{v}(\theta_{j-1/2}, \lambda_i) \hat{V}(\ell, \theta_j)] \sigma(\theta_{j-1/2}) \\ &+ W_\phi(\theta_j, \lambda_i) [\hat{\phi}(\theta_j, \lambda_i) \hat{\Phi}(\ell, \theta_j)] \sigma(\theta_j) \} \exp(-ik\lambda_i)/I^{1/2} \end{aligned} \quad (3.55)$$

W_u and W_ϕ are the weights for winds and mass, respectively.

σ is the same as in (3.25)-(3.27). Because no attempt is made to put a vertical variation in the weights, the vertical mode index has been dropped from these equations.

The inverse of (3.46) is

$$\hat{\tilde{Y}} = \sum_{k=0}^{I-1} \sum_{\ell=1}^N C_k^\ell \hat{\tilde{Y}}_k^\ell \quad (3.56)$$

If $\hat{\underline{y}}_I$ is the balanced initial condition and $\hat{\underline{y}}_0$ the analysis, then an optimal initial condition is that obtained from a minimization of

$$I = \langle (\hat{\underline{y}}_I - \hat{\underline{y}}_0) \cdot (\hat{\underline{y}}_I - \hat{\underline{y}}_0) \rangle \quad (3.57)$$

with respect to the modal coefficients.

The balanced data have components on both the rotational and gravitational manifolds, i.e.,

$$\hat{\underline{y}}_I = \hat{\underline{y}}_R + \hat{\underline{y}}_G, \quad (3.58)$$

where

$$\hat{\underline{y}}_R = \sum_{k=0}^{I-1} \sum_{\ell=1}^R x_{\ell}^k \hat{\underline{y}}_{\ell}^k \quad \text{and} \quad (3.59)$$

$$\hat{\underline{y}}_G = \sum_{k=0}^{I-1} \sum_{\ell=1}^G G_{\ell}^k \hat{\underline{y}}_{\ell}^k. \quad (3.60)$$

x^k and G^k represent the rotational and gravitational mode coefficients, respectively. Notice that G plus R equals N , which is the total number of modes. The nonlinear balance relationship requires that the gravitational component be a function of the rotational component only (Phillips, 1981; Baer and Tribbia, 1977; Daley, 1981), i.e., $G_{\ell}^k = G_{\ell}^k(\underline{x})$, therefore minimizing (3.57) requires that

$$\frac{\partial I}{\partial x_{\alpha}^{\beta}} = 0 \quad (3.61)$$

for the rotational mode coefficients X , or

$$2 \left\langle \left(\sum_{k=0}^{I-1} \sum_{\ell=1}^R X_{\ell}^k \hat{\gamma}_{\ell}^i + \sum_{k=0}^{I-1} \sum_{\ell=1}^R G_{\ell}^k \hat{\gamma}_{\ell}^k - \hat{\gamma}_0 \right) \cdot \left(\hat{\gamma}_{\alpha}^{\beta} + \sum_{k=0}^{I-1} \sum_{\ell=1}^R \frac{\partial G_{\ell}^k}{\partial X_{\alpha}^{\beta}} \hat{\gamma}_{\ell}^k \right) \right\rangle = 0 \quad (3.62)$$

As Tribbia (1982) notes, this equation is not easily solved. This is particularly true for non-zero values of G . To make this equation more tractable, an iterative solution is possible where the first pass is solved using

$$\hat{\gamma}_I^{(1)} = \hat{\gamma}_R^{(1)} \quad (3.63)$$

The superscript is iteration cycle. This simplifies (3.62) where

$$2 \left\langle \left(\sum_{k=0}^{I-1} \sum_{\ell=1}^R X_{\ell}^k \hat{\gamma}_{\ell}^k - \hat{\gamma}_0 \right) \cdot \left(\hat{\gamma}_{\alpha}^{\beta} \right) \right\rangle = 0 \quad (3.64)$$

reduces to a linear equation set

$$\underline{A} \underline{X}^{(1)} = \underline{Z} \quad (3.65)$$

$$\underline{A} \underline{X} = \left\langle \left(\sum_{k=0}^{I-1} \sum_{\ell=1}^R X_{\ell}^k \hat{\gamma}_{\ell}^k \right) \cdot \left(\hat{\gamma}_{\alpha}^{\beta} \right) \right\rangle \quad \text{and}$$

$$\underline{Z} = \left\langle \hat{\gamma}_0 \cdot \hat{\gamma}_{\alpha}^{\beta} \right\rangle$$

for all $\hat{\gamma}_{\alpha}^{\beta}$ on the rotational manifold.

If the weights are unity everywhere, then the orthonormality of the modes makes A an identity matrix, and \hat{Y}_I is simply equal to the rotational component of \hat{Y}_0 .

Subsequent values for X may be computed using (3.62). G is evaluated from Machenhauer's equation (3.52) using the value of X from the previous cycle. The variation of G with respect to X_α^β is computed numerically. The benefits of following this complex procedure are almost certainly not worth the effort.

To avoid the computational workload of (3.62), the variational balance is performed on the analyzed corrections. Assuming the corrections are much smaller than the total analysis, the approximate equation (3.64) is more accurate than it would be if the balance were performed on the total analysis.

The solution is still not very easy. For total variability of the weights, the equation set (3.65) represents $(I/2 \cdot R)$ or 1656 equations. The corresponding size of \underline{A} is over 2.5 million elements. Therefore, the computation of the inverse of \underline{A} is extremely cumbersome, especially when the computer memory available is only about 100,000. Restricting the variations of the weight to latitude only decreases the size of \underline{A} to 23×23 . But now we must solve 216 different arrays, one for each vertical and horizontal mode configuration. These are solved only once and stored.

Some attempts were made to add longitudinal variation to the weights by iterating, but this did not work. Firstly, it was not possible to keep $\hat{\gamma}_I$ on the rotational manifold. Secondly, the variations in the magnitude of the weight required to influence significantly the result were too large for convergence.

Ultimately, it is hoped that a subset of the rotational manifold may be found that still defines the important meteorological information that needs to be retained by the initialization and yet has reasonable array sizes.

A summary of how the final method works is given by a Leith (1981) manifold schematic in Fig. 5. Prior to the update, the model is assumed to be on the slow manifold (M), say at point 0. Adding the rotational component puts the model on the data manifold. This step is represented by the line between 0 and 1, and is equivalent to linearly balancing the corrections and inserting them into the model. Note that only the rotational modes are affected by this step, where (3.65) is solved for \underline{x} and then the rotational component of the corrections is determined from (3.59). The imbalances introduced by updating are removed by solving (3.52) and then (3.60). This is the nonlinear step and is represented by the line between 1 and 2.

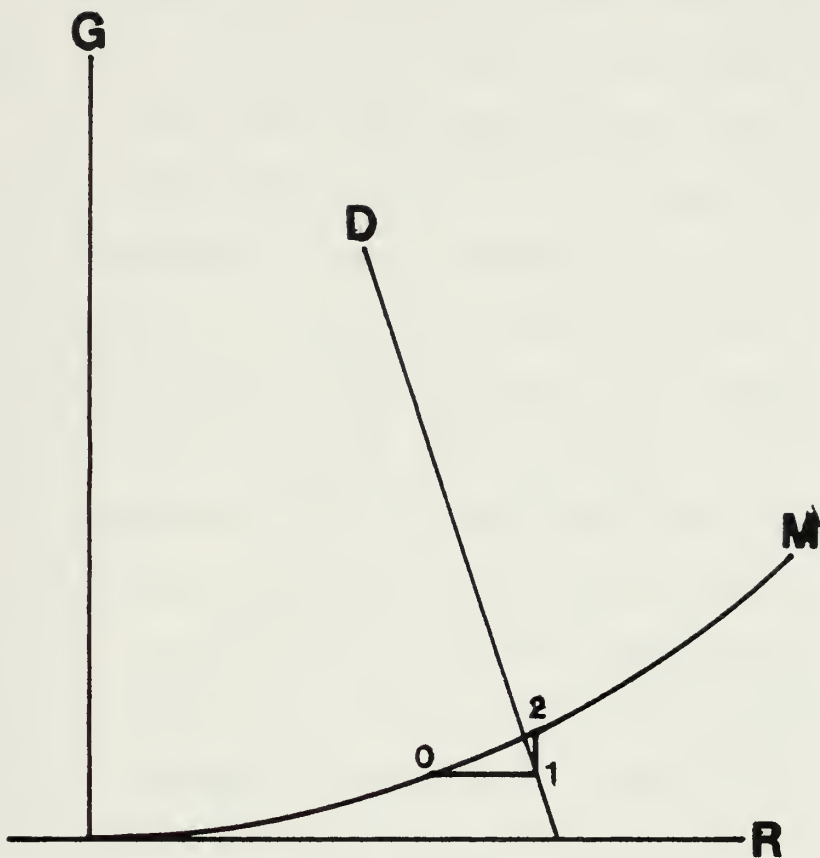


Fig. 5. Manifold schematic of the update and balance procedure used in the data assimilation. Point 0 represents the forecast before the update. The path between 0 and 1 represents the linear balance step. The path between 1 and 2 represents the nonlinear balance step.

E. TESTS OF THE NORMAL MODE METHOD

The magnitude of the rotational and gravitational components of the analyzed corrections were computed from real data taken from the 00 GMT 16 Nov 1979 analysis (see Figs. 6 and 7). The surprising thing about these curves is that the gravitational component is as large or larger than the rotational component. This is especially true of the surface pressure. In fact, the surface pressure gravitational component is so large that the two components must be of opposite signs over much of the globe. Because the nonlinear component of the initialized fields is determined from the rotational component only, the gravitational component of the analysis is not used and therefore represents lost information. It is also a measure of how well the analysis dynamically matches the wind to the mass.

Completeness theorems for the normal modes require that the sum of the rotational and gravitational components of the data be equal to the original data. As a test of the approximations and final code, the degree to which the completeness theorem applied was determined. This was done by computing the rotational component of the corrections, and then computing the gravitational component from what remained of the corrections after the rotational component was removed. The corrections were then reconstructed by adding the rotational and gravitational components. These

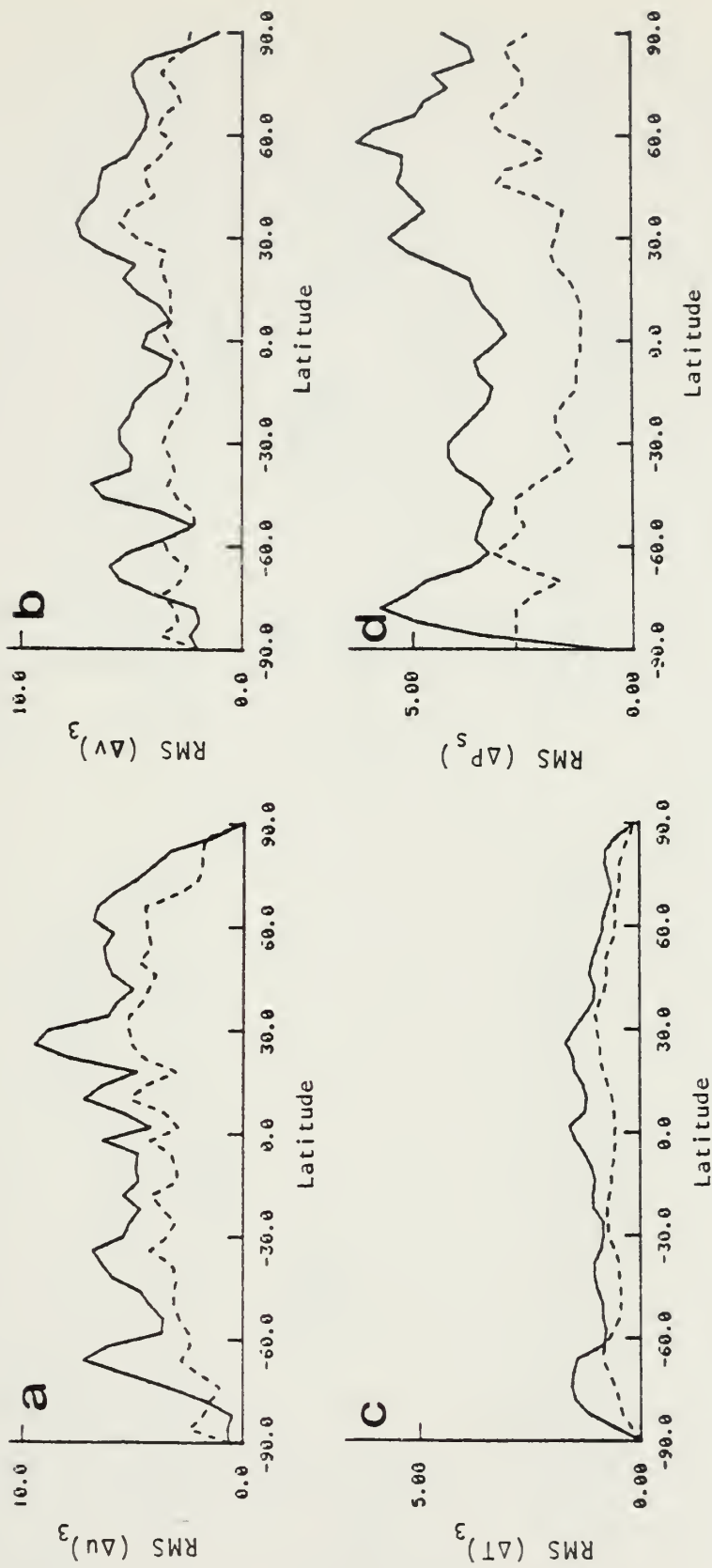


Fig. 6. Update analysis (solid line) and its rotational component (dashed line). Subscript 3 designates level 3.

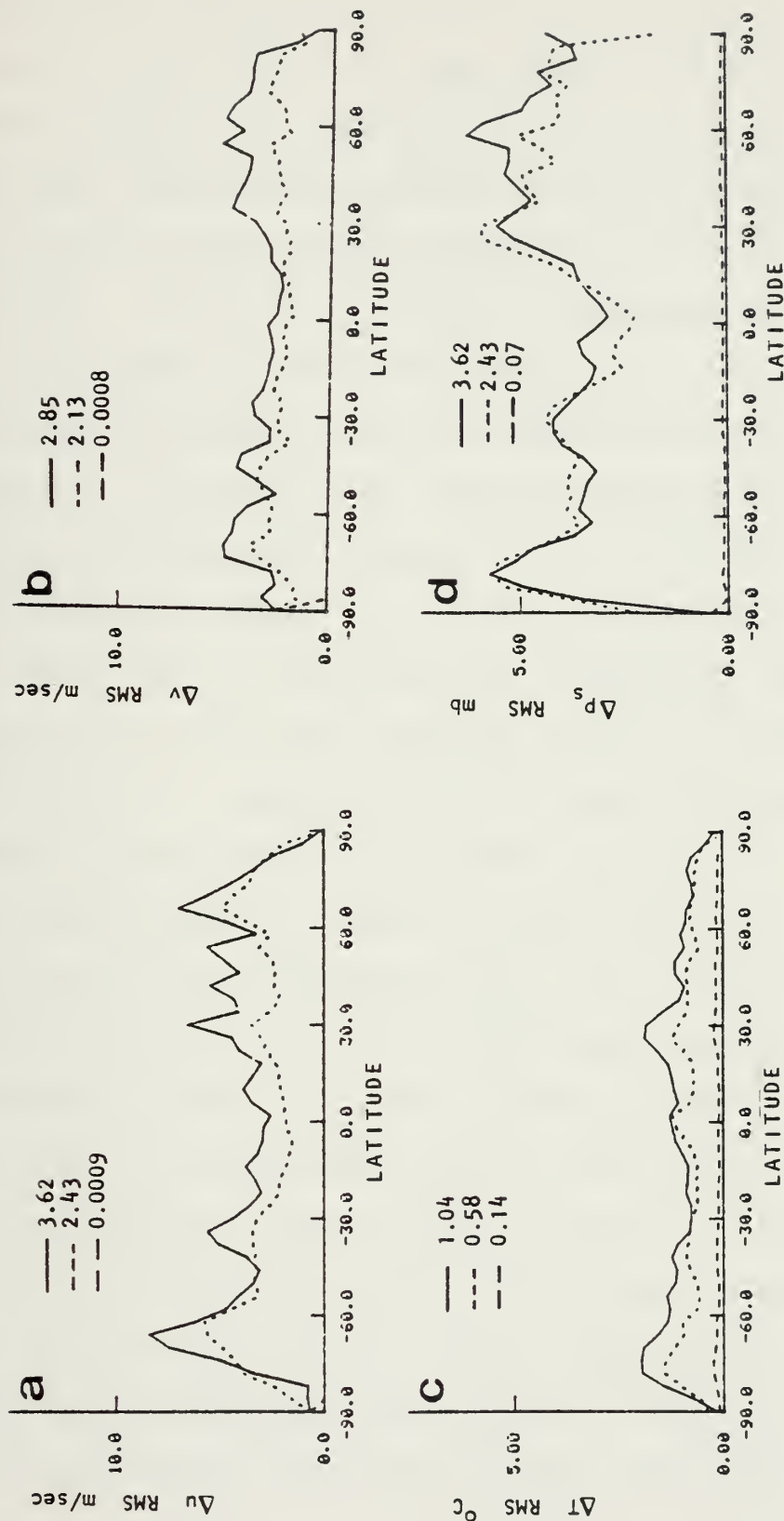


Fig. 7. Analyzed corrections and their gravitational components (dashed line) for third level from the top of the model. The residual of the temperature and surface pressure not resolved onto either the gravitational or rotational manifold is shown by the dark dashed line near the abscissa of (c) and (d).

reconstructed data were compared to the original data by computing RMS differences (see Fig. 7). The differences between the two wind variables were essentially zero, but nonlinear relationships between surface pressure and temperature caused significant residuals to remain in the mass variables. The long dark dashed lines near the abscissa in Fig. 7 (c) and (d) show the residual for level three of the model and the numbers above the curves give the global RMS averages. It can be seen that the temperature residual is largest, and represents about 14% of the total correction. The pressure residual is only about 2%, however.

As a test of the variational technique, the linear balance was rerun with different weights on the mass variable each time. Figure 8 shows the global RMS residuals between the balanced and analyzed variables for the different weight values. Clearly, the most sensitive region is for weight values between 0 and 1. For a loss in the wind residual of about 0.4 m sec^{-1} , the improvement in the mass variables is 0.3°C and 1 mb. Increasing the weight from 1 to 10 does not dramatically improve the fit of the balanced mass variables to the analysis. Eventually, for very large weight on geopotential, the wind residual becomes as poor as the forecast first guess. It is interesting to note the limit in the residual of the wind variables. Even when the weight on the mass variables is zero, the wind residual is

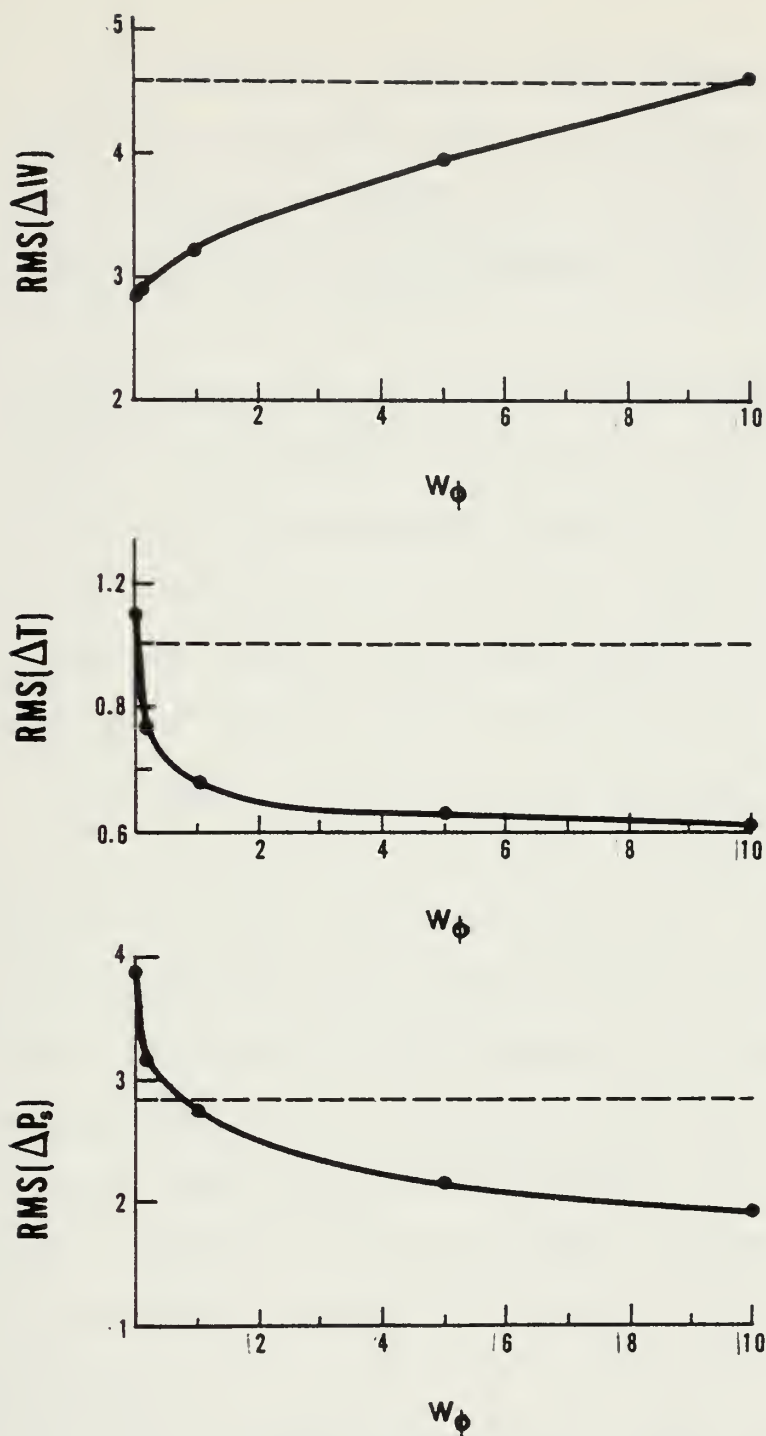


Fig. 8. The RMS differences between the analyzed and initialized variables for different weighting on the mass analysis, W_ϕ . The averages are for the entire globe and all levels. The dashed straight line shows the RMS differences between the analysis and the forecast first-guess.

2.8 m sec⁻¹. The reason for this is that the analyzed wind contains unrealistic divergence that is orthogonal to the rotational manifold (Daley, 1980), and regardless of the weighting, this component has no influence on the rotational component.

As a further demonstration of the variational method, the same analysis was balanced two different ways. In one, the mass variables were weighed very heavily ($W_\phi = 1000$) poleward of $\pm 30^\circ$ latitude. In the other, they were given no weight. The 500 mb vorticity and geopotential fields are shown in Figs. 9 and 10 with the analyzed contours for these two cases. From these figures, it is clear that this range of weighting is sufficient to map exactly either vorticity or geopotential onto the rotational manifold. This is probably not a good method for computing mass from motion and vice versa, because the relationships are linear. In fact, winds computed from the method compare less favorably with observations than the 12-hour forecast first guess. To correct this problem, Phillips (1982a) proposes a method whereby the nonlinear component is removed from the analysis prior to balancing.

The variational method described in this section is too cumbersome to impose full variability into the weights. As a result, restrictions that only allow variations with latitude were imposed. Such limitations are only necessary



Fig. 9. Updated 500 mb vorticity when (a) weight on mass is zero, (b) weight on mass is 1000 poleward of 30°. The unprocessed analysis is dashed and the contour interval is $25 \cdot 10^{-6} \text{ sec}^{-1}$.

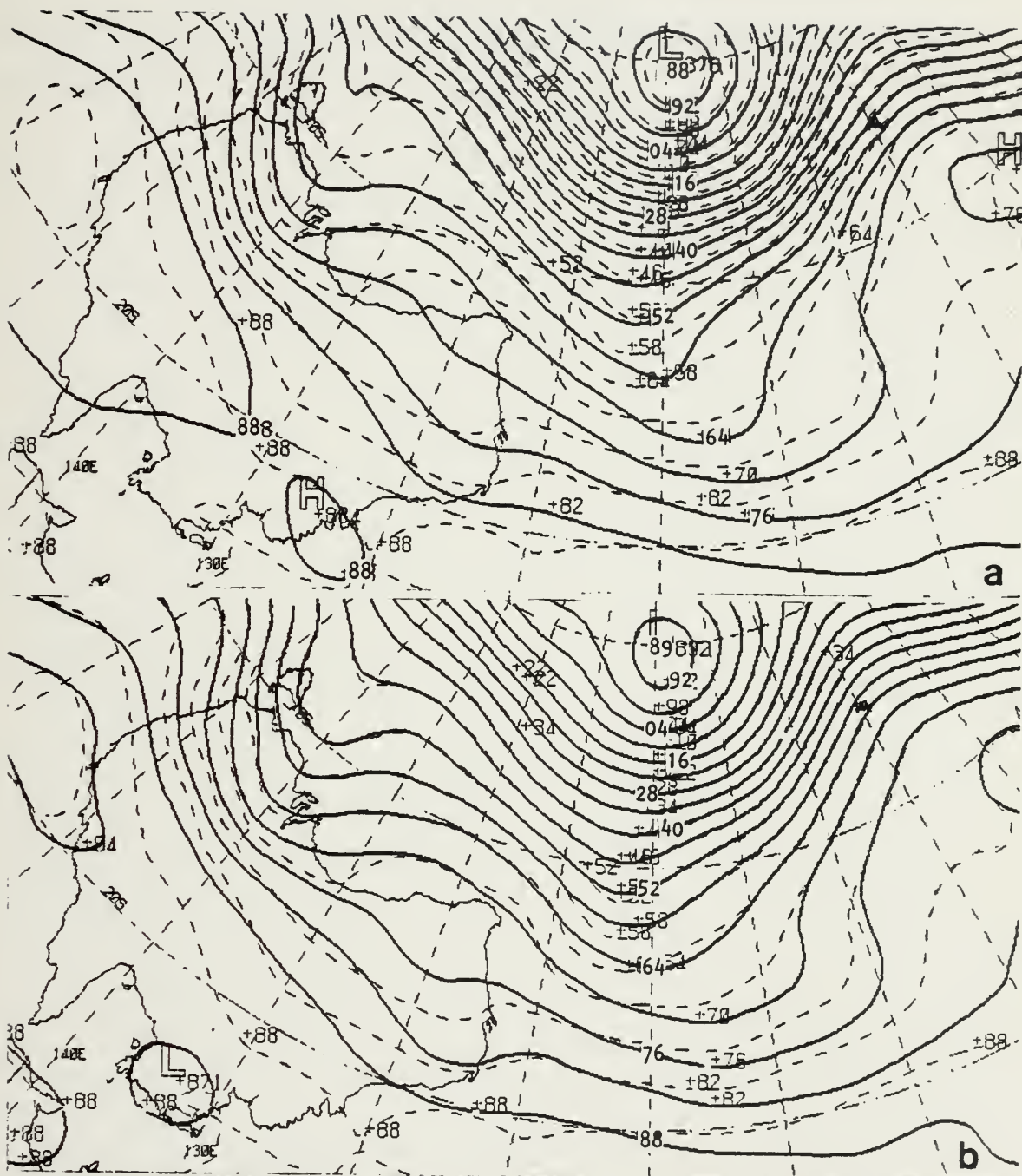


Fig. 10. Updated 500 mb geopotential when (a) weight on mass is zero, (b) weight on mass is 1000 poleward of 30° . The unprocessed analysis is dashed and the contour interval is 60 m.

in the normal mode method. As shown in the next section, the variational method that uses the balance equation as a constraint is capable of using weights with large spatial variation.

IV. THE BALANCE EQUATION INITIALIZATION

A. THE VARIATIONAL FORMULATIONS

For simple models, the nonlinear normal mode balance is nearly equivalent to applying the balance and omega equations as constraints to the initial conditions (Leith, 1980). In the variational method developed by Sasaki (1958, 1970), Stephens (1972) and Haltiner et al. (1976), and described in this section, the balance equation is utilized. But, instead of the omega equation, the vertical motion is derived from the forecast first-guess divergence.

To impose the balance equation as a constraint, the functional

$$I(\phi, \psi) = \int_A (\phi - \phi_0)^2 + \beta (W - W_0)^2 + 2\lambda_B m(\psi, \phi) dA \quad (4.1)$$

is minimized. Here, ϕ is geopotential, W is the vector wind, ψ is stream function, A is the horizontal area over which the integral is applied, and λ_B is the Lagrange multiplier. The constraint is

$$m(\psi, \phi) = \nabla \cdot f \nabla \psi + 2J(u, v) - \nabla^2 \phi = 0, \quad (4.2)$$

where u and v are the east and north components of wind, respectively, J is the Jacobian operator and all operators are applied in spherical coordinates. The minimization is achieved when the first variation of $I(\phi, \psi)$ with respect to ϕ , λ_B and ψ is set to zero. Neglecting the variation of $J(u, v)$ and noting that

$$\int_A \nabla \cdot () dA = 0 \quad (4.3)$$

for integration over the globe gives

$$\phi = \tilde{\phi} + \nabla^2 \lambda_B \quad (4.4)$$

and

$$\beta \nabla^2 \psi = \nabla \beta \cdot \nabla (\psi - \tilde{\psi}) + \beta \nabla^2 \tilde{\psi} + \nabla f \cdot \nabla \lambda_B + f \nabla^2 \lambda_B. \quad (4.5)$$

The Euler-Lagrange equations are (4.2), (4.4) and (4.5) and the unknowns are ψ , ϕ and λ_B . The solution of the Euler-Lagrange equations is accomplished by eliminating ψ and ϕ in (4.2) using (4.4) and (4.5). This gives:

$$\nabla^4 (\Delta \lambda_B)^n - \frac{f^2}{\beta} \nabla^2 (\Delta \lambda_B)^n = m(\phi^{n-1}, \psi^{n-1}), \quad (4.6)$$

$$(\Delta \phi)^n = \nabla^2 (\Delta \lambda_B)^n, \quad \text{and} \quad (4.7)$$

$$\nabla^2 (\Delta \psi)^n = \frac{f \nabla^2 (\Delta \lambda_B)^n + \nabla f \cdot \nabla (\Delta \lambda_B)^n}{\beta} \quad (4.8)$$

The superscript, n , is the iteration count and the delta specifies the difference between the current and previous iteration, i.e.,

$$(\Delta \phi)^n = \phi^n - \phi^{n-1}, \quad (4.9)$$

where

$$\phi^{n-1} \equiv \tilde{\phi} \quad \text{when } n=1. \quad (4.10)$$

Note that all boundary conditions are automatically eliminated when the solution is desired for a full sphere. The second term on the right of (4.8) was dropped because it caused unrealistic adjustments to the winds near the equator. Consequently, only elliptic equation solutions for

$\nabla^2(\Delta\lambda)$ and $\Delta\psi$ are necessary to solve (4.6)-(4.8). Each iteration through (4.6)-(4.8) reduces the residual of the balance equation constraint by an order of magnitude, therefore two cycles produce sufficiently balanced results. A direct solution technique for elliptic equations was used to solve (4.6) and (4.8) (see Swarztrauber and Sweet, 1975; Rosmond and Faulkner, 1976).

The forecast first-guess divergence is retained at the update time in the following manner: First, the variables are balanced as described above. Secondly, the rotational component of the forecast first-guess wind field is computed and subtracted from the balanced wind. Finally, the variables are interpolated to model coordinates where the wind, which is now a nondivergent correction, is added to the forecast first-guess wind field. The mass variables, however, are balanced and interpolated to model coordinates in the conventional manner. In this way, the erroneous divergence near steep terrain regions remains small, and the first-guess divergence is untouched.

Another method of retaining the forecast first-guess divergence is to balance the corrections rather than the updated values. This makes the nonlinear term a little more cumbersome, but this procedure has the advantage of not affecting areas without new data. In this case, the nonlinear term is defined as

$$J'(u,v) = J(u,v) - J(u_0,v_0), \quad (4.11)$$

where the prime is used to designate a correction value rather than an updated value. The integral to be minimized is

$$I(\phi', \psi') = \int_A (\phi')^2 + \beta (W')^2 + 2\lambda_B m(\psi', \phi') dA,$$

where the constraint is

$$m(\psi', \phi') = \nabla \cdot f \nabla \psi' + 2J'(u, v) - \nabla^2 \phi' = 0.$$

This basic approach has also been proposed by Phillips (1977).

B. VERTICAL FILTERING WITH EMPIRICAL ORTHOGONAL FUNCTIONS

The major problem with the foregoing formulations is that the temperature adjustments are not small everywhere. For example, if balancing caused the 925 mb height to change 10 m and the 1000 mb height did not change, the resulting temperature correction between these two levels would be 4°C. Such inconsistencies are difficult to avoid for grids covering very large regions.

To minimize the effects of these inconsistent modifications in the vertical, the variables are vertically coupled by projecting them onto basis functions prior to the balance. Because filtering requires that some of the unimportant components be dropped, the empirical orthogonal functions are the most suitable functions for this purpose. These functions are derived so that they form a basis set

that produces the least error when a partial series is used to describe a particular three-dimensional field, such as geopotential (see Appendix C).

An example of the efficiency of the empirical orthogonal functions is shown in Fig. 11 for a ten-level analysis of geopotential. Here, the first mode explains 95% of the total variance, whereas the first two modes explain 98%. Only four modes are necessary to explain 99.9% of the total variance. Projecting the wind analysis onto the first four modes retained the details of the jet streams produced by the analysis. Holmstrom (1963) first noticed this very rapid convergence of the empirical orthogonal functions in representing geopotential profiles. The smoothness of the first four empirical orthogonal functions insures that inconsistent vertical variations of wind or geopotential between adjacent levels will be truncated when used to form a partial series of the analyzed fields prior to balancing. Another advantage of this method is that considerable computer time is saved. Rather than treating 10 levels, only the four vertical modes need to be balanced.

To show how empirical orthogonal functions are incorporated into the variational balance, the balance equation is written in vertical vector form

$$\underline{m}(\psi, \phi) = \nabla \cdot (f \nabla \underline{\psi}) + \underline{A} - \nabla^2 \underline{\phi}, \quad (4.14)$$

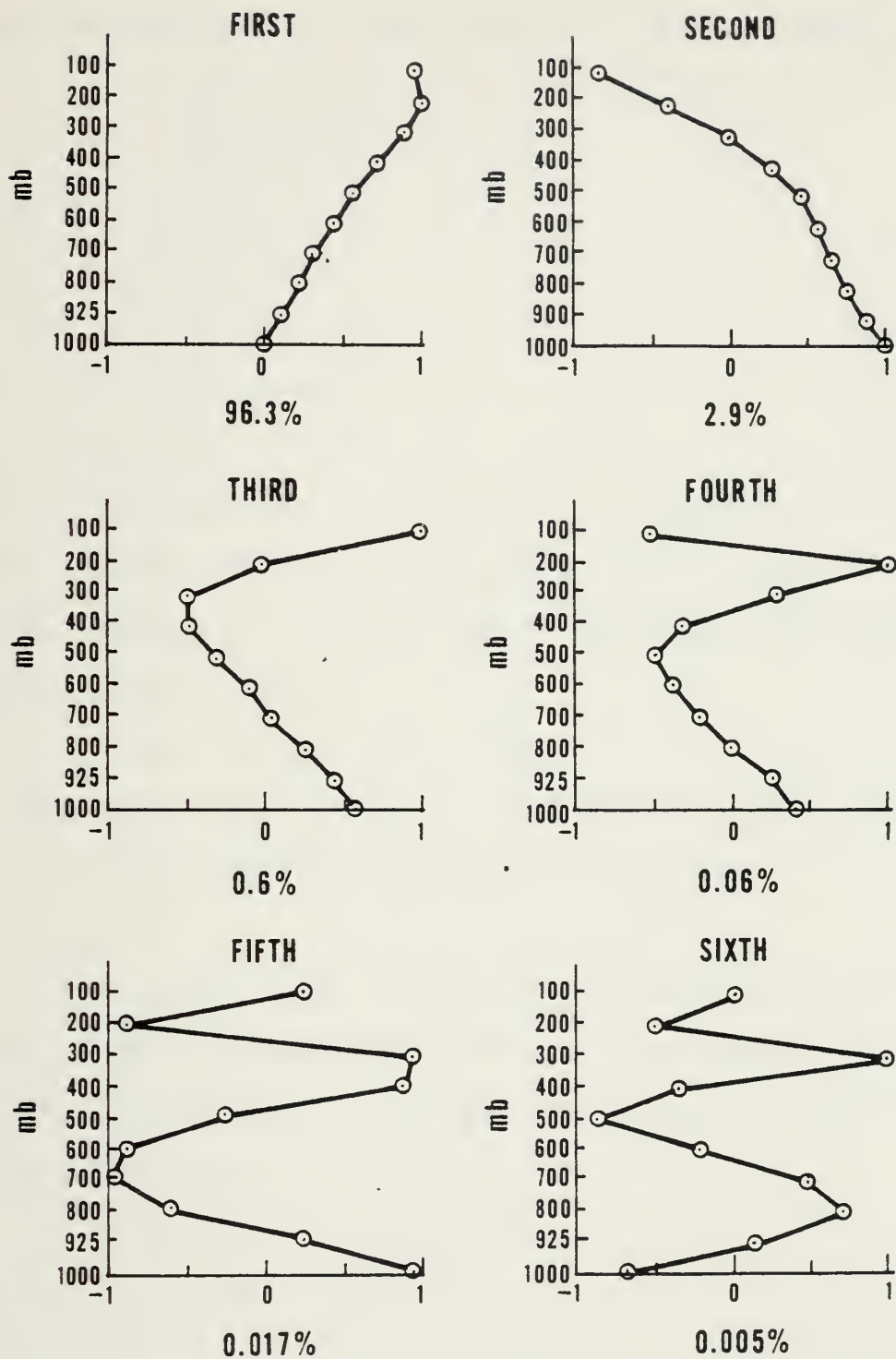


Fig. 11. The first six empirical orthogonal functions derived from a ten-level analysis of geopotential.

where the underlying tilde signifies a column vector, such as

$$\tilde{\phi} = \begin{bmatrix} \phi_{10}(\lambda, \theta) \\ \phi_9(\lambda, \theta) \\ \vdots \\ \phi_1(\lambda, \theta) \end{bmatrix} \quad (4.15)$$

Here λ is longitude, θ is latitude and the subscript is the level number. A is the Jacobian given in (4.2).

Multiplication of (4.14) by one of the empirical orthogonal functions, E_i^T , gives

$$m_i = \nabla f \cdot \nabla \psi_i + A_i - \nabla^2 \phi_i = 0, \quad (4.16)$$

and the variational integral imposing this constraint is

$$\int_A (\phi_i - \phi_{0i})^2 + \beta (W_i - W_{0i})^2 + 2\lambda m_i dA \quad (4.17)$$

The solution of (4.17) exactly follows that for (4.1).

After (4.17) is solved for N of the most significant empirical orthogonal functions, the balanced fields are constructed from

$$\tilde{\phi}_B = \sum_{i=1}^N \phi_i \tilde{E}_i \quad (4.18)$$

and

$$\widetilde{\nabla \times W}_B = \sum_{i=1}^N (\nabla \times W_i) \tilde{E}_i \quad (4.19)$$

As shown by (4.19), the balanced vorticity is constructed from the empirical orthogonal functions, and then the

balanced winds are computed from vorticity. The degree of filtering is governed by the size of N , which was set to four to keep the jet streams sufficiently strong.

The filtering described in this section greatly improved the erroneous temperature problem. A temperature adjustment profile for a filtered and unfiltered balance is shown in Fig. 12. As has been typical, the lowest layers were particularly poor in the nonfiltered balance, where adjustments were in excess of 3° . Zonal averages of the temperature adjustments of the lowest layer in the tropics were -3°C to -4°C . The filtered balance, on the other hand, produced adjustments that were much smaller. The zonal averages of the adjustments were everywhere less than 0.5°C , and individual adjustments in the lowest layers were about 1°C .

C. WEIGHT STRUCTURE

Typically, the weight a variable receives during the variational balancing depends on an intricately computed error structure function, which can be derived from optimum interpolation methods such as given by Gandin (1963). Such error structures are not easily derived from successive correction methods, but the amount of data that influences any point can be used to infer analysis accuracy to some extent.

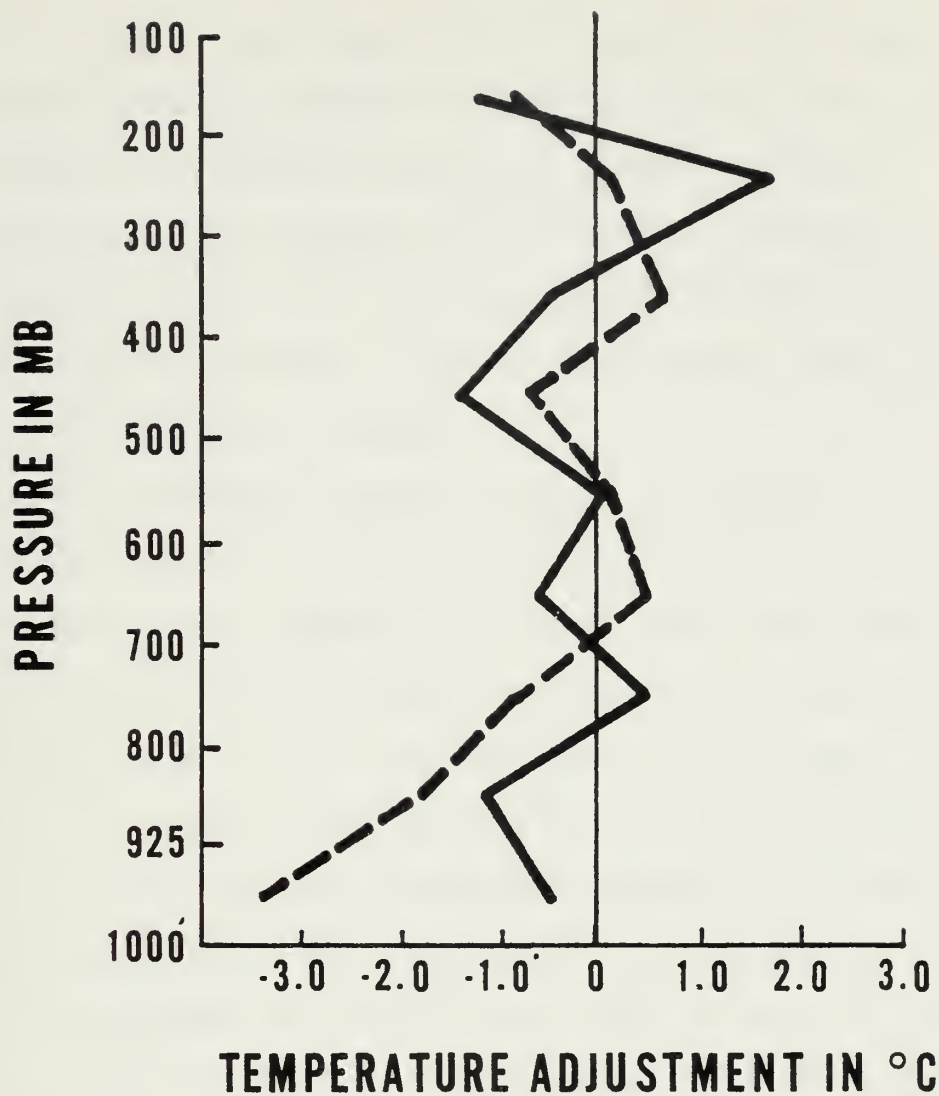


Fig. 12. Adjustments made to the temperature in order to balance wind at 60°E, 30°N on 27 Mar 1982. No vertical coupling (dashed line) and vertically coupled using empirical orthogonal functions (solid line).

In the methods described in this section, the weight on the geopotential is unity and the weight on the winds is β , thereby keeping the weight function a single variable. Limitations to β were necessary in the region bounded by $\pm 30^\circ$ latitude. Here, β had to be at least $10^4 \text{ m}^2 \text{ sec}^{-2}$ to avoid convergence problems. Outside this region, no such limitations were found to exist.

The wind weight has two basic parts. One part is purely a function of latitude and is prescribed without regard to observation density. For this part, the weight was set at $40,000 \text{ m}^2 \text{ sec}^{-2}$ over the region bounded by $\pm 30^\circ$ and at $4,000 \text{ m}^2 \text{ sec}^{-2}$ over the remainder of the globe. This means that a 5 m sec^{-1} modification in wind would correspond to a 100 m or a 30 m change in height, depending on where the change took place. The second part of the weight depends on the number of observations used to describe mass or motion, and has a range of values from $-2000 \text{ m}^2 \text{ sec}^{-2}$ to $2000 \text{ m}^2 \text{ sec}^{-2}$. For example, if a motion variable were influenced by five or more observations and there were no mass observations, the second part would have a value of $2000 \text{ m}^2 \text{ sec}^{-2}$. But if the reverse were true, i.e., the mass variables were supported by five or more observations, then the second part would have a value of $-2000 \text{ m}^2 \text{ sec}^{-2}$. The final weight value is the sum of the first and second parts.

In this chapter, the classical balance equation has been incorporated into a global initialization that uses calculus of variations. The method involves the solution of elliptic equations on a sphere, but otherwise the method is simple and flexible in terms of variable weighting. This system was thoroughly tested by Barker (1981a). In the next section, the role of the balance equation in data assimilation will be compared to that of the nonlinear normal mode method.

V. COMPUTATIONAL RESULTS

A. EXPERIMENT DESCRIPTION

The results comparing the different initialization methods were obtained using the FGGE level IIa data set for the period between 16 Nov 1979 and 21 Nov 1979. The level IIa data were available on an operational basis, consequently no special processing was performed for this set. The observing systems available at this time are described by Fleming et al. (1979).

Four different initialization methods were tested in data assimilation tests that covered the period of the data set. Two of the methods tested used some form of the balance equation, and the other two used the variational nonlinear normal mode method.

In the two balance equation methods, the divergence was obtained from the forecast first guess. In the first method, hereafter referred to as BE1, the corrections to the forecast were balanced and interpolated to the model coordinate. This maintained a balance between mass and motion and preserved the divergence that was present in the forecast just prior to the time of the update. The second method, which shall be called BE2, balanced the total analysis (forecast first guess plus corrections) and then converted the balanced winds to nondivergent corrections. The motion

variables were then treated as in BE1, except the mass variables were treated as the new values in the model. The main difference between the two methods is that the corrections were balanced in BE1 and the updated variables were balanced in BE2. Both methods used the same weight assignment described in Chapter IV.

Two variations of the normal mode approach were used. In the first case (NM1), the weights were varied with latitude. Poleward of ± 30 degrees, the weight on the geopotential was 10, that is an order of magnitude larger than naturally occurs in the normal mode method. Further increases in geopotential weight make only slight improvements in the fit of geopotential, as discussed in Chapter IV.D. Equatorward of ± 30 degrees, the geopotential weight was 0.5. In the second case (NM2), the geopotential weight was unity everywhere.

B. DIFFERENCES BETWEEN BALANCED AND ANALYZED VARIABLES

The objective analysis method described above is used to fit the available observations relative to the first-guess fields from the forecast model. Unfortunately, large regions of the earth have inadequate data coverage in terms of quantity and quality. Mass corrections are frequently made in regions without motion corrections and vice versa. This, in turn, causes large imbalances between the mass and

wind fields which often cause the model to reject much of the analyzed information (Daley, 1980; Daley and Puri, 1980). Similarly, the initialization may reject updated information by balancing to the motion variables when the mass variables are more correct. To show how the balanced conditions differ from the analyzed ones, the differences between the balanced and analyzed variables were plotted for the different balancing methods.

The RMS averages of the analyzed corrections and the differences between the balanced and unbalanced conditions are shown in Fig. 13 for BE1 and BE2. Except for temperature, the two methods produced about the same modifications to the analyses. Surprisingly, these changes to the analyses were nearly as large as the original corrections.

The globally averaged temperature modifications are much larger for the BE2 method than the BE1 method, primarily because of the adjustments made to the lower levels of the model. These adjustments were much smaller in subsequent update cycles (0.8 degrees), but were consistently twice as large as the BE1 method.

The large differences between analyzed and balanced winds are related to the inability of the objective analysis to project the corrections onto the rotational component of the wind. This is further illustrated in Fig. 14.

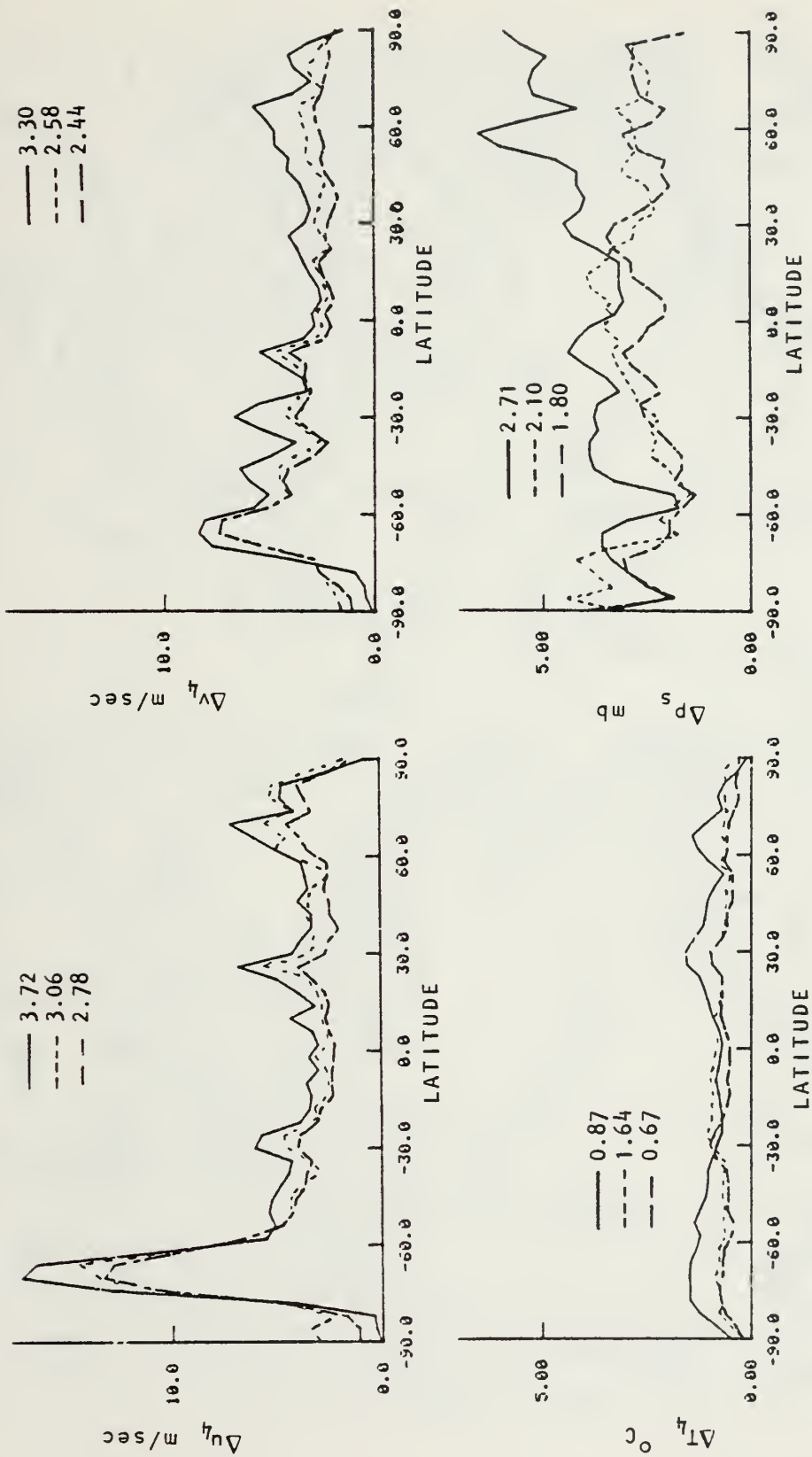


Fig. 13. RMS differences between the first guess and analysis (solid line), and RMS differences between balanced values and analysis (dashed lines) where BE1 is represented by long dashes and BE2 is represented by short dashes. The subscript 4 designates level 4, and the global RMS values are given above the respective plots.

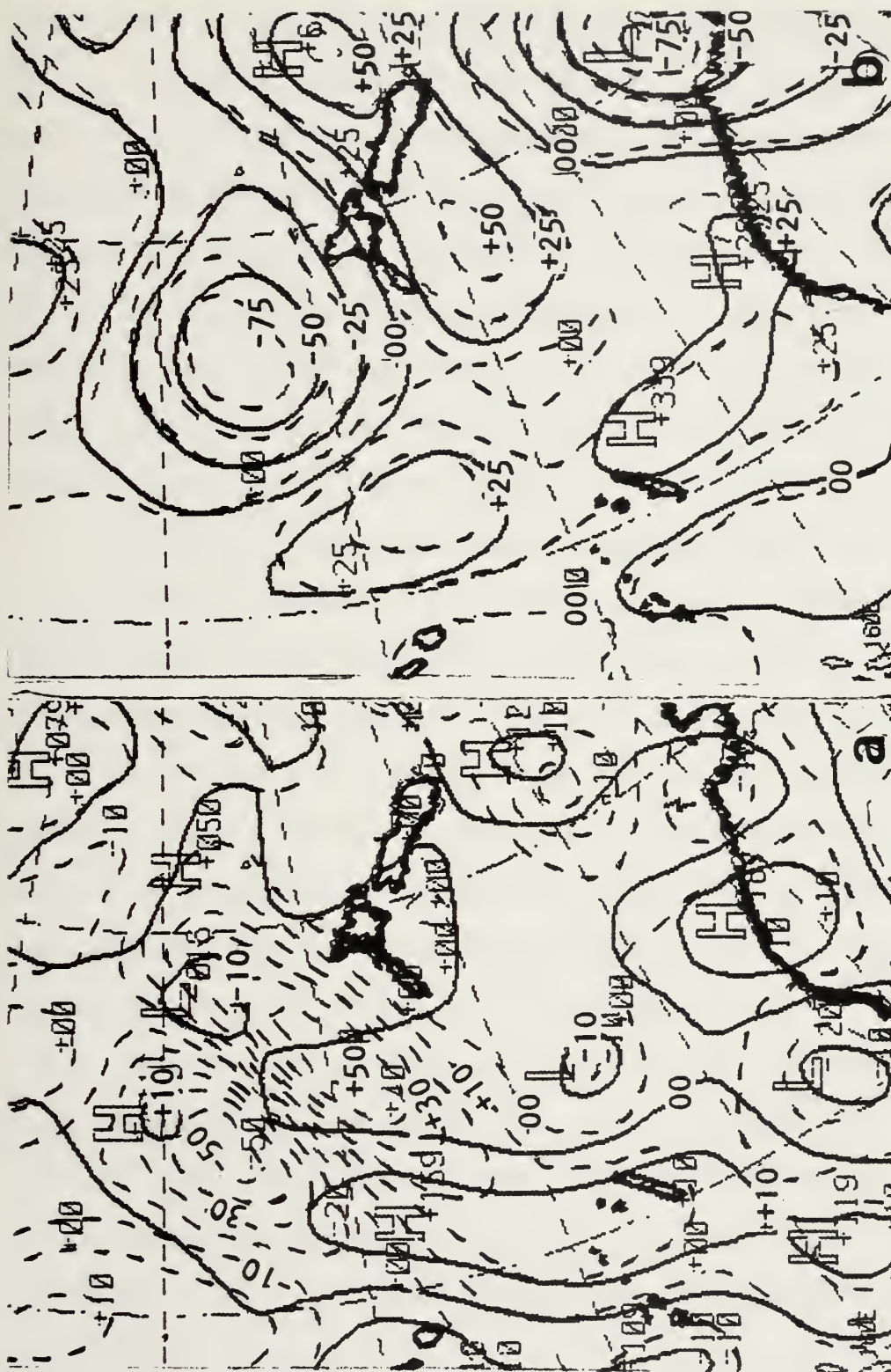


Fig. 14. Divergence (a) and vorticity (b) at 500 mb in the region of New Zealand. The values after balance are depicted with a solid line and the analyzed values are depicted with a dashed line. Contour interval is $10 \cdot 10^{-6} \text{ sec}^{-1}$ for divergence and $25 \cdot 10^{-6} \text{ sec}^{-1}$ for vorticity. The time is 00Z GMT 11 Nov 1979.

Regions such as the one shown have few wind observations. When there is an isolated report, it produces a correction that is largely divergent (see Barker, 1981b), and regardless of the weighting on the winds, this divergence is rejected during the balance. The rotational component, however, can be fit as accurately as desired (see Chapter IV.D), by adjusting the wind weights. The vorticity shown in Fig. 14 is reasonably close to the analyzed values considering the moderate values of weighting applied to the winds in this area, $(\frac{\Delta\phi}{\Delta V})^2 \sim 4000 \text{ m}^2 \text{ sec}^{-2}$.

The RMS average differences between normal mode balanced and unbalanced variables were also compared to the RMS average of the analyzed corrections (see Fig. 15). In these comparisons, however, the divergent component of the wind correction was removed from the analysis before interpolation to the model coordinates. The method with stronger weight on geopotential produced closer fits of temperature and pressure than did the other method, but it failed to fit the winds as well. This is to be expected in the variational method. The globally averaged wind differences were between 1.0 and 1.5 m sec^{-1} , but when divergence was not removed from the analysis, the differences were consistently larger (between 2.0 and 2.7 m sec^{-1}). The surface pressure differences were as large as the analyzed corrections over much of the earth.

Comparing the balance equation results (Fig. 13) to those of normal mode methods (Fig. 15) indicates that both techniques were similar in the way that they modified analyzed variables. The balanced winds differ from the analyzed winds by about the same amount for all methods when the analyzed divergence was not removed prior to balancing (these curves are not shown). The normal mode methods were slightly better at fitting the analyzed temperature, but poorer at fitting the surface pressure.

The modifications to the analyzed variables were significantly large in all experiments performed. However, whether the impact of the balancing can be considered beneficial to the data assimilation process principally depends on the magnitude of the gravity wave noise that still exists. In the next section, the noise levels that are present in the model before and after balancing are compared for the balance equation and normal mode methods.

C. ELIMINATION OF GRAVITY WAVE NOISE

In this section, gravity noise produced in forecasts initialized with no balance, the balance equation and the normal mode method are compared. In these comparisons, surface pressure tendency was used as a measure of the gravity noise. Although this quantity reflects only the presence of external gravity waves, the highest frequencies

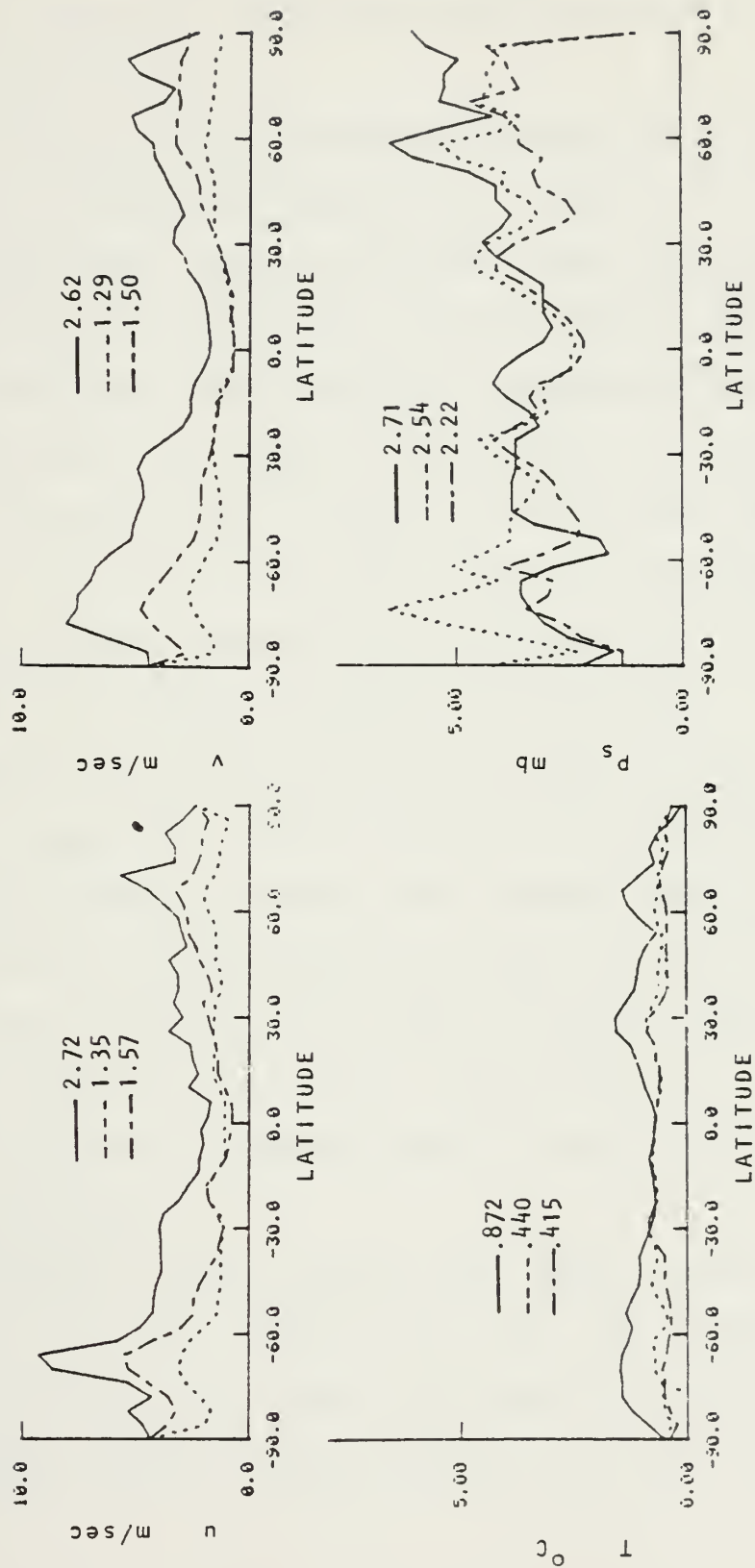


Fig. 15. Similar to Fig. 13 except for the normal mode methods. NM1 (long dashes) and NM2 (short dashes).

come from these external waves. Except where stated otherwise, a dry version of the global model was used to perform the integrations.

In the first comparison, the effectiveness of the balance equation was tested by comparing it with an initialization that just removed divergent winds from the update corrections. In the balance equation method used for testing, the corrections were balanced, interpolated to model coordinates and then added to the forecast first guess (method BE2). As can be seen in Fig. 16, the balance equation forecast is less noisy than the forecast initialized with nondivergent winds, particularly during the final hours of the forecast. The slower adjustment rate of the unbalanced forecast is probably due to the scale of the gravity waves, since global models may carry large gravity waves that do not readily disperse their energy (Bourke, 1972). This version of the balance equation initialization, on the other hand, is effective at removing these large scale waves, but it does not balance around terrain. Consequently, the balance equation method contained noticeable small scale noise.

Using the model's normal modes, the linear balance was compared to the nonlinear balance (Fig. 17). The nonlinear balance forecast required one hour adjustment time and resulted in about one half as much noise as did the linear

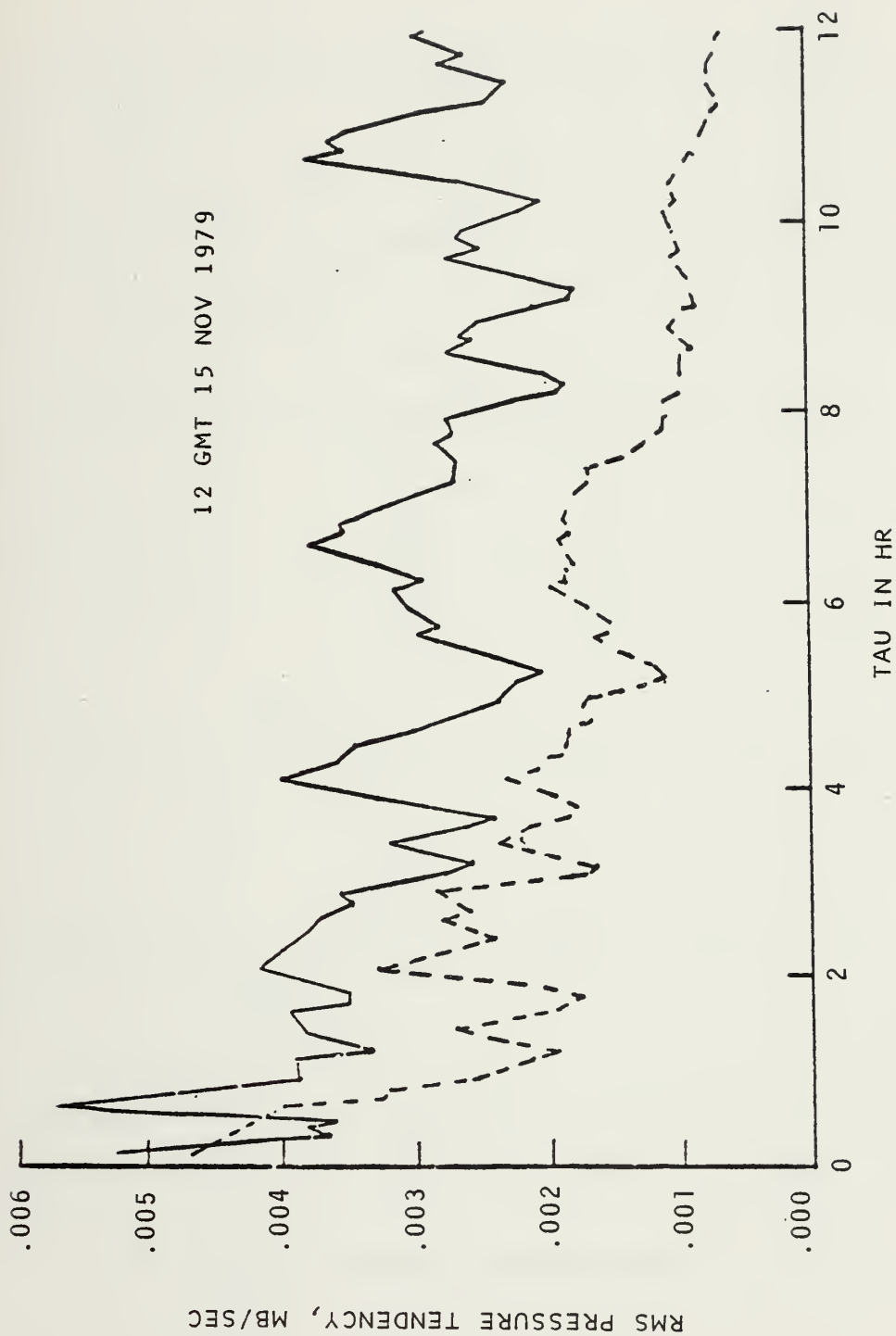


Fig. 16. Global RMS average of surface pressure tendency from a forecast initialized with no divergence (solid line) and a forecast initialized with the balance equation (dashed line).

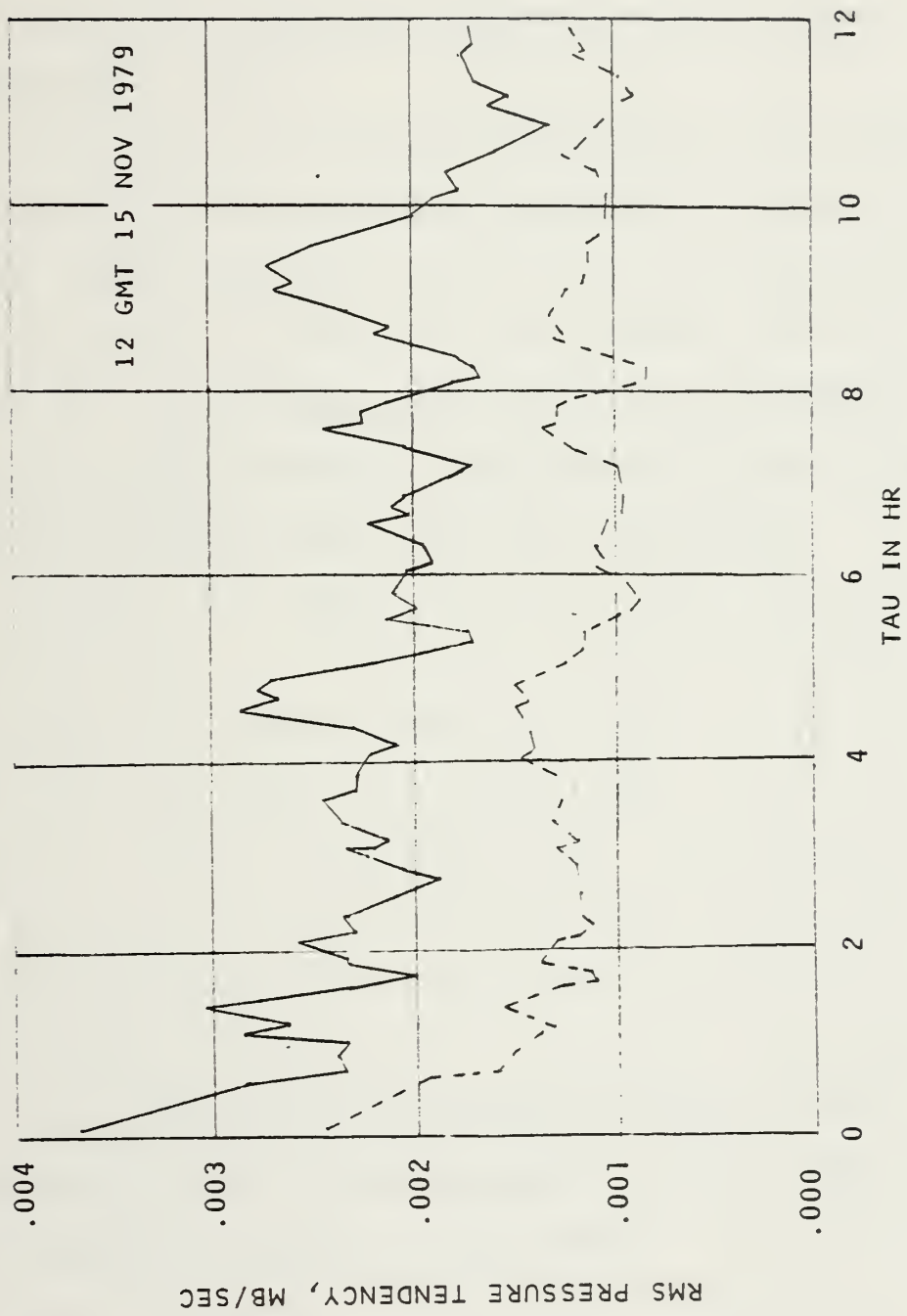


Fig. 17. Global RMS average of surface pressure tendency from a forecast initialized with linear normal mode balance (solid line) and nonlinear normal mode balance (dashed line).

balance forecast. These results illustrate the effectiveness of the nonlinear balance step, which can balance around terrain (Daley, 1979; Williamson and Temperton, 1981) and can include the nonlinear component of the balance (Machenhauer, 1977).

Plots of surface pressure tendencies from predictions initialized with the balance equation and with the nonlinear normal mode method are shown in Fig. 18. These results show the superiority of the normal mode method over the balance equation. After seven hours, however, the forecast started from the balance equation contained only slightly more noise than the forecast from the normal mode method.

Finally, the impact of adding latent heating effects to the forecasts is illustrated in Figs. 19 through 21. The increased noise level is most noticeable in the normal mode runs (Fig. 20) where the forecast seems to have required about six hours of adjustment time. The balance equation run was only slightly affected by the heating (Fig. 19), possibly because less precipitation was generated during the early hours of the forecast. In any case, the result is that the normal mode method was no better at noise suppression than the balance equation when latent heating effects were included in the forecast. This result was observed consistently several times during the course of development of the methods.

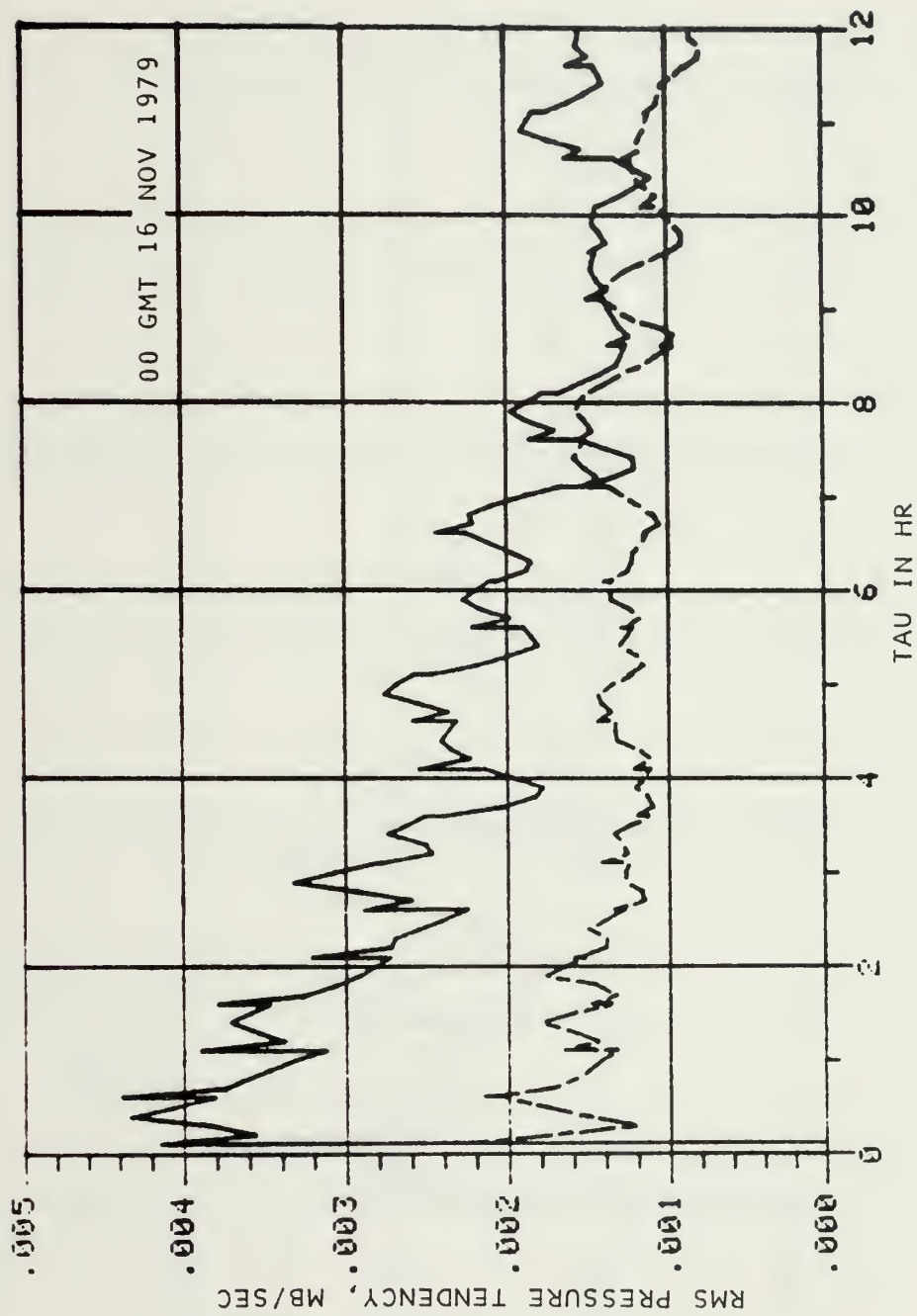


Fig. 18. RMS of surface pressure tendency for the normal mode initialization (dashed line) and for the balance equation (solid line) when latent heating is not included in the forecast model.

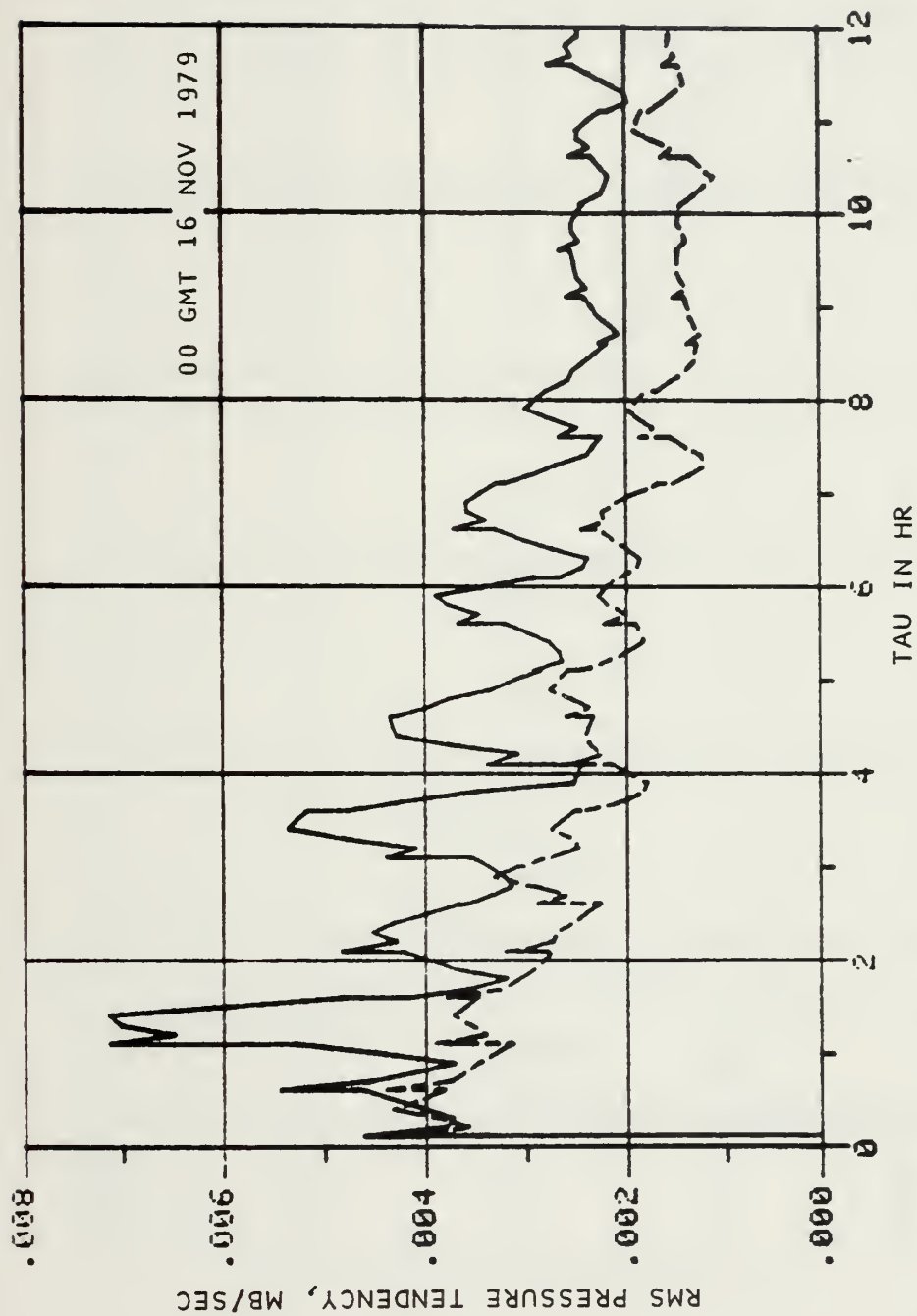


Fig. 19. RMS average of surface pressure tendency in forecasts initialized with the balance equation method. The adiabatic forecast is represented by a dashed line and the forecast including latent heat effects is represented by a solid line.

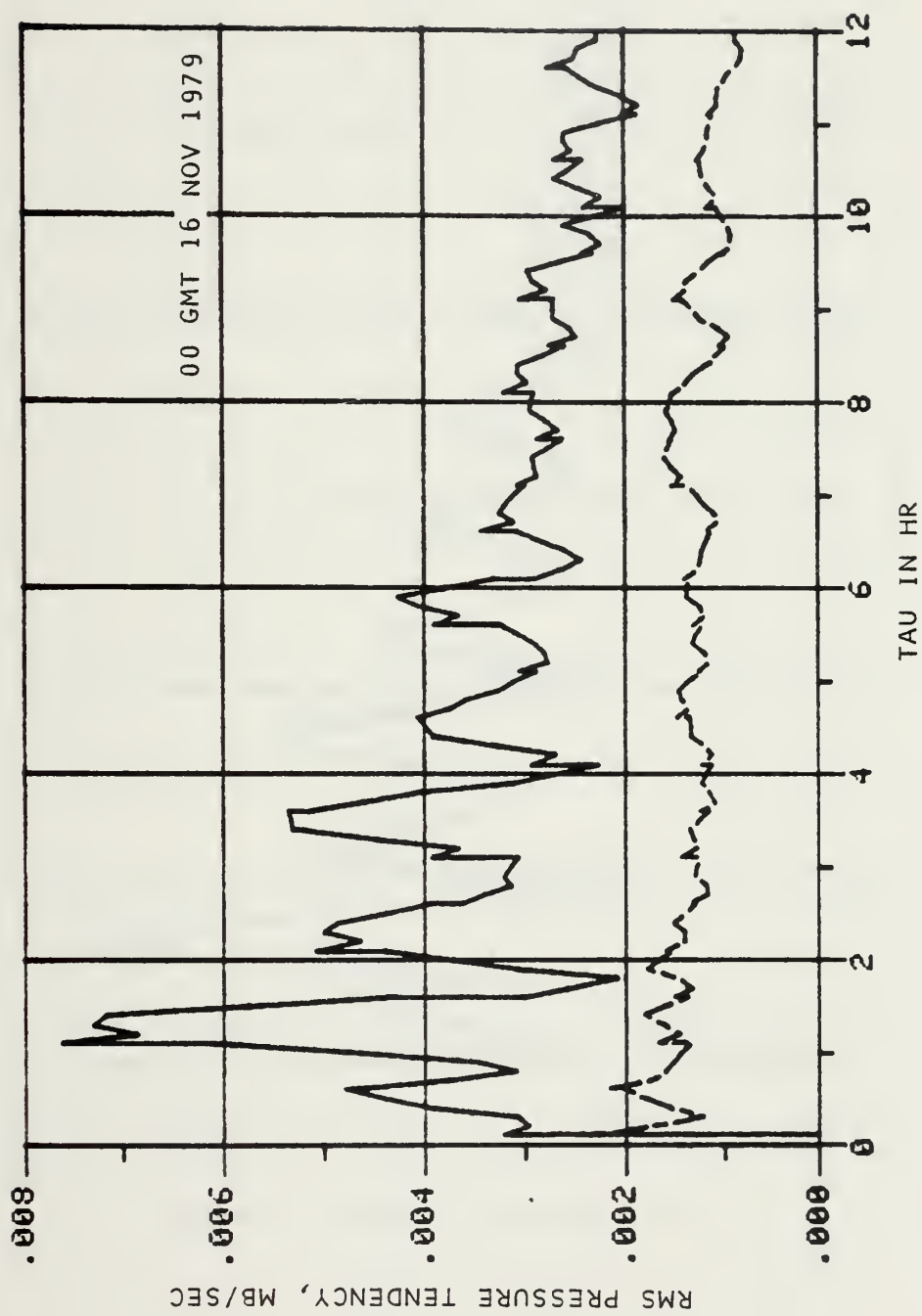


Fig. 20. Similar to Fig. 19 except for the nonlinear normal mode technique.

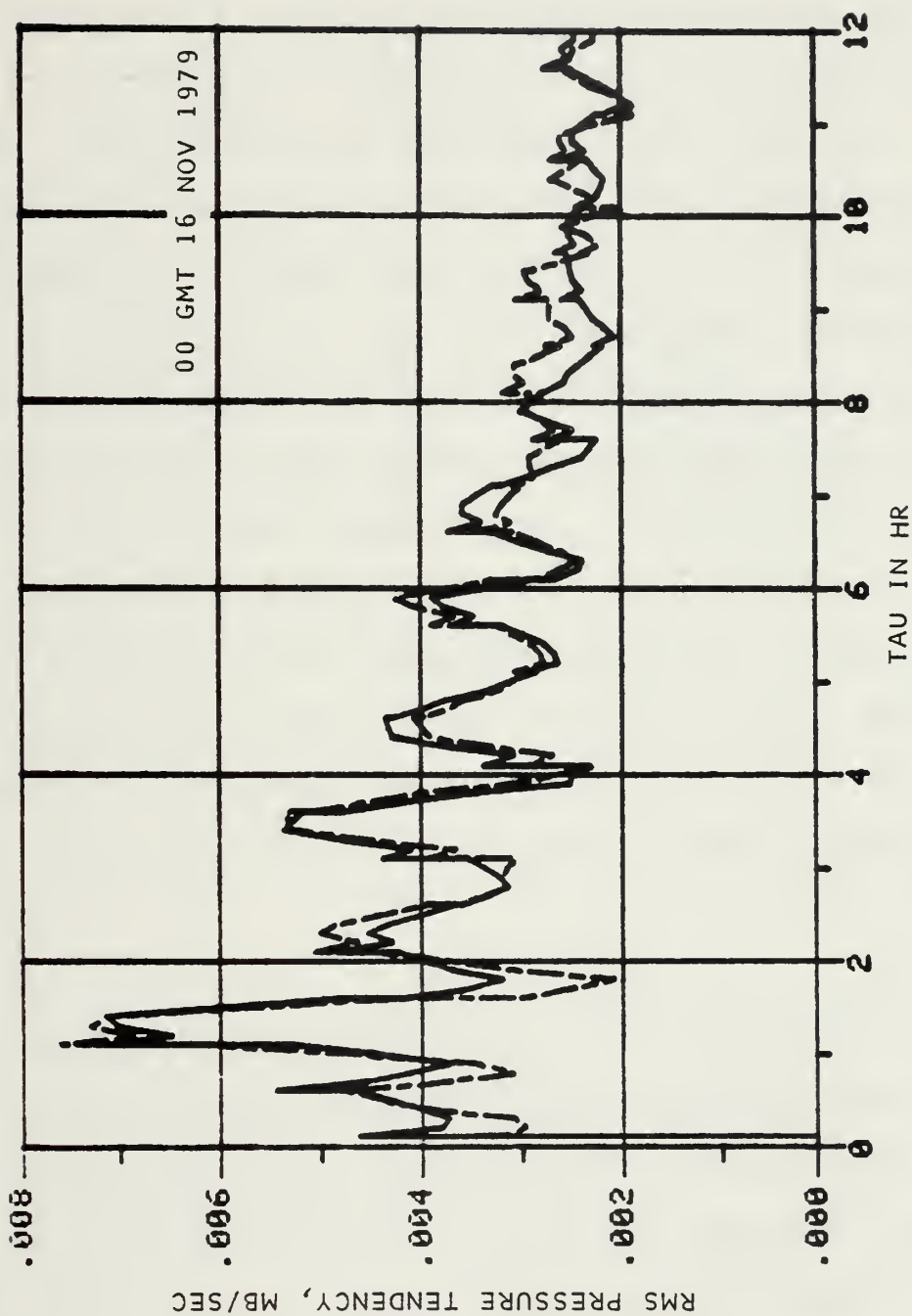


Fig. 21. RMS of surface pressure tendency for the nonlinear normal mode initialization (dashed line) and for the balance equation (solid line) when latent heating is included in the forecast.

In summary, the normal mode method was most affected by latent heating in the forecast. This was probably because it allowed more precipitation to occur during the early hours of the forecast compared to the balance equation method. Considering that one problem associated with initialization has been the lack of precipitation early in the forecast, the noise level increase in the forecast including latent heating may be a symptom of a beneficial result. It is noteworthy that latent heating effects generated twice as much gravity noise as the integrations that did not include latent heating. This was true even after the initial adjustment period was complete. To explore the question of latent heating effects more fully, comparisons of the precipitation, vertical motion and cyclogenesis during data assimilation runs were made. The results from these runs are described in the following section.

D. VERTICAL MOTION PRECIPITATION AND CYCLOGENESIS

The lack of precipitation early in the forecast is considered to be a major problem in the initialization of numerical models (Tarbell et al., 1981; Bengtsson, 1981; Daley, 1981). This is particularly true of forecasts initialized without vertical motion. An example of the problem is shown in Fig. 22. These two forecasts were

initialized with the balance equation with no provisions to include vertical motion. The forecasts for the region west-northwest of the Hawaiian Islands predicted large precipitation rates after six hours, but only slight amounts before this time.

These initially small precipitation rates occur when no vertical motion is included in the initialized data. Inclusion of the omega equation (Tarbell et al., 1981), nonlinear normal mode initialization (Leith, 1980) and retention of the forecast first-guess vertical motion provide possible solutions to this problem. Unfortunately, the omega equation and normal-mode methods have not worked well in the tropics (Bengtsston, 1981; Tribbia, 1981), and the forecast first guess may suffer from inaccuracies in the forecast.

The balance equation methods discussed in Chapter III use the forecast first guess divergence. The normal mode initialization partially recomputes this divergence through the nonlinear balancing of the external and first internal vertical modes. The forecast and derived divergence from the normal mode methods are given in Fig. 23. A sequence of forecast and computed divergence fields is given in Fig. 24. Notice that only small differences exist between the forecast and computed divergence patterns. This similarity between the two divergent winds suggests that the forecast divergence is a fairly accurate quantity.

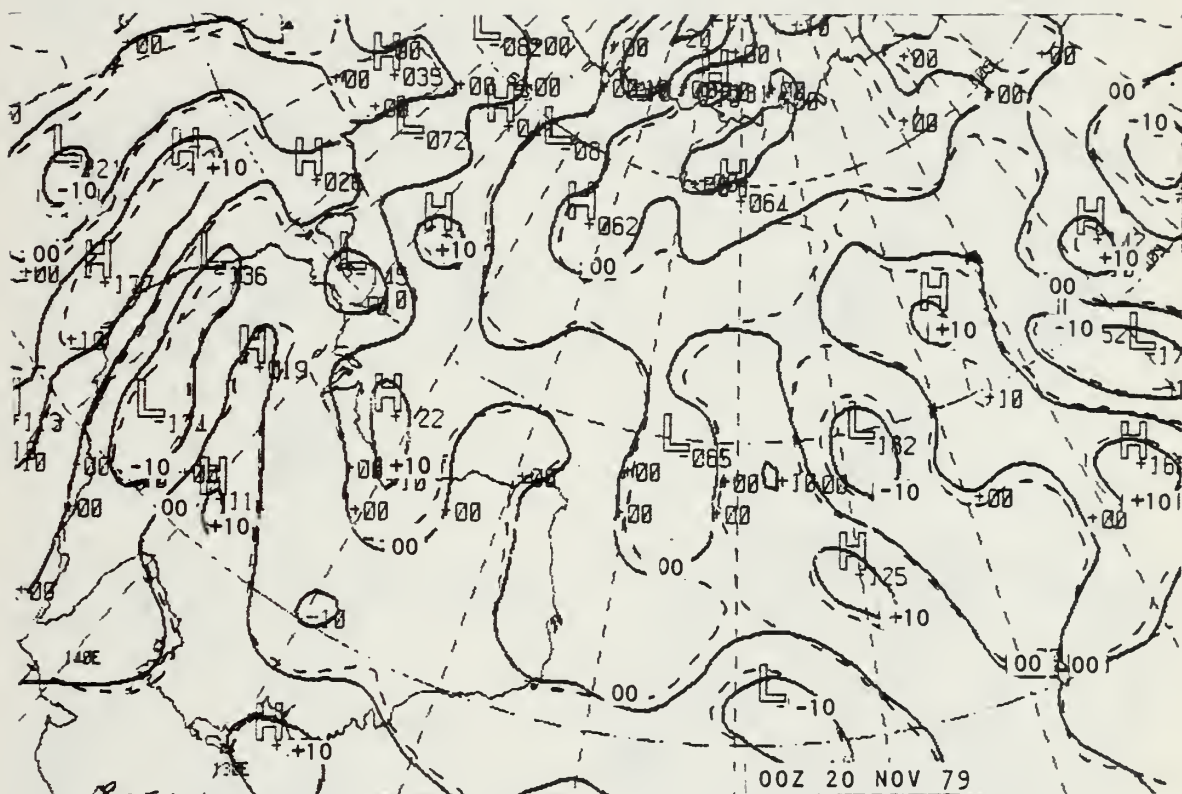


Fig. 23. The first-guess divergence (dashed line) and normal mode computed divergence (solid lines) at 500 mb valid at 00 GMT 20 Nov 1979. The contour interval is 10^{-5} sec^{-1} .



Fig. 24. Forecast first-guess divergence (a, c, e) and divergence computed using the normal mode method, NM2 (b, d, f), for three successive 12-hourly updates beginning at 12 GMT 17 Nov 1979. Contour interval is 10^{-5} sec^{-1} . The interval between $-1 \cdot 10^{-5} \text{ sec}^{-1}$ and $-2 \cdot 10^{-5} \text{ sec}^{-1}$ is cross-hatched and the interval between 10^{-5} sec^{-1} and $2 \cdot 10^{-5} \text{ sec}^{-1}$ is cross-hatched twice.

Precipitation rates from five forecasts that are identical except for the initialization procedure are shown in Fig. 25. In the first case (Fig. 25a), no initialization was used. Even the excessive divergence produced by the analysis was included in the initial data. The other methods, which are designated BE1, BE2, NM1 and NM2, are described in Chapter V.A. These forecasts all produced a nearly identical precipitation pattern along the coast of North America. The normal mode methods (NM1, NM2), however, produced less precipitation in the central Pacific than did the balance equation methods (BE1, BE2). However, on the other hand, normal mode methods have produced the largest precipitation rates south of Japan. None of the methods produced a persistent bias in the strength of precipitation rates. Considering the sensitivity of precipitation rate to small changes in initial data, however, the similarity of the patterns is quite remarkable. In particular, the lack of spurious precipitation in the forecast without any balancing is most surprising.

The precipitation rates during the first twelve hours of forecasts initialized by the balance equation and normal mode methods are shown in Fig. 26 for a region just north of South America. Separate rates are given for the first and second six-hour periods to illustrate the impact of initialization. During the first six hours of the forecast, the



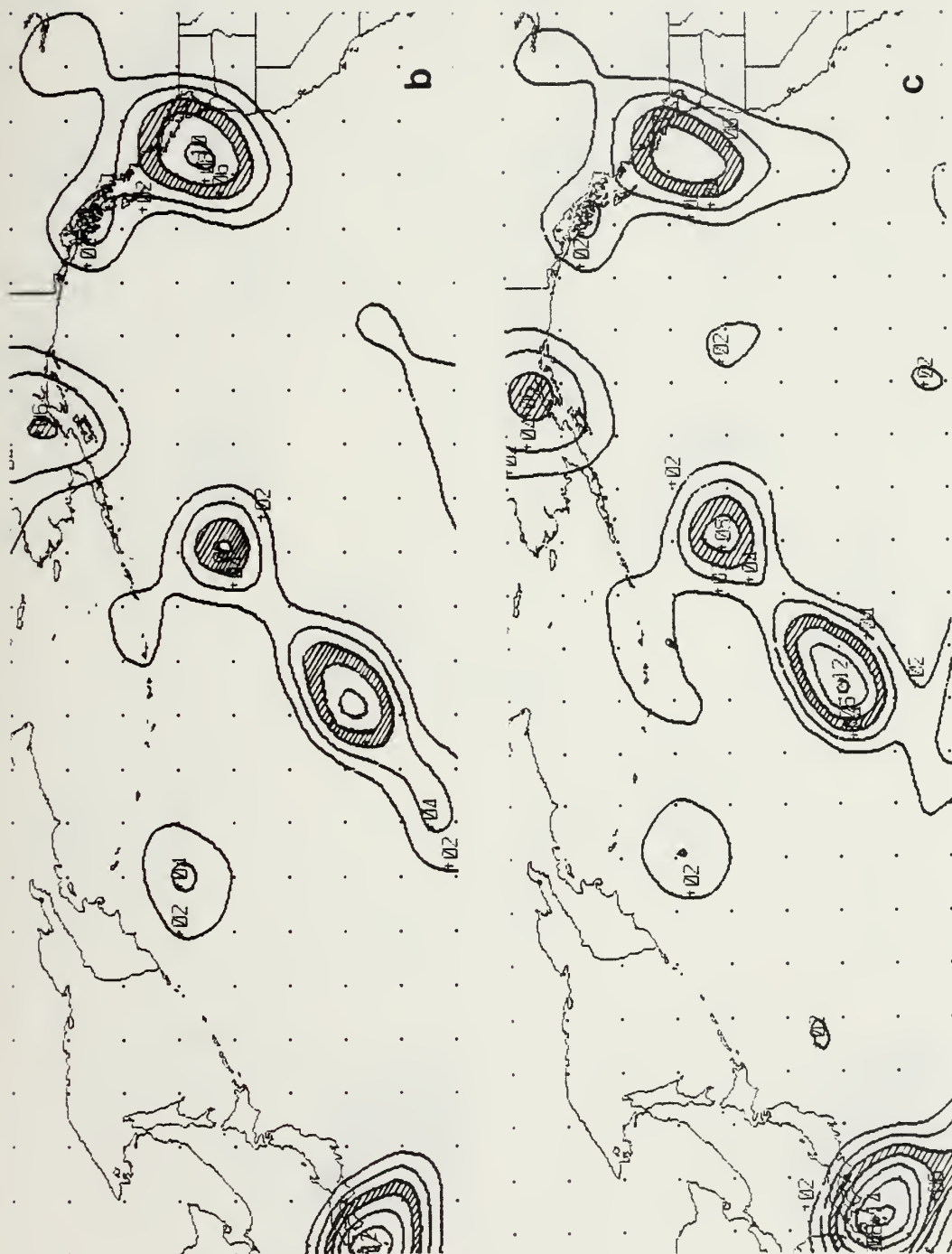


Fig. 25. Continued.



Fig. 25. Continued.

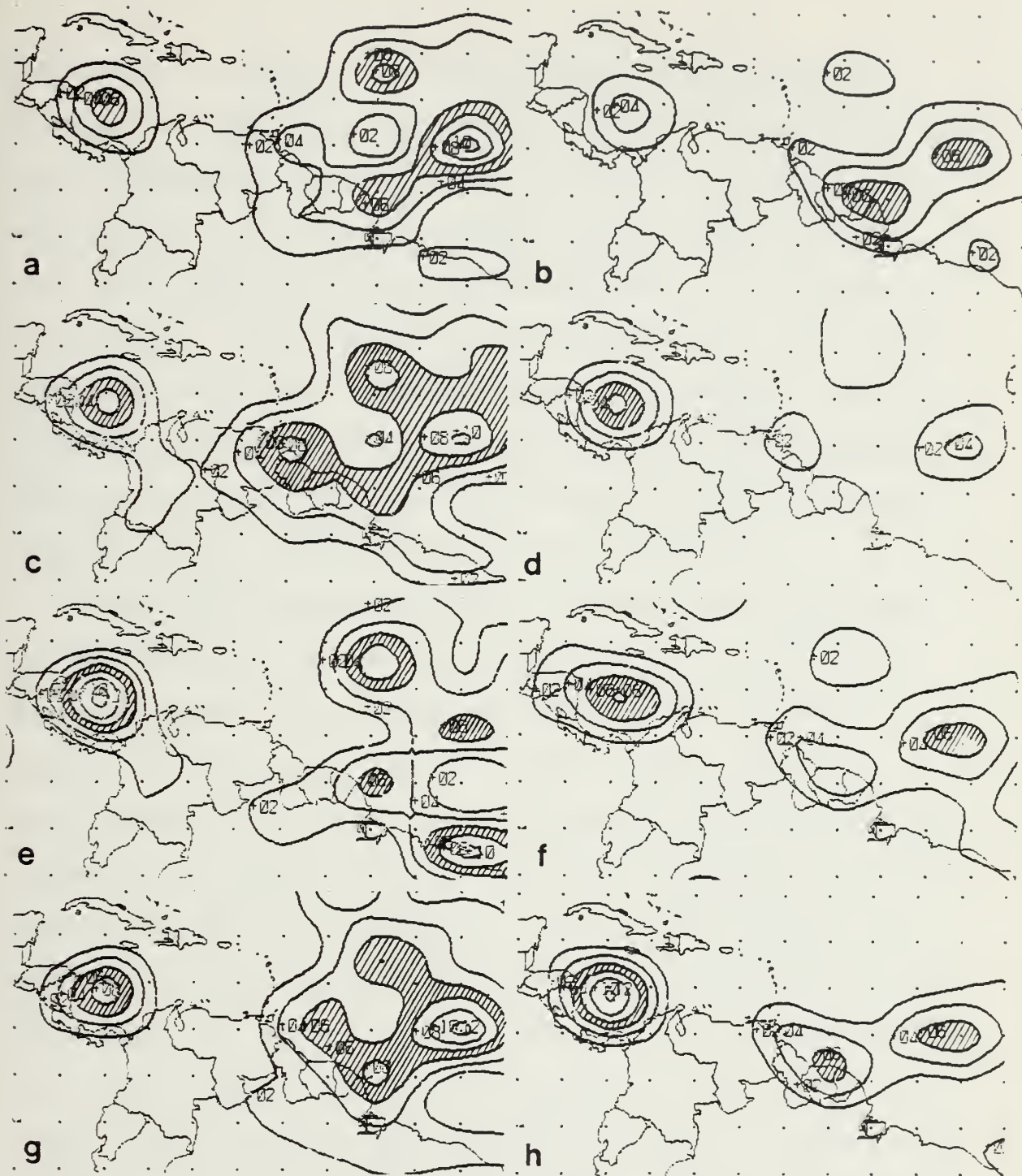


Fig. 26. Precipitation rate during the first six hours from forecasts initialized with BE1 (a), BE2 (c), NM1 (e) and NM2 (g), and precipitation rate during the second six hours for BE1 (b), BE2 (d), NM1 (f) and NM2 (h). The contour interval and cross-hatching are as in Fig. 25. The starting time is 00 GMT 11 Nov 1979.

precipitation extended over much larger regions and was stronger than during the second six hours. This tendency is just the opposite effect observed in the nondivergent case, and helps to explain why the model produces more gravity wave noise when the latent heating effects are included in the forecast. The precipitation patterns appear to be less similar between the forecasts during the second six hours than during the first six. In fact, after several update cycles, the precipitation fields produced by the different methods contain little similarity in the tropics.

Slight differences due to the various initialization methods may cause the assimilation runs to diverge slowly from each other. The largest differences are likely to occur in regions of strong baroclinic instability where precipitation can play a role. To examine this possibility, a moderately intense surface low, which developed along the Aleutian Islands, was studied. This case of surface cyclogenesis of 20 mb in 24 hours was supported by an upper level short wave that traveled along the island chain in twenty-four hours. Three twelve-hour forecasts are shown for the various initialization methods tested (Figs. 27 through 34). Comparing forecasts rather than analyses helps to eliminate the possibility that gravity modes allow a closer fit to the data than actually exists by the meteorological modes. As can be seen from the verifying analyses (Fig. 35), none of

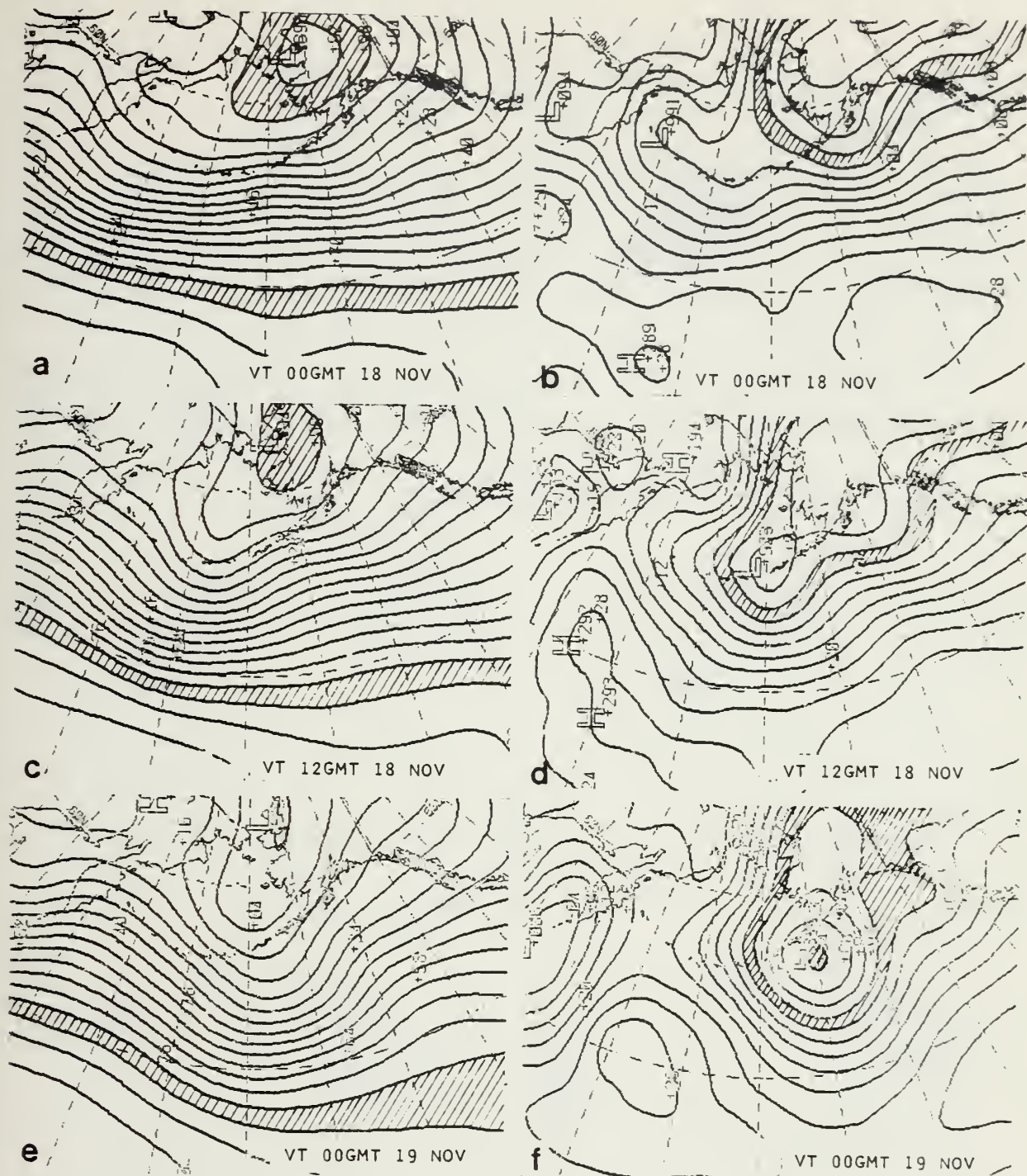


Fig. 27. Twelve hour forecasts of 500 mb geopotential (a, c, e) and sea-level pressure (b, d, f) during the assimilation run using the BE1 initialization method. Contour interval for geopotential is 60 m and for sea-level pressure is 4 mb. The 4920 to 4980 m interval is cross-hatched in the 500 mb maps. The 996 to 1000 mb and 980-984 mb intervals are cross-hatched in the sea-level pressure maps.

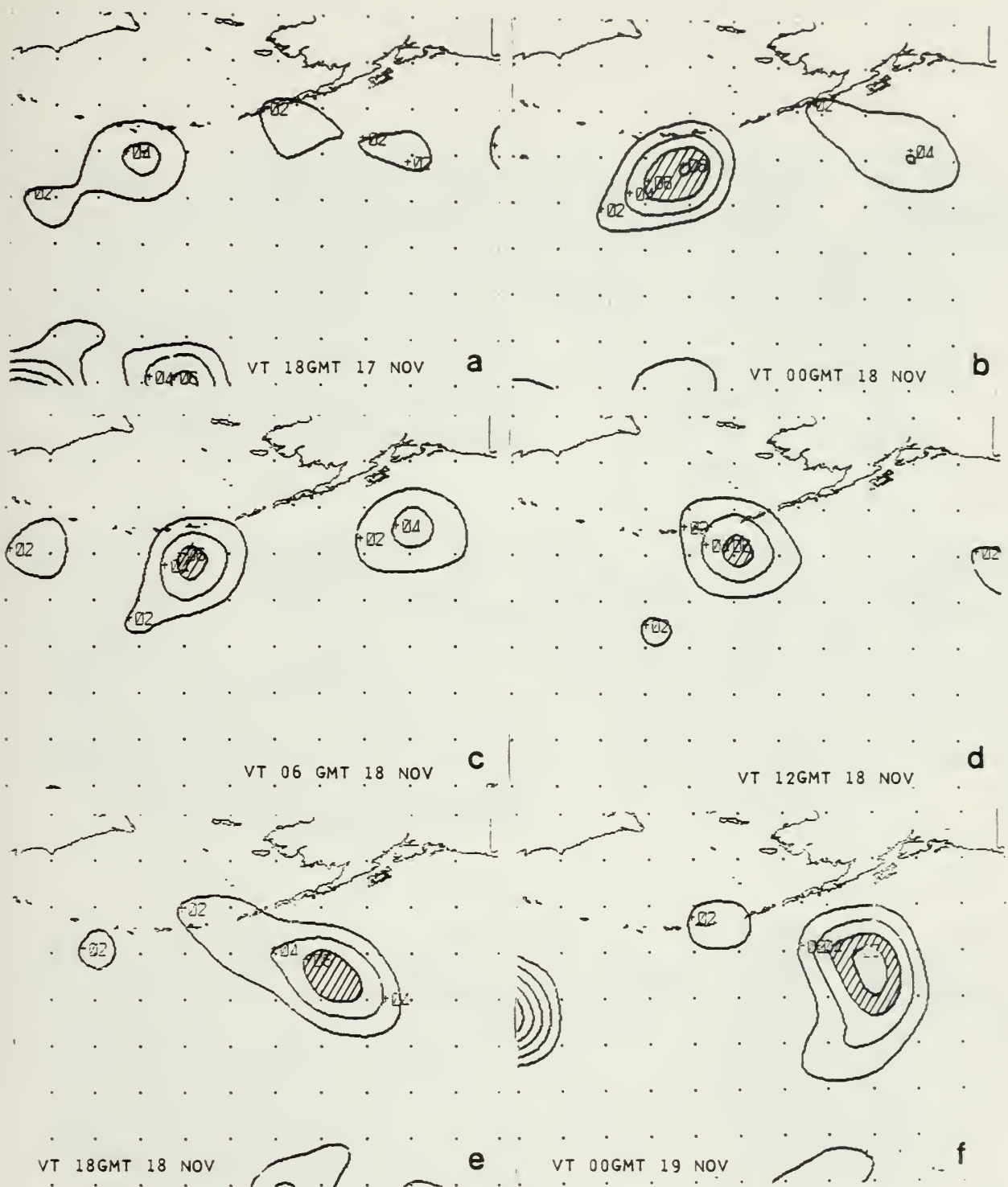


Fig. 28. Precipitation rate during the first six hours (a, c, e) and second six hours (b, d, f) of the forecasts from the BE1 initialization. Contour interval is 2 cm hr⁻¹ and the contour interval between 2 and 4 cm hr⁻¹ is cross-hatched.

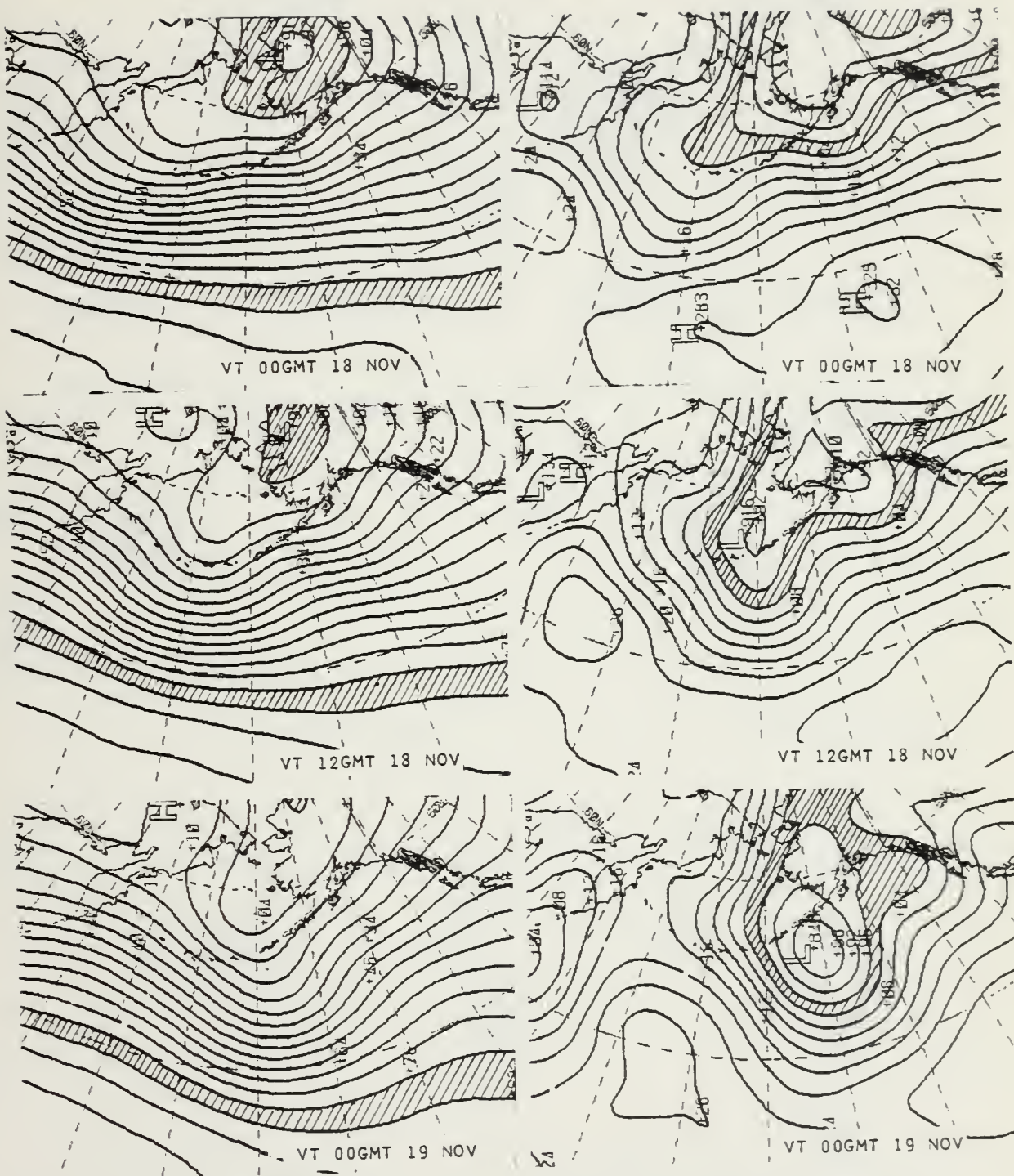


Fig. 29. Similar to Fig. 27 except for the BE2 method.

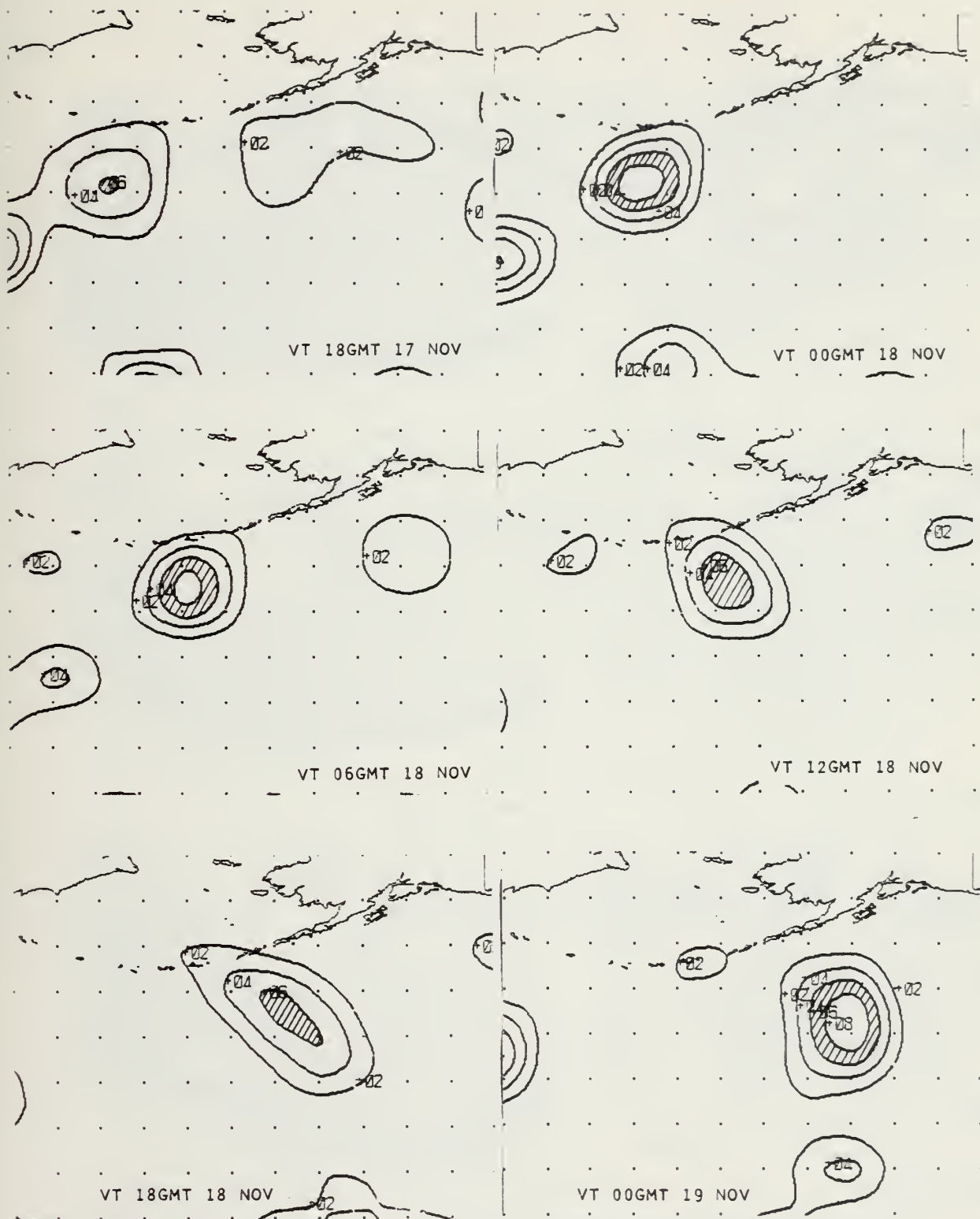


Fig. 30. Similar to Fig. 28 except for the BE2 method.

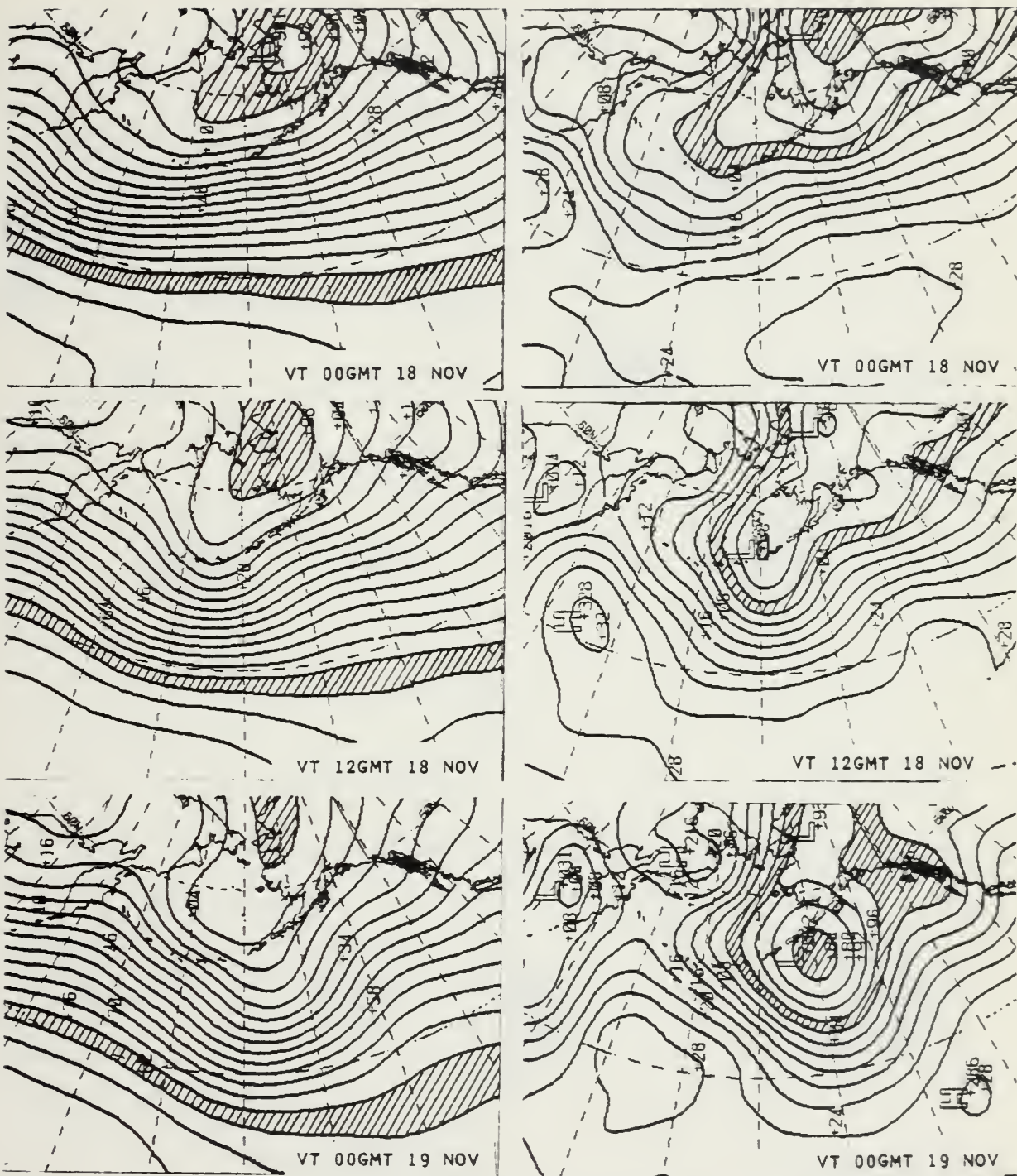


Fig. 31. Similar to Fig. 27 except for the NM1 method.

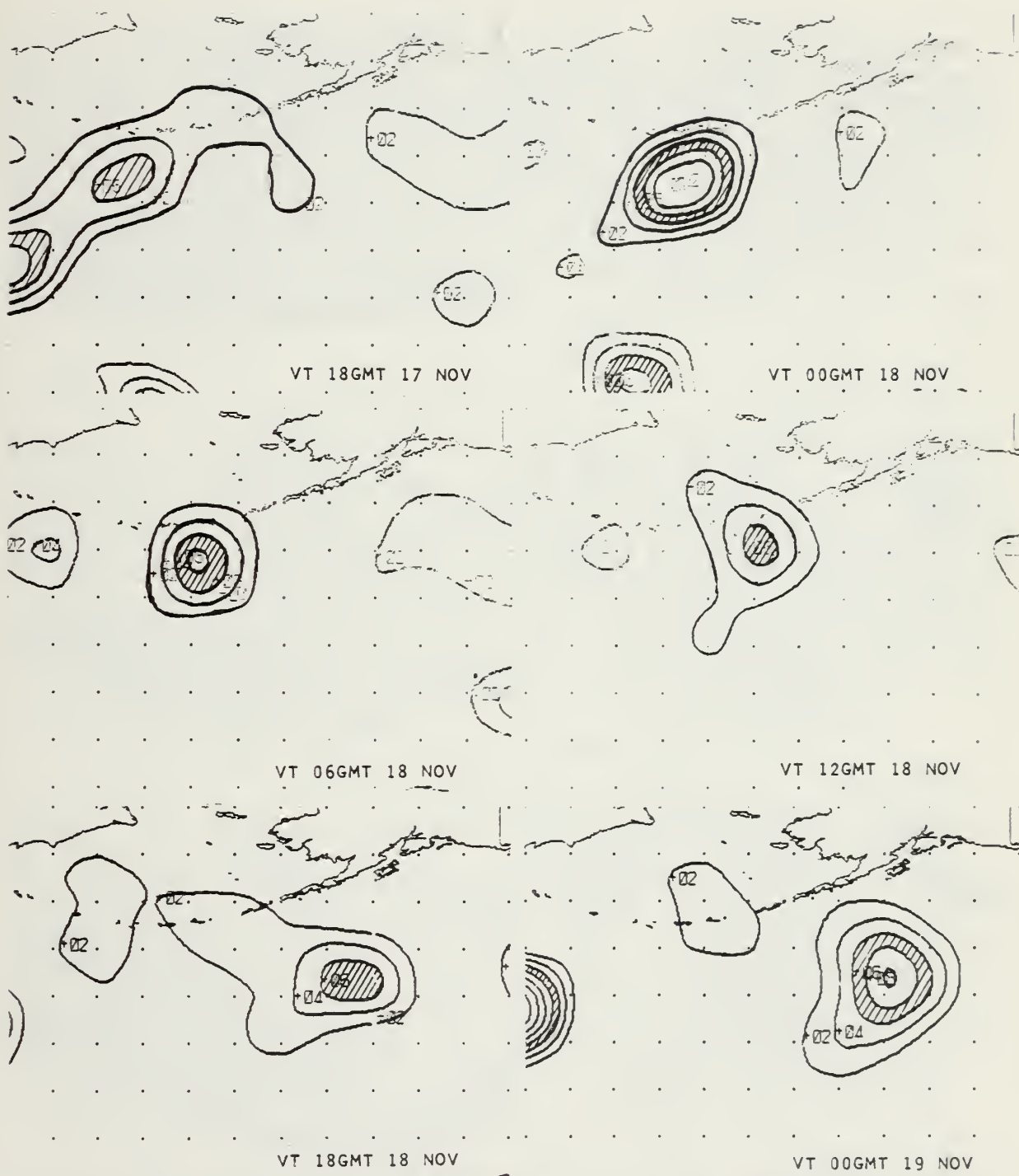


Fig. 32. Similar to Fig. 28 except for the NM1 method.

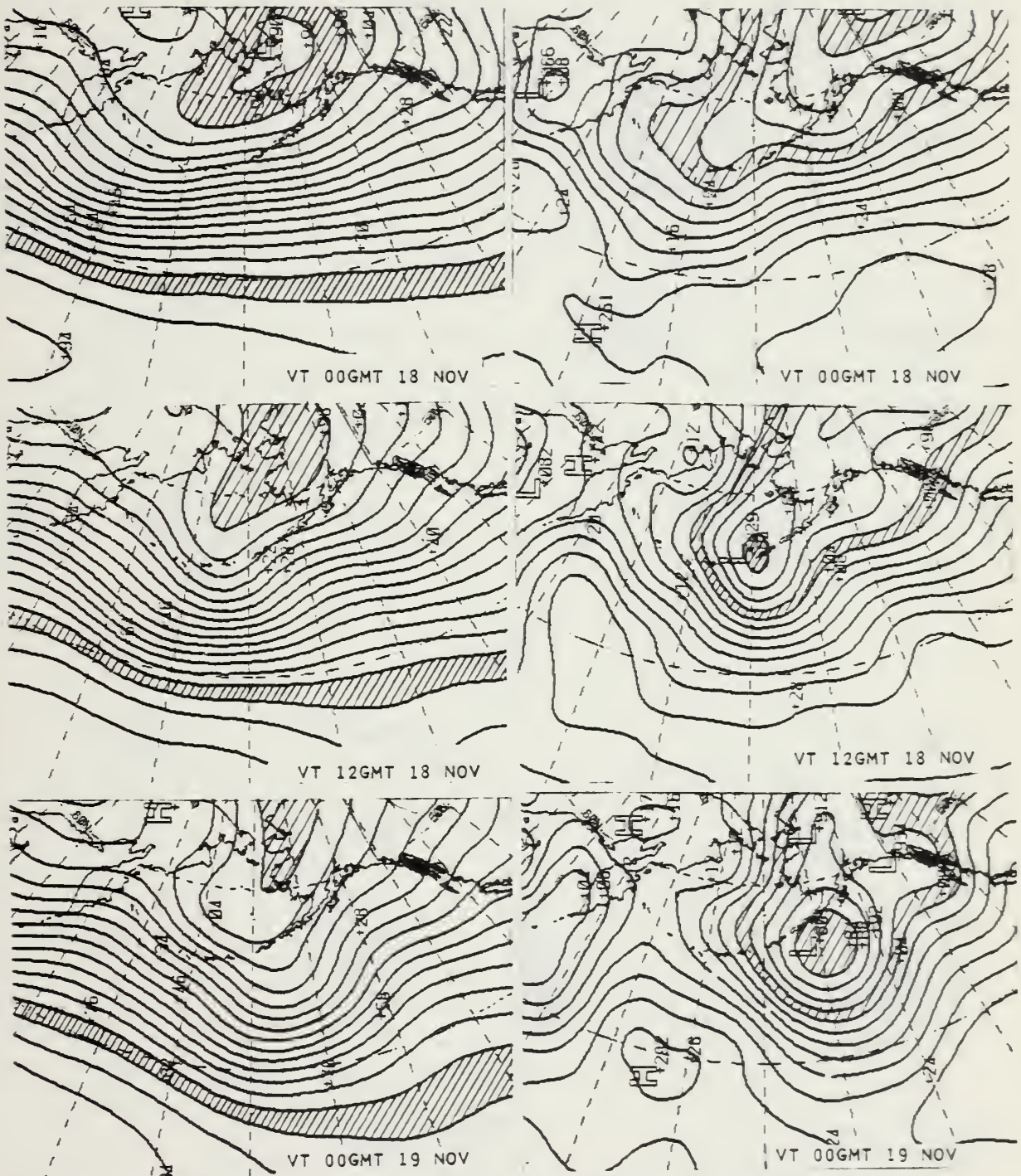


Fig. 33. Similar to Fig. 27 except for the NM2 method.

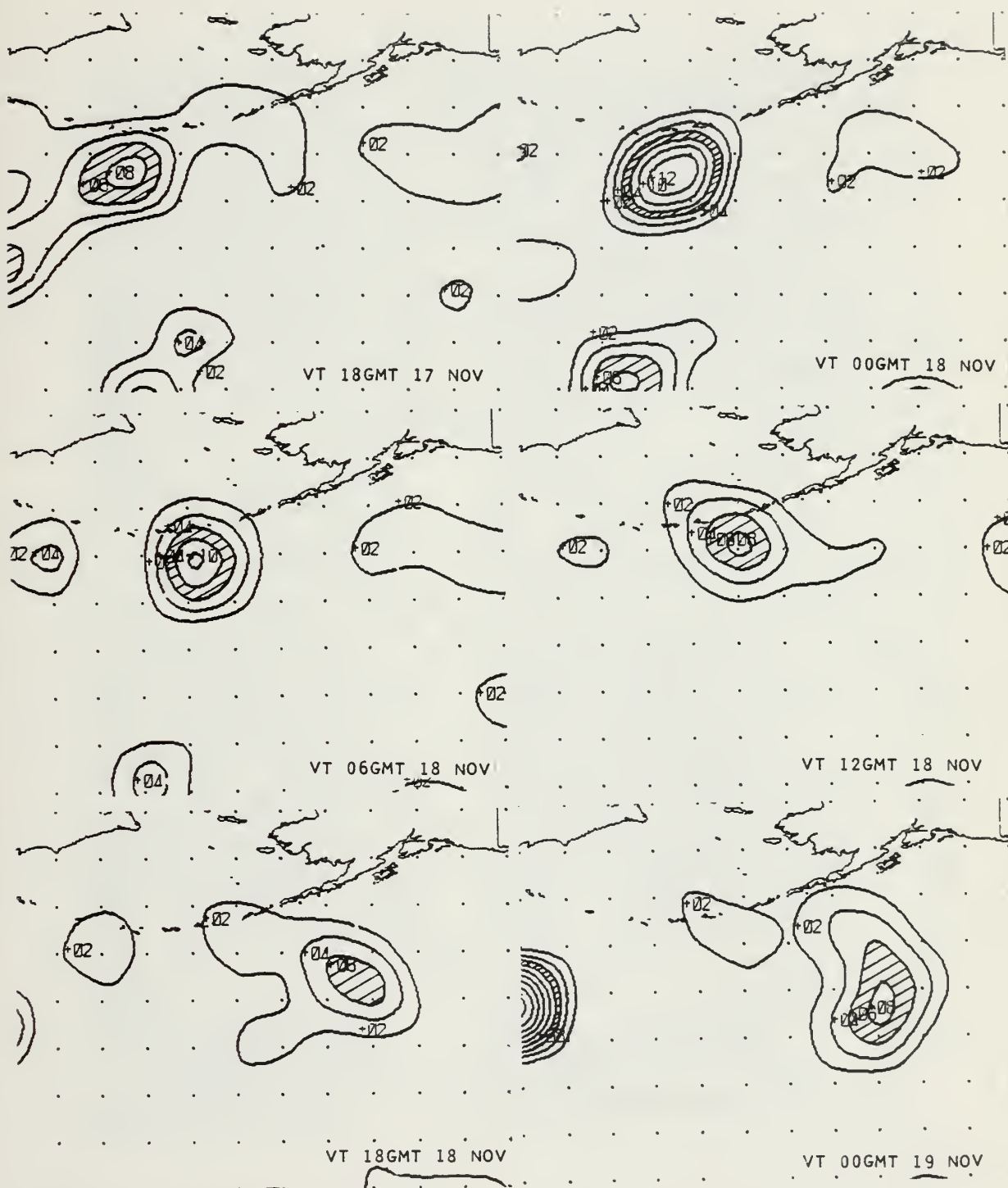


Fig. 34. Similar to Fig. 28 except for the NM2 method.

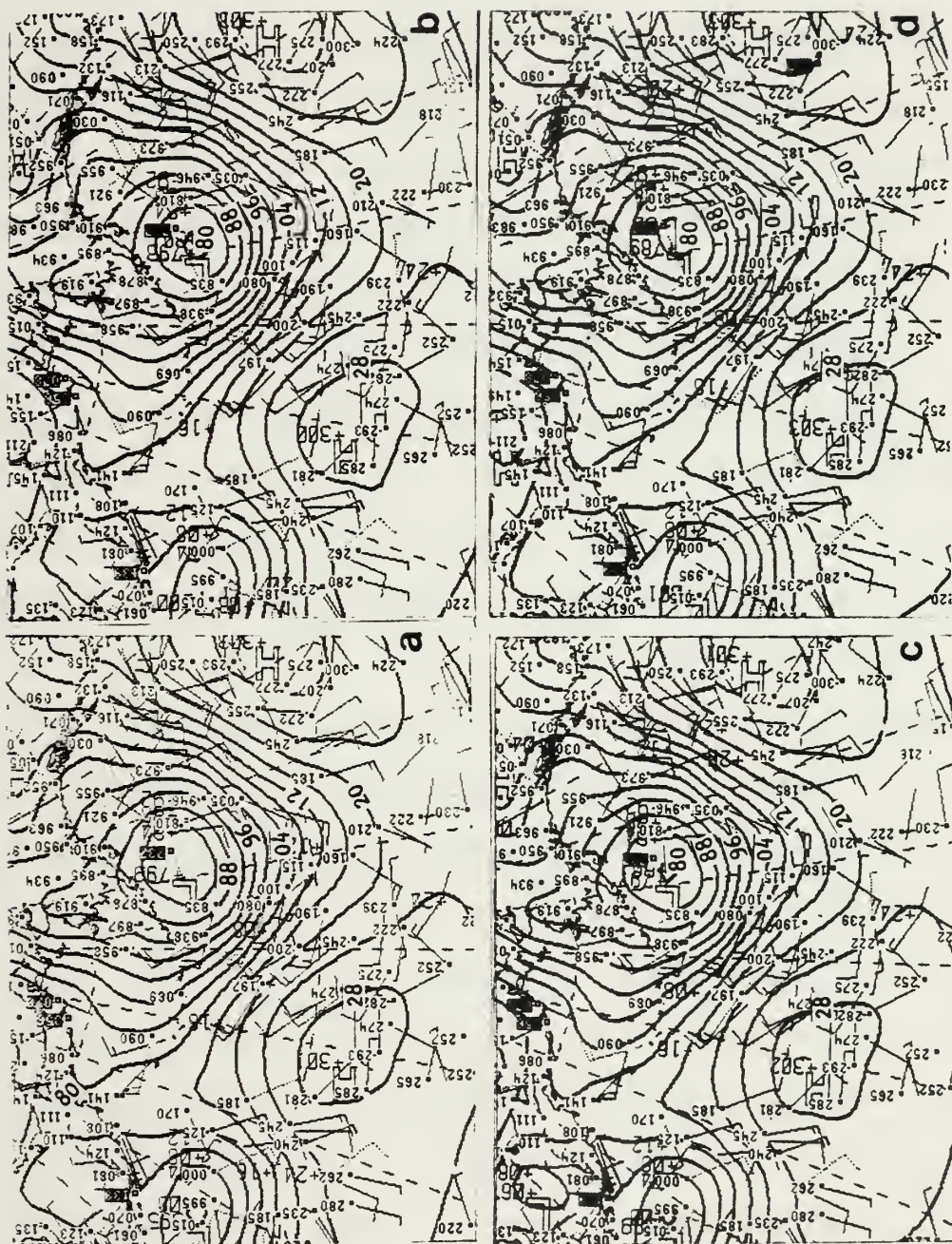


Fig. 35. Sea-level pressure analysis for 19 Nov 00 GMT produced by the BE1 (a), BE2 (b), NM1 (c) and NM2 (d) assimilation runs.

the forecasts developed the system as rapidly as the atmosphere. However, the normal mode method came closest by developing slightly deeper systems each time. The NM2 method managed to do slightly better than the NM1 method. The weakest system was produced by the BE2 method, but it was only 4 mb too weak. The normal mode methods generated the largest precipitation amounts. This is particularly true during the 6 to 12 hour forecast made from the 17 November 1979 12 GMT data. During most of the period, however, the precipitation differences were quite small.

In general, forecast experiments that used divergence in the initial conditions produced precipitation rates in the early hours of the forecast that were larger than those produced after six hours. This is the opposite effect observed in forecasts using a nondivergent initialization. Whether the divergence was computed from the normal mode method or derived from the forecast first-guess seemed to make little difference in the resulting precipitation and divergence. During data assimilation experiments lasting several days, however, these differences between the methods became more pronounced. A study of cyclogenesis over the North Pacific showed that while the normal mode methods tended to deepen the system faster and somewhat more accurately, the balance equation methods were nearly as effective.

Unfortunately, these results which describe a single case are hardly conclusive. To extend the verification of the different initialization methods over broader areas and more cases, comparisons of many forecasts to observations are made in the next section.

E. FORECAST VERIFICATION

Justification for balancing during data assimilation runs is readily demonstrated with the verification comparison of a balanced and unbalanced forecast. Forecast verifications against all observations for these runs are plotted versus latitude in Fig. 36 for geopotential and winds. The results indicate that although the wind verification is unaffected by the presence of gravity wave noise, the geopotential verification is drastically affected. This forecast from an unbalanced initial state has RMS errors almost double that of the balanced forecast over much of the earth. Such large errors in a forecast first guess may cause the quality control programs to reject observations that should not be rejected and to add noise to the resulting analysis. (Heavy damping filters applied during integration may make the forecasts more usable, however.)

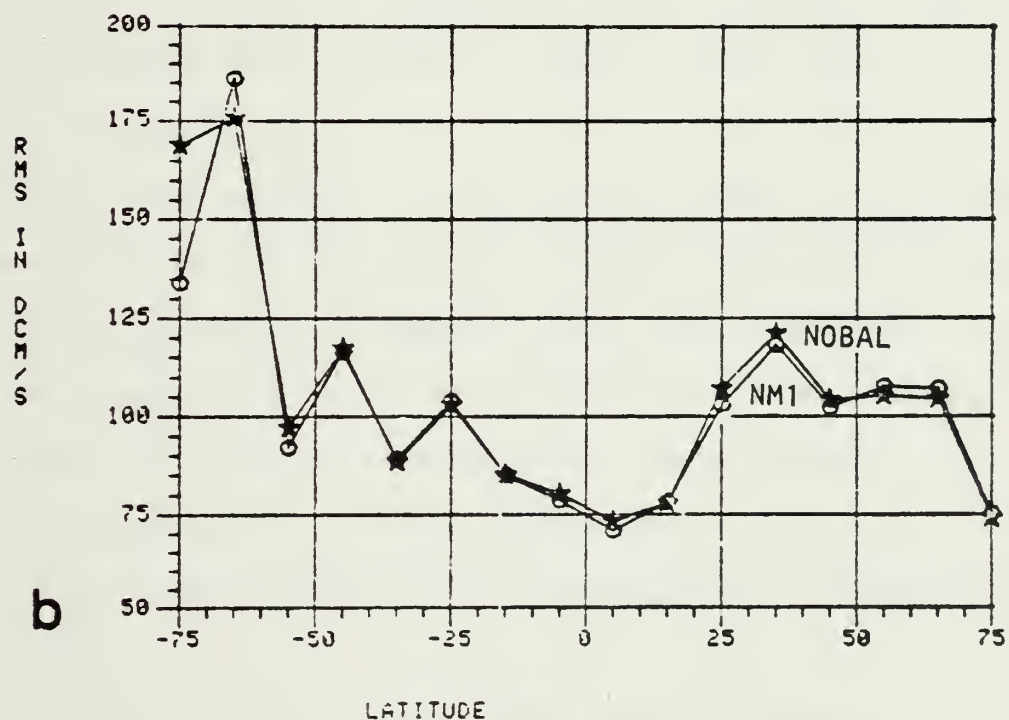
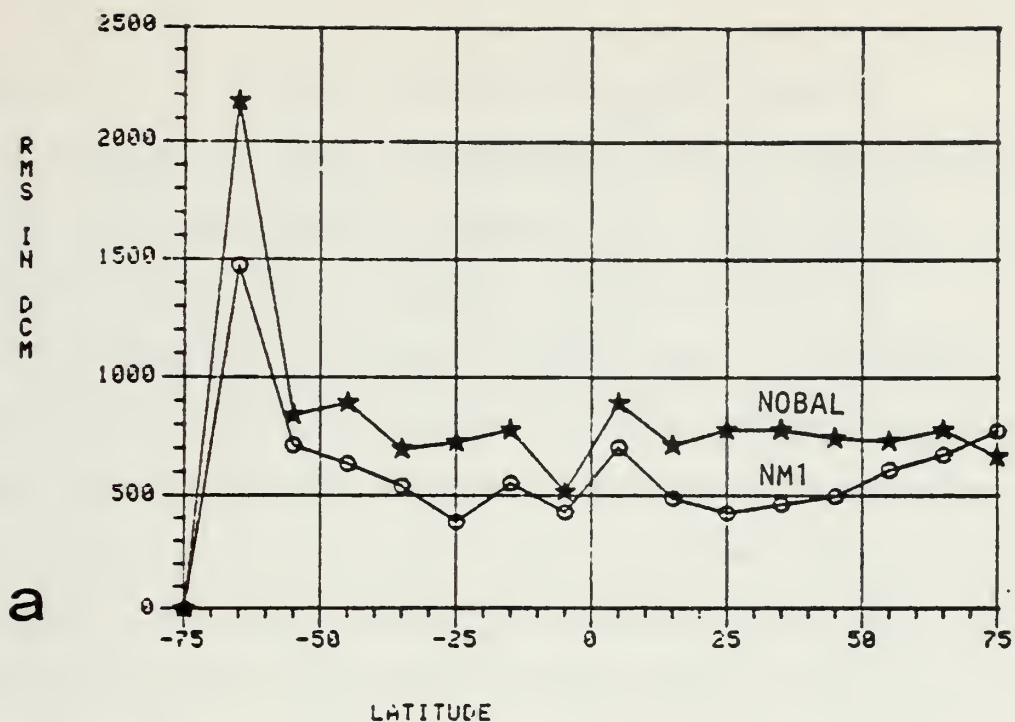


Fig. 36. Latitudinal variation of RMS (a) pressure height and (b) wind differences between observations and 12-hr forecasts without balance (stars) and with NM1 initialization (circles).

While it is certain that the forecasts from an unbalanced initial state are unsuitable as a first guess for an analysis of geopotential observations, and therefore are not useful in data assimilation, the most effective balancing procedure to be used is not clear. Some small differences do exist between the assimilation results using different initialization methods. This can be seen (Fig. 37) in the analysis of a short wave upstream of Australia. The 12-hour forecasts (rather than analyses) are shown for this system so that data resolved onto gravity waves could be dispersed by the model. The normal mode methods (NM1 and NM2) produced a slightly deeper wave than did the balance equation methods (BE1 and BE2). This is consistent with the results in Chapter V.C.

An extensive objective verification study was performed for the different methods, where the RMS differences between the 12-hour forecasts and observations were computed. These computations were made for ten forecasts covering the period of the data assimilation experiments. Unfortunately, this type of test may tend to favor the smoother forecasts, and therefore the interpretation of results should be made with this in mind.

Although verification was performed by region as well as globally, the regional verification added no new information not readily apparent in the global statistics. The

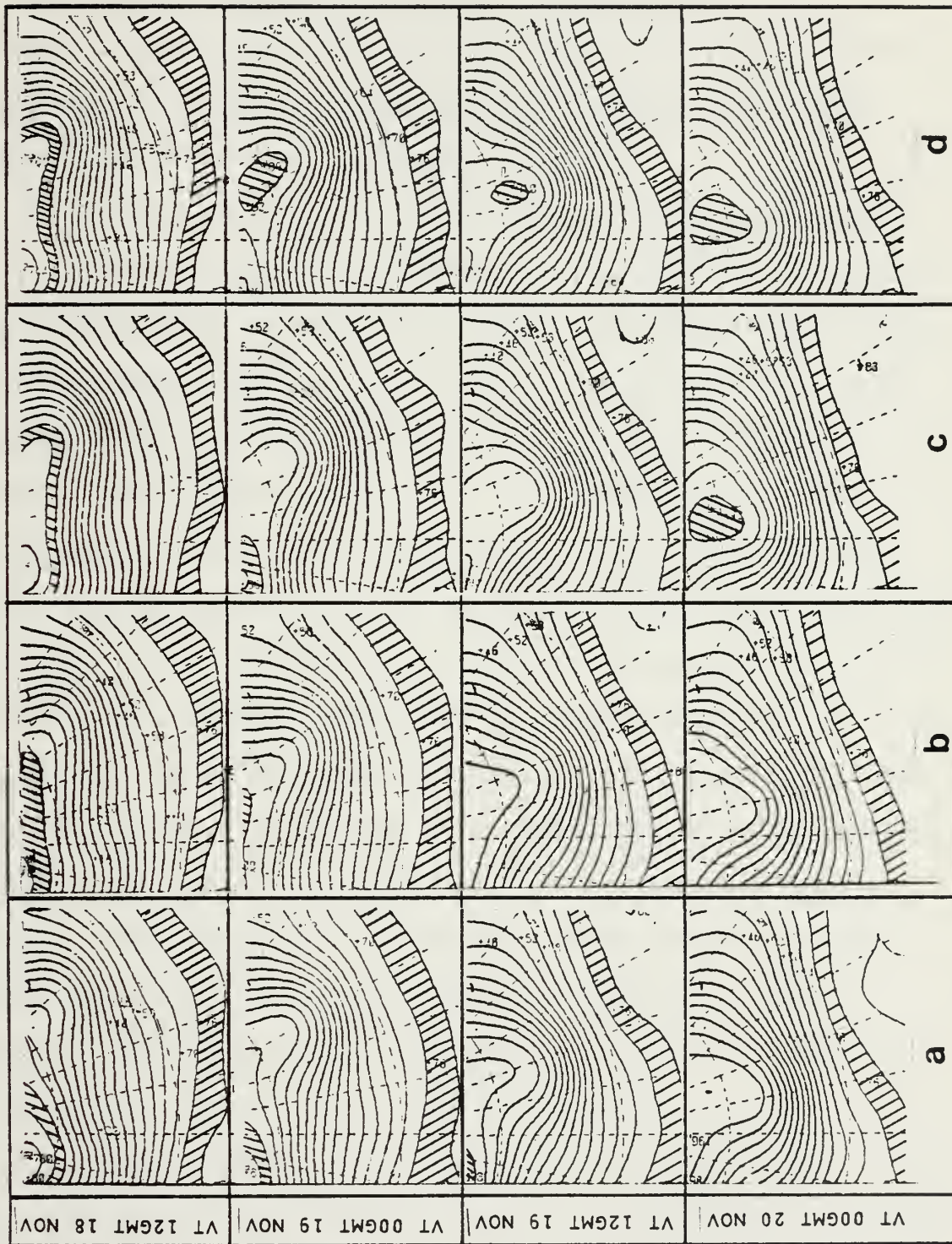


Fig. 37. Sequence of 12-hr forecasts of 500 mb height from assimilation runs using BE1 (a), BE2 (b), NM1 (c) and NM2 (d) initialization methods. The contour intervals 4860-4920 m and 5760-5820 m are cross-hatched.

verification is presented by observation type, which tends to regionalize the verification to some extent. For example, observations from ships, satellites and aircraft are primarily taken over the oceans, whereas radiosonde observations are mostly taken over land.

Forecast verification against radiosonde geopotential and wind observations are presented in Figs. 38 and 39 for the four methods of initialization. The lowest RMS differences between forecasts and observations occurred in the balance equation method, BE2. However, the differences between methods are very small. For geopotential, the differences produced by the various methods are generally less than 2m, which is only about 4% of the total RMS error. For wind, this difference is generally less than 3 m sec⁻¹, which also represents about 4% of the total error. Comparing the normal mode methods, it can be seen that NM1 verified against geopotential observations slightly better, whereas NM2 verified against wind observations slightly better. This reflects the emphasis that the variational balancing placed on the respective variables. However, notice that BE1 verified geopotential as well as the NM1 method and wind as well as the NM2 method.

Forecast verifications against ship observations of sea level pressure, which were converted to geopotential through the hydrostatic equation, are given in Fig. 40. The

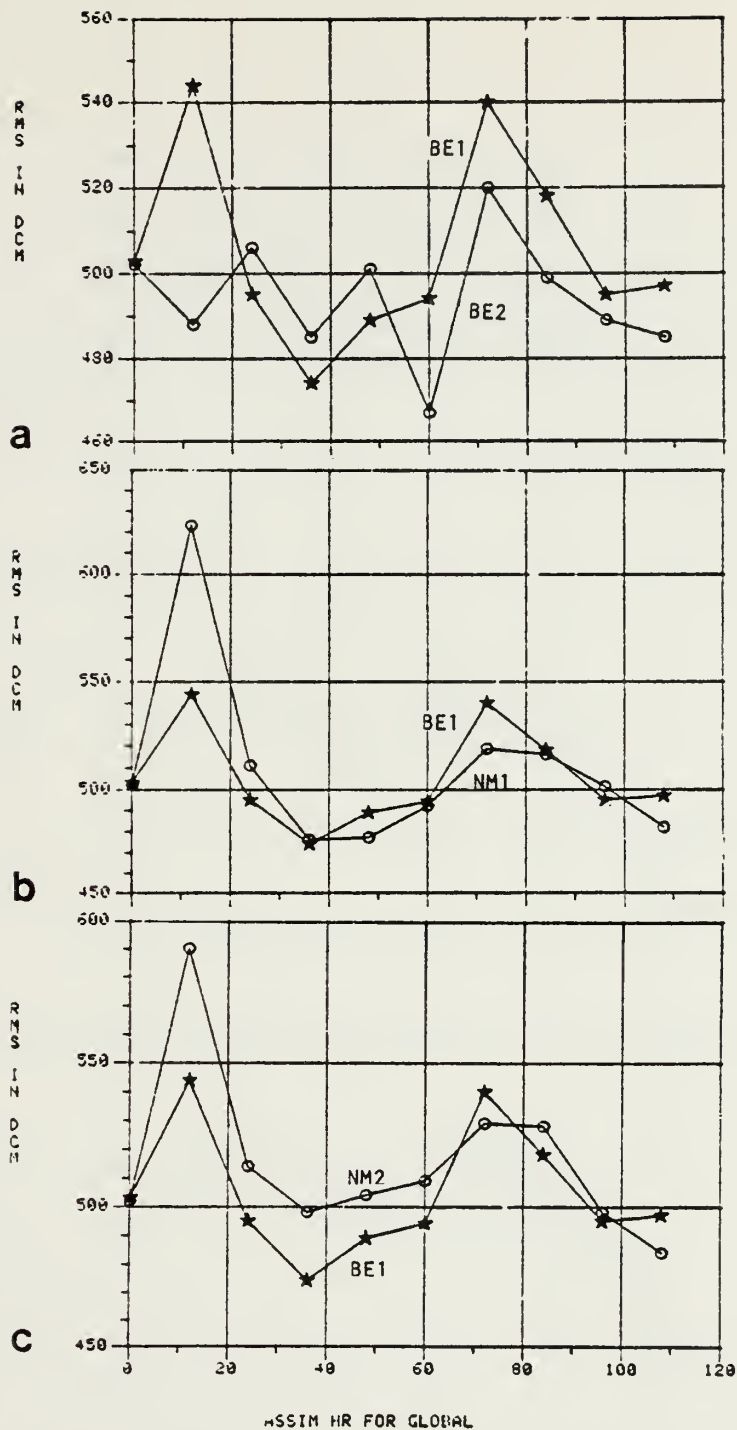


Fig. 38. RMS differences between radiosonde observations of pressure height and 12-hr forecasts for the assimilation runs comparing BE2 (a), NM1 (b) and NM2 (c) with BE1 initialization methods. Each data point represents the error in the assimilation model just prior to the update. Abscissa labels are hours after start of the assimilation run.

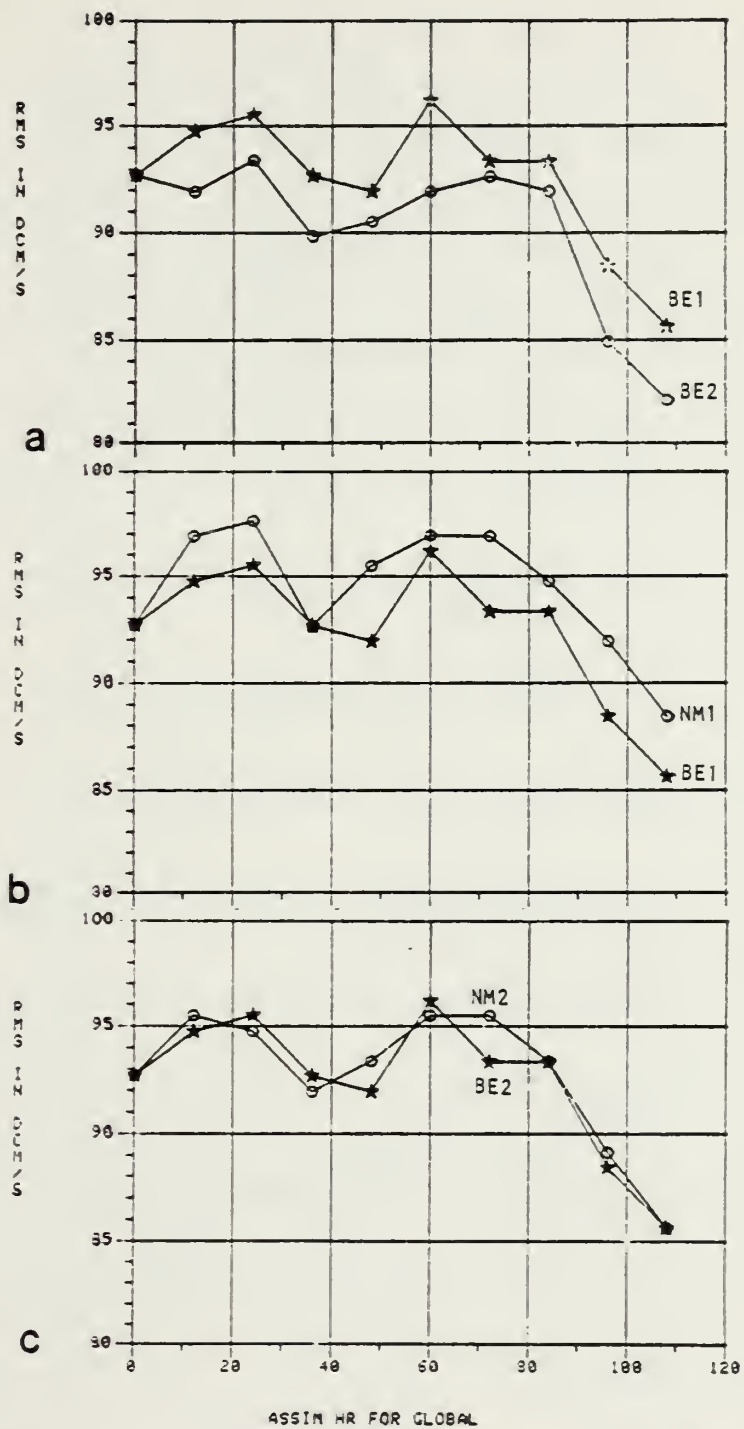


Fig. 39. Similar to Fig. 38 except for radiosonde wind observations.

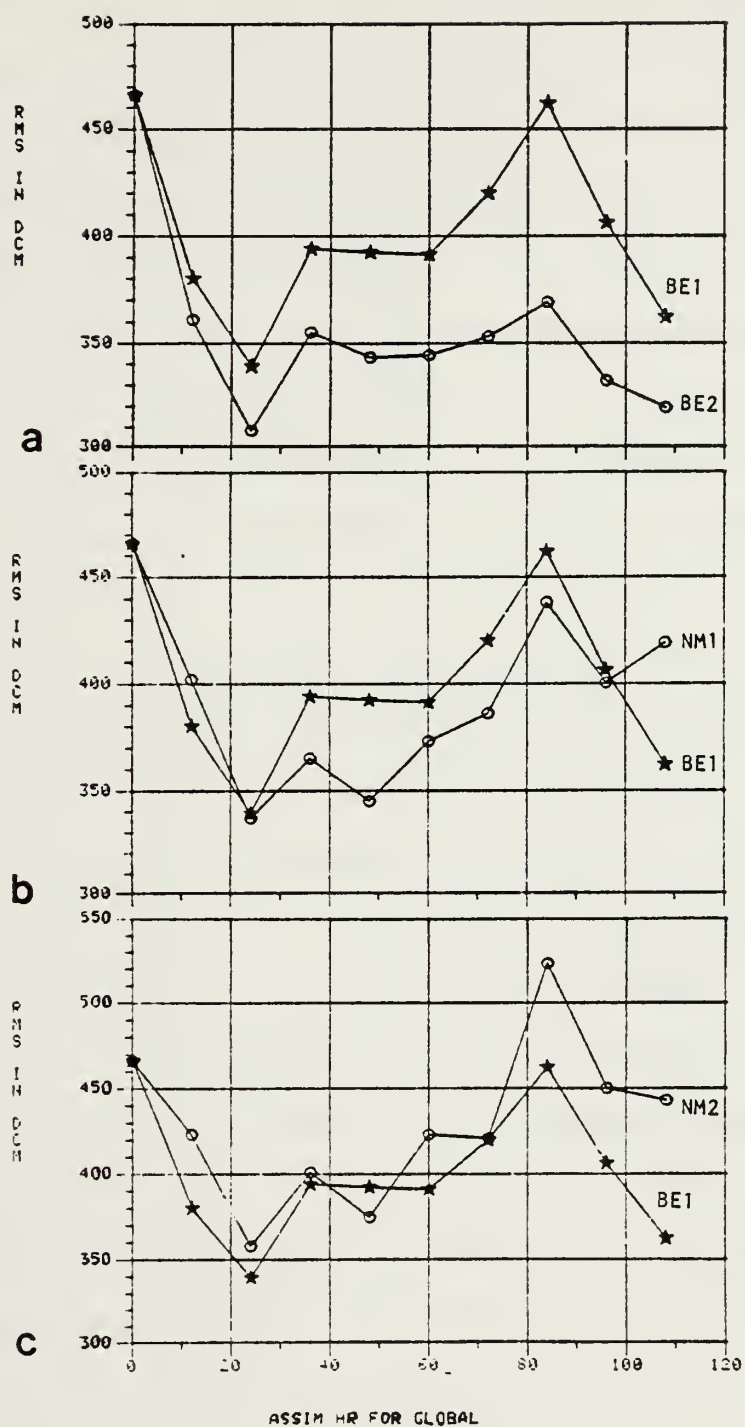


Fig. 40. Similar to Fig. 38 except for surface ship observations converted to geopotential height.

improvement of the BE2 method over the other methods is much more significant for this data. Compared to BE1, the improvement is as high as 10% of the total RMS error. The NM1 method, which weighted the geopotential analysis more than the NM2 method, verified somewhere between BE2 and BE1, whereas NM2 produced approximately the same results as BE1.

Verification using satellite-generated geopotentials (Fig. 41) again show the BE2 method to be superior to the other methods. The improvement ranges between 6 and 12%. The other initialization methods resulted in rather similar verifications.

Satellite wind forecast verification (Fig. 42) shows that the BE2 method gave about 0.5 m sec^{-1} smaller forecast error, or about a 5% improvement over the other methods. This verification is based mainly on the low level (925 mb) satellite observations in the tropics. Once again, the other verifications are similar to each other.

Unlike the other types of data, aircraft wind forecast verification failed to show much difference between the methods (see Fig. 43). Since aircraft observations are primarily taken between 300 and 250 mb, this suggests that the four methods produced comparable results at the upper levels over the oceans.

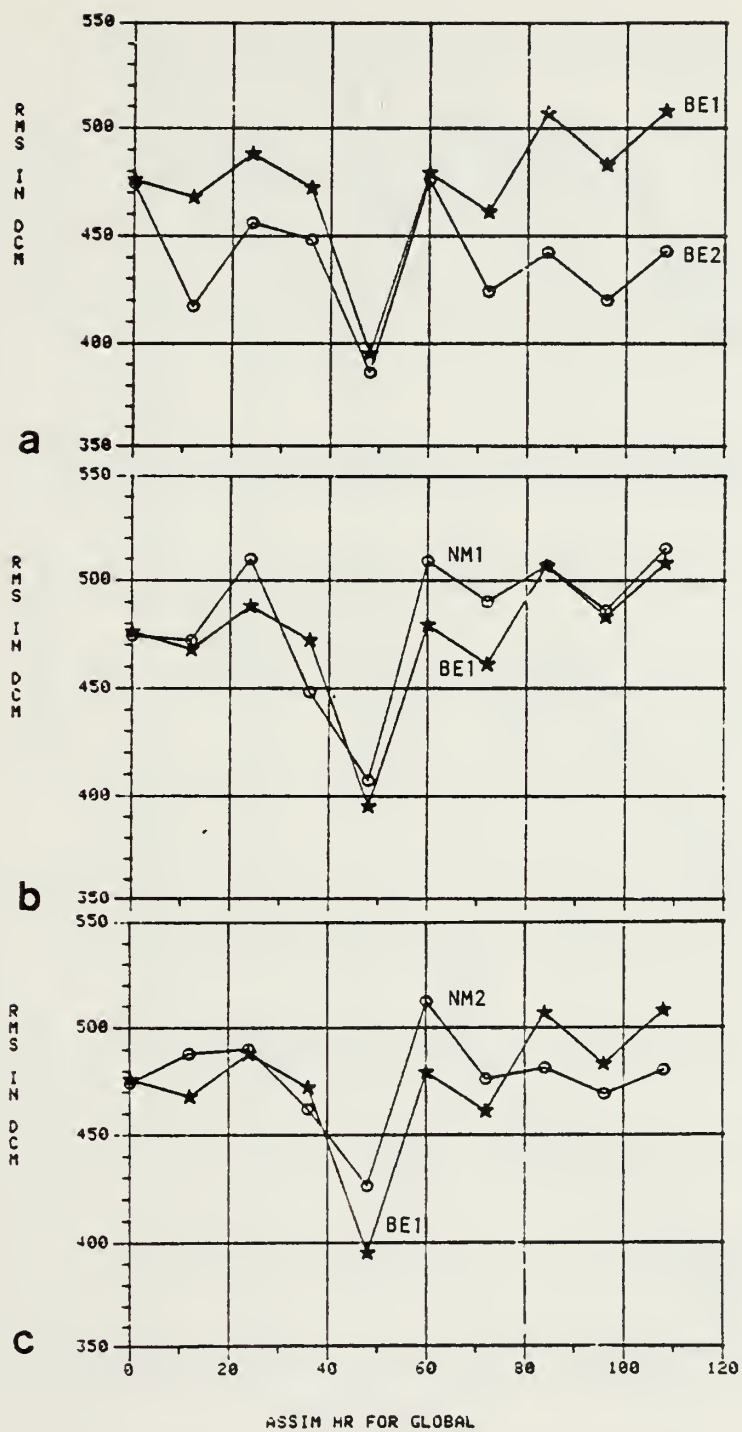


Fig. 41. Similar to Fig. 38 except for satellite derived geopotentials

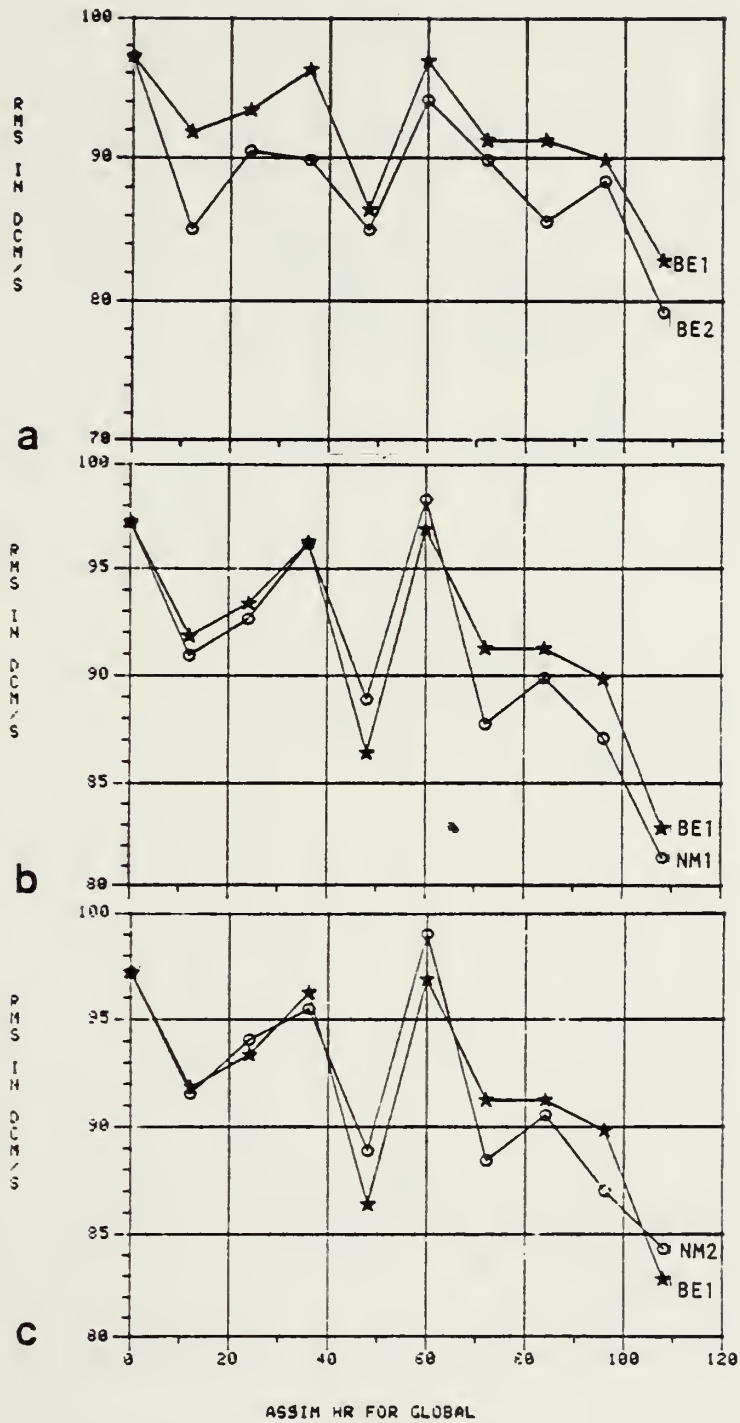


Fig. 42. Similar to Fig. 38 except for satellite wind observations.

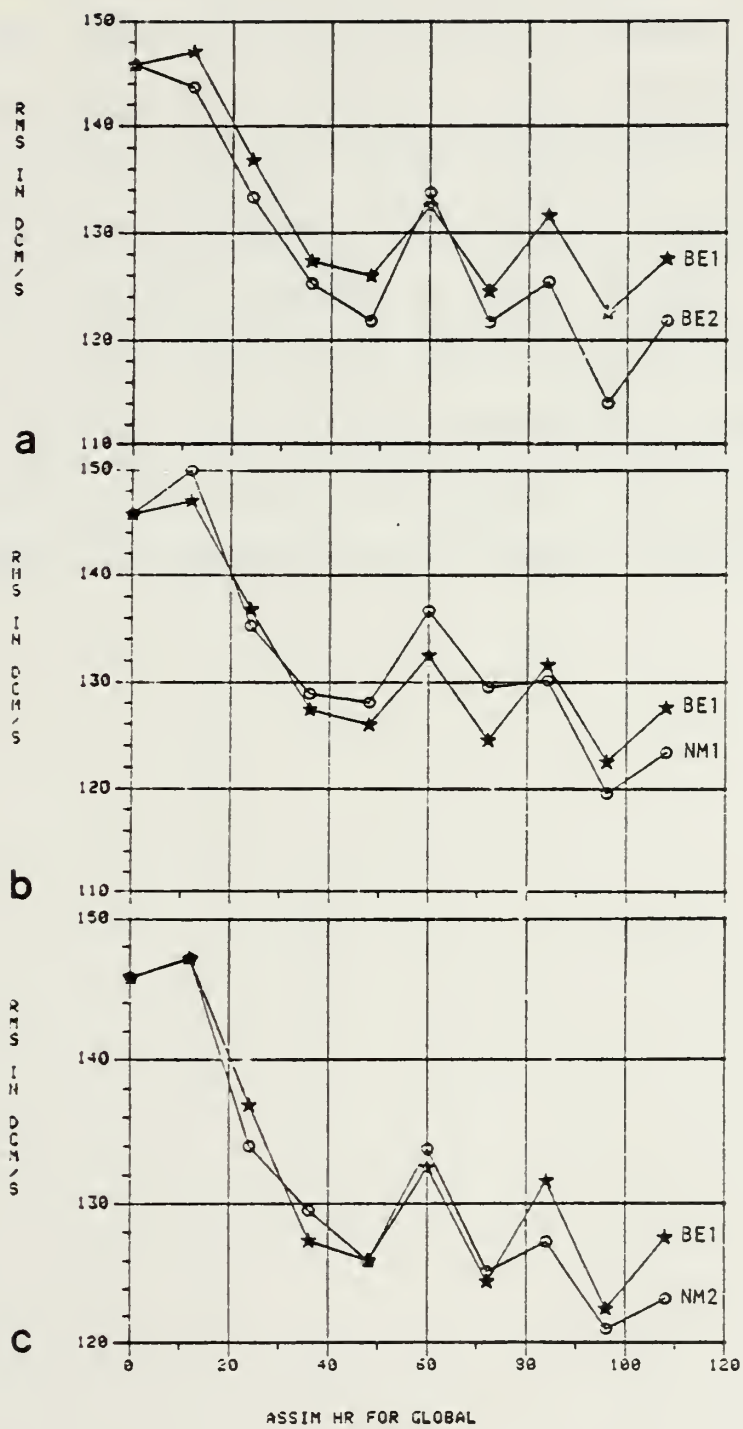


Fig. 43. Similar to Fig. 38 except for aircraft wind observations

In summary, the BE2 method, which uses the balance equation to variationally balance the complete analysis (forecast first guess plus corrections), produced the best verification scores. This result is most pronounced at the low levels over the oceans. Visual inspection of the forecasts produced by this method indicate that they were also smoother than forecasts produced by other methods. While RMS scores tend to be better for smooth fields, the much better verifications against ship observations produced by the BE2 method are difficult to dispute. The differences among the remaining methods are too small to conclude which is best.

VI. SUMMARY AND CONCLUSIONS

In this study, two different static initialization methods have been developed and tested in data assimilation experiments. These methods not only reduce gravity wave noise, but they also fit the meteorological modes to the most accurately analyzed variables through calculus of variations. The methods are based on the balance equation and a nonlinear normal mode procedure. Of the two methods, the normal mode method would be the more cumbersome to apply, because the most general form with the weighting fully variable in the horizontal requires more computer memory than was available.

The two methods were compared in various ways. The comparison tests were designed to show how the analyzed fields were modified during the balancing, how each controlled gravity wave noise, how precipitation varied during the early hours of the forecast, how the forecast of a rapidly developing system was affected, and finally, how short range forecasts from the various methods verified against observations.

Both methods modified the analyzed fields during the balance by a large amount when compared to the size of the corrections (differences between analysis and forecast first guess). Surface pressure modifications were particularly

large, sometimes exceeding the magnitude of the corrections. Modifications to the winds were primarily caused by unrealistic divergence patterns in the analyzed winds, which were nearly as large as the analyzed corrections. When the divergence was removed prior to balancing, the modifications were much smaller. For wind and surface pressure, the magnitude of the adjustments was very nearly the same for the two methods. However, the modifications to the temperature analysis were larger for the balance equation method when it was used to balance the total analysis (corrections plus first guess) than when it was used to balance just the corrections.

In terms of gravity wave noise removal, the normal mode methods performed significantly better in a dry version of the prediction model than did the balance equation method. Adding the effects of latent heating, however, tended to mask this improvement, because the heating effects caused gravity wave noise to more than double relative to the dry version of the model.

The increased gravity noise due to the heating may be caused by many factors. It is partly caused by the way in which the heating effects are included. Each fifth time step, the heating effects are added. A Matsuno time step is then used prior to resuming the leapfrog time stepping. The gravity wave amplitudes produced are larger than if the

heating effects are added incrementally over each time step. Another factor that may make the latent heating effects more pronounced is that the model tends to be warmer and drier in the lower layers than observed in the atmosphere (Johnson, 1976; Payne, 1981). After each update, the solution tends toward the model equilibrium state. Also, because no analysis is made of moisture, changes in the mass and motion structure may require that the model undergo some adjustment before latent heating matches the updated systems. None of these effects are controllable by the initialization procedures under study, however.

Integrations performed without divergence (vertical motion) required several hours to develop realistic precipitation rates. This was particularly true in the tropical regions in a test with the balance equation initialization that did not include divergence from the forecast first-guess.

Comparisons of divergence from the forecast first-guess and that computed using the nonlinear normal mode balance applied to the external and first internal vertical modes revealed only small differences. Other comparisons of precipitation forecasts from the balance equation, normal mode and no balance conditions showed only minor differences. In the balance equation and no balance methods, the forecast first-guess divergence was present in the initial

conditions. The unbalanced forecast surprisingly produced no noticeable spurious precipitation forecasts, even when the unrealistic divergence produced during the wind analysis was included. Unlike the forecast initialized without divergence, however, largest precipitation rates were predicted during the first few hours of the forecast. It appears, then, that whether the forecast first-guess divergence is partially recomputed using the normal mode methods or even mixed in with unrealistic divergence, little difference will exist in the precipitation forecast.

The effectiveness of the model in assimilating data around a rapidly developing surface low over the Pacific was examined for the different initialization methods. The representation of the cyclone development was very similar for the various methods. The maximum central pressure difference between the methods was 4 mb. The more intense, and slightly more accurate representation of the low was produced by a normal mode method, whereas the least accurate was produced by the balance equation method that balanced the total analysis and used the forecast first-guess divergence. The results from this single example are only suggestive, however.

To produce results over a wider number of cases, the forecast first-guess fields were verified for the four data assimilation methods. Two methods used variations of the

balance equation method and two others used variations of the normal mode method. The results from these runs showed that while minor differences existed between the forecasts for much of the data, the balance equation method that balanced the total analysis, rather than the corrections, produced the most accurate short-range forecasts near the surface over the oceans. The forecasts produced from the normal mode methods tended to contain slightly stronger systems than the balance equation methods, which may have actually reduced all the verification scores for this method relative to the smoother fields from the balance equation method.

In conclusion, the results of this study show that it is possible to initialize a model with the forecast first-guess divergence. This allows continuity in the precipitation rates produced by the model during the updates. Consequently the variational balance equation method produced results that are competitive with, and in some respects, better than the more elegant nonlinear normal mode method. This conclusion is based on precipitation rates during the early hours of the forecast, gravity wave noise and short-term forecast results. In terms of variational weight assignment, the balance equation methods are less cumbersome, and thereby allow more flexibility.

As a note of caution, however, it should be mentioned that assimilation systems, such as the ones tested, are too complicated to guarantee absolutely that the tests were without flaws. For example, the balance equation method that scored the highest forecast verification scores was also the only method that used a slight variation of the interpolation to model coordinates. It interpolated updated mass variables instead of corrections. Interpolation of corrections did not insure that the sea level pressure under terrain matched observations corrected to sea level. Consequently, regions such as the Himalayas contained sea-level features that were not present at terrain level. Another factor is the type of assimilation-prediction that was used. The version of the UCLA model used in the assimilation produces much larger surface pressure tendencies than does a dry version of the same model. This factor, which masked the benefits of the normal mode initialization, may not be so prevalent in future generation models.

APPENDIX A

DATA ANALYSIS WITH SIMULTANEOUS FILTERING

The inherent smoothing of a successive correction scheme can be determined by neglecting discrete spacing of the observations and assuming isotropy in the weight specification (Barnes, 1973). Under these conditions,

$$F(r) = \int_{-\infty}^{\infty} \omega(\epsilon) f(r-\epsilon) d\epsilon. \quad (A1)$$

The convolution theorem allows us to take the Fourier transform of this equation or

$$\hat{F}(K) = \hat{\omega}(K) \hat{f}(K) \quad (A2)$$

where K is the wave number equal to $2\pi/\lambda$, and λ is wavelength. The hat is used to show that the variable is transformed into wave number space, e.g.,

$$\hat{\omega}(K) = \int_{-\infty}^{\infty} \omega(\epsilon) e^{iK\epsilon} d\epsilon \quad (A3)$$

Recall that \hat{F} is a complex quantity whose magnitude is represented by

$$|\hat{F}| = \sqrt{\hat{F} \hat{F}^*} \quad (A4)$$

or

$$|\hat{F}| = |\hat{\omega}| |\hat{f}|, \quad (A5)$$

which means that the spectral response of the analysis may be identified by $|\hat{\omega}(K)|$.

If the analysis is repeated to converge on the data more closely, the resulting product will be

$$F_T(r) = F_1(r) + \int_{-\infty}^{\infty} \omega_2(\epsilon) [f(r-\epsilon) - F_1(r)] d\epsilon \quad (A6)$$

where F_1 is the result of applying (A1) with weight function ω_1 . This equation transforms to

$$\hat{F}_T(K) = \hat{F}_1(K) + \hat{\omega}_2(K)\hat{f}(K) - \hat{\omega}_2(K)\hat{F}_1(K), \quad (A7)$$

or

$$\hat{F}_T(K) = [\hat{\omega}_1(K) + \hat{\omega}_2(K) - \hat{\omega}_2(K)\hat{\omega}_1(K)]\hat{f}(K) \quad (A8)$$

and the spectral response of two passes is identified by

$$|\omega_T| = |\omega_1 + \omega_2 - \omega_2\omega_1| \quad (A9)$$

Specifying the weight function as Gaussian, where

$$\omega_1(\epsilon) = a_1 \exp(-\epsilon^2/B^2), \quad (A10)$$

$$\omega_2(\epsilon) = a_2 \exp(-\epsilon^2/\gamma B^2), \quad (A11)$$

simplifies the computation of spectral response. γ and B^2 are arbitrary constants and a_1 and a_2 are normalizing coefficients, e.g.,

$$a_1 = \left[\int_{-\infty}^{\infty} \exp(-\epsilon^2/B^2) d\epsilon \right]^{-1}. \quad (A12)$$

The Fourier transform of (A10) and (A11) are

$$\hat{\omega}_1(K) = \exp(-B^2 K^2/4) \quad \text{and} \quad (A13)$$

$$\hat{\omega}_2(K) = \exp(-\gamma B^2 K^2/4). \quad (A14)$$

It is now possible to design the spectral response, $\hat{\omega}_T$, by appropriate choices for γ and B .

The objective analysis for discrete spacing of the observations is

$$F'(\underline{r}) = \sum_{k=1}^N \omega_1(\underline{\varepsilon}_k) f'(\underline{r} - \underline{\varepsilon}_k). \quad (A15)$$

In this equation and those that follow in this section, the upper case letters, such as F' , designate gridded fields of the variable being analyzed, whereas the lower case letters are related to observations that are irregularly located in space and time. The vector, $\underline{\varepsilon}_k$, specifies the separation in space and time between the observation, f_k , and the grid at point \underline{r} . The quantity f' represents the difference between the observation and the forecast that is to be updated and F' is the analyzed correction field that results from A15.

The weighting function, ω , determines how the observations are weight-averaged at each point on the grid. There is no upper limit to the size of ε , but a practical limit occurs when ω_1 is sufficiently small as to make correction meaningless. The volume over which computation is performed is referred to as the scan volume, and it represents the region from which observations are weight averaged to produce a value for point \underline{r} . Equation A15 was first developed by Bergthorsson and Doos (1955). Cressman (1959) overcame some of the inherent oversmoothing of this technique by incorporating multiple analysis scans, with

each scan using a progressively smaller radius. In this successive correction method, the second pass uses a weight, ω_2 , to reduce the remaining discrepancy between the analysis after the first pass and the observation, f'' , i.e.,

$$F''(r) = \sum_{k=1}^N \omega_2(\epsilon_k) f''(r - \epsilon_k). \quad (A16)$$

The resulting correction is equal to the sum of F' and F'' .

Although the Cressman method is usually designed to perform three or more passes through the data, Barnes (1964, 1973) and Stephens (1967) have shown that careful design of the weight function may provide adequate results after only two passes. The weight functions defined by Barnes are

$$\omega_1 = a_1 \exp(-\epsilon^2/B^2) \quad (A17)$$

and

$$\omega_2 = a_2 \exp(-\epsilon^2/\gamma B^2). \quad (A18)$$

As already shown, an analysis that uses (A18) and (A19) to compute the weights, and has a sufficiently dense observational coverage, will produce a spectral response

$$\hat{\omega}_T(K) = \exp(-B^2 K^2/4) + \exp(-\gamma B^2 K^2/4) \exp[-(1+\gamma)B^2 K^2/4], \quad (A19)$$

where B and γ are arbitrary parameters, and K is the wave number ($2\pi/\lambda$, where λ is wavelength). The symbol $(\hat{})$ signifies that the variable is transformed into wave-number space. It is possible to use this equation to design

variable filtering characteristics that are dependent on observation type in the analysis. The parameter B is used to limit the volume of influence of an observation, and the parameter γ is used to specify the degree of inherent filtering.

To design the desired filtering into the analysis, it is convenient to define the weight function as the product of three functions, i.e.,

$$\omega = \omega_H(\epsilon_H)\omega_V(\epsilon_V)\omega_t(\epsilon_t) \quad (A20)$$

where the subscripts H , v and t designate the functions describing the horizontal, vertical and temporal dependence, respectively. In this form, it is possible to make the filtering different for each dimension in the analysis.

A vertical weighting function that allows ample vertical variability while maintaining some vertical coupling is desirable. The weight function, ω_V , in (A20) is proportional to $\exp(-\epsilon_V/B_V^2)$, where $\epsilon_V = \ln(P_k/P_r)$ represents the pressure separation between the observation and analysis level. The constant B_V is 0.6, which produces a vertical scan radius that corresponds to the positive values of the prediction error covariances computed by Hallett (see Rutherford, 1976). The vertical filtering parameter, γ_V , is allowed to vary with observation type. For satellite soundings it is 0.8, whereas for other data types it is 0.3. Thus the satellite sounding corrections

are very smooth with height, thereby avoiding the problem of removing inversions that are formed by the model or are present in the other observations (Tracton et al., 1980). For example, updates from satellite soundings containing vertical wavelengths of 0.5 are damped to 20% of their original values, whereas this same wavelength in a radiosonde is damped only 50%.

As is the case for the vertical function, the horizontal weighting function is designed to limit the influence of an observation to an area that roughly corresponds to the positive values of correlation structure function. Using the curves produced by Buell (1972), B_H is then 3.24 grid intervals on the 2.5° mesh used by the analysis. To account for the spherical geometry, the horizontal separation between observation and grid point is defined by

$$\varepsilon_H^2 = (\mu x)^2 + y^2, \quad (A21)$$

where x and y are the zonal and meridional distances in grid intervals, μ is the map factor

$$\mu = \max[\cos \theta, 0.5], \quad (A22)$$

and θ is latitude. The lower limit on μ distorts the region of influence an observation may have poleward of 60° , but it prevents obvious computational problems near the poles.

Inman (1970) has shown that successive correction methods have a tendency to diffuse narrow jets such as occur in the upper troposphere. An ellipsoidally shaped weighting function with the major axis aligned along the wind direction tends to avoid the difficulty. Therefore, the weighting function for the wind is computed from

$$\omega_H(\epsilon_H) = \exp(-\epsilon_H^2 m_V/B_H^2), \quad (A23)$$

where

$$m_V = [0.7 + 3.0 \sin(\theta_V - \theta_\epsilon)] , \quad (A24)$$

$$\theta_V = \arctan (v/u) \quad \text{and} \quad (A25)$$

$$\theta_\epsilon = \arctan (y/x). \quad (A26)$$

Inclusion of the map factor in (A26) made no impact in the analysis and therefore was omitted to save considerable computer time.

. The present assimilation system updates the forecast every twelve hours, which means that during any single analysis time, there are likely to be data whose observation time differs from that of the analysis by six hours. As is the case in spatial dimensions, a poorly defined time weight function will result in damping and shifting of the small scale waves. If the weight in time is determined from (A17) and (A18) where ϵ_t is the separation in hours between observation time and analysis time, the inherent temporal filtering of the analysis depends on the values of B_t and γ_t . It is desirable to compute B_t from time correlations of

different data types, however very little literature exists on this type of study. Barnes (1973) used the phase speed of the meteorological systems to compute values for B_t that are consistent with the spatial parameters. Assuming a phase speed, C , of the order of 20 kt, then B_t can be determined from B_H/C , which is about 20 hours. For the update interval used, however, the temporal variations of the weights is only about 10%.

The amount of horizontal and temporal filtering inherent in the analysis is governed by γ_H and γ_t , respectively. The observational accuracy may be a factor in the determination of these values, as observations containing large random error tend to produce fictitious short waves which should be filtered more than the longer waves. The density of reports also becomes a factor, since aliasing may result when insufficient reports are used to describe a wave (Stephens, 1972). The filtering parameters selected ($\gamma_{H,t} = 0.3$) give a response for the four-grid increment wave of only 25% with a fairly steep rise to 80% for the eight-grid increment waves.

The error checking procedures used in analysis schemes may account for sizeable differences between various techniques. Even the most sophisticated schemes are not immune to large errors in the analysis that are caused by improper rejection of the observations. The most difficult

problem is avoiding the rejection of observations that result from a poor forecast. This is most likely to happen if the forecast is used to check the data, rather than the more desirable "buddy check" method, in which observations are compared. In the design of the error rejection procedure, an attempt was made to retain as many observations as possible, even at the expense of accepting data with errors. These erroneous data cause small scale effects that tend to diminish during the balancing procedure.

Three separate procedures are used to detect erroneous data. First, the radiosonde data are subjected to a vertical consistency check that requires the lapse rate be stable. Data is corrected through interpolation from adjacent levels with good data whenever possible. Secondly, gross errors are removed by rejecting the data that disagree with the forecast by more than five standard deviations of the expected error at that level. Finally, the remaining observations are used to perform a single pass, two-dimensional analysis. Each observation is then checked by first removing its effect from the analysis. This is done by determining the effect the observation in question has on the analysis at the closest grid point,

$$\Delta f_R = \frac{\sum_{k=1}^N \omega_k f_k - \omega_R f_R}{\sum_{k=1}^N \omega_k - \omega_R} \quad (A27)$$

where ω_R is the weight given f_R at this location. The analysis at this point excluding the observation being tested becomes

$$F_C = F - \Delta f_R. \quad (A28)$$

The observation is rejected whenever disagreement between F_C and f_R exceeds three standard deviations of the forecast error and there exists the equivalent of two other observations within one grid interval of the observation in question. This procedure rejects less than 0.2% of the total observations. An advantage of this method is that it utilizes computer code that is used to perform the analysis, which decreases the size and complexity of the computer program.

The successive corrections procedure described above is both simple and very fast compared to other methods, such as the multivariate optimum interpolation method (Schlatter, 1975). Furthermore, in experiments performed by Otto-Bliesner et al. (1977), the more sophisticated and time consuming methods did not produce significantly better results. Unfortunately, the successive corrections method is univariate, which means that no attempt is made to constrain the corrections to be consistent dynamically. This makes the balancing component of the assimilation system critical if the analyses are to be optimally combined to produce meteorologically consistent updates.

APPENDIX B

LINEARIZED HYDROSTATIC, THERMODYNAMIC AND CONTINUITY EQUATIONS

The vertical grid (see Fig. B1) has all variables except pressure are defined at odd levels and therefore

$$\phi_k - \phi_{k+2} = C_p (P_{k+2} - P_k) \hat{\theta}_{k+1} \quad \text{for } k = 1, 3, \dots, k-2 \quad (\text{B1})$$

and

$$\phi_k = \hat{\phi}_s + C_p (\hat{P}_s - P_k) \theta_k. \quad (\text{B2})$$

Interpolation formulas

$$P_k = \frac{1}{P_0^\kappa} \frac{1}{1+\kappa} \frac{\hat{P}_{k+1}^{1+\kappa} - \hat{P}_{k-1}^{1+\kappa}}{\hat{P}_{k+1} - \hat{P}_{k-1}}, \quad (\text{B3})$$

$$P_k = \frac{1}{P_0^\kappa} \frac{1}{1+\kappa} \frac{P_s^{1+\kappa} - P_{k-1}^{1+\kappa}}{P_s - P_{k-1}}, \quad (\text{B4})$$

and

$$\hat{\theta}_{k+1} = A_{k+1} \theta_k + B_{k+1} \theta_{k+2} \quad (\text{B5})$$

are used to produce energetically consistent equations where

$$p_k = \sigma_k (p_s - p_0), \quad (\text{B6})$$

$$\hat{P}_k = \left(\frac{\hat{P}_k}{P_0} \right)^\kappa, \quad (\text{B7})$$

$$A_{k+1} = \frac{\hat{p}_{k+1} - p_k}{p_{k+2} - p_k} \quad \text{for } k=1,3\dots k-4 \quad (B8)$$

$$B_{k+1} = \frac{p_{k+2} - \hat{p}_{k+1}}{p_{k+2} - p_k} ,$$

$$A_{k-1} = \frac{\frac{p_k p_{k-2}}{\hat{p}_{k-1}} - p_{k-2}}{p_k - p_{k-2}} , \quad (B9)$$

$$B_{k-1} = \frac{p_k - \frac{p_k p_{k-2}}{\hat{p}_{k-1}}}{p_k - p_{k-2}} , \quad (B10)$$

T is temperature, p is pressure and C_p is the specific heat at constant pressure.

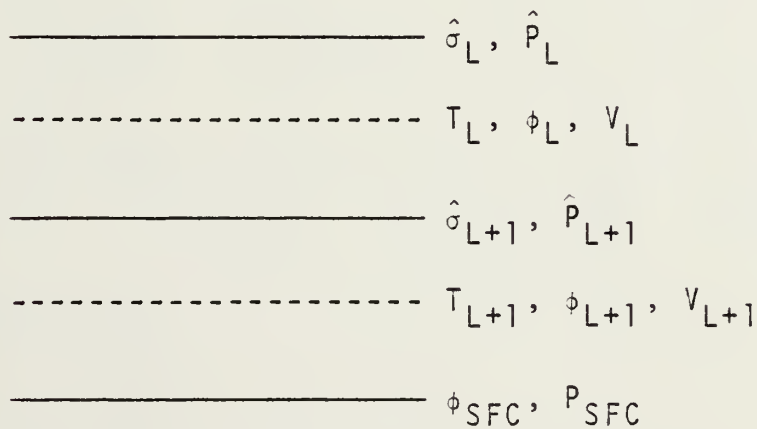


Fig. B1. Grid configuration.

The geopotential at each level is computed through integration, or

$$\phi_K = \hat{\phi}_S + C_p (P_S - P_K) \theta_K \quad (B11)$$

and

$$\begin{aligned} \phi_k = \hat{\phi}_S + \sum_{n=k}^{K_1} C_p (P_{n+2} - P_n) (A_{n+1} \theta_n) + \\ \sum_{n=k+2}^{K_1} C_p (P_n - P_{n-2}) (B_{n-1} \theta_n) . \end{aligned} \quad (B12)$$

The primed sum indicates increments of 2. Now we can write the hydrostatic equation as

$$\phi_k - \hat{\phi}_S = \sum_{n=1}^{K_1} C_{kn} T_n \quad (B13)$$

where

$$C_{kn} = \begin{cases} 0 & n < k \\ C_p (P_{n+2} - P_n) A_{n+1} / P_n & n = k \\ C_p (P_{n+2} - P_n) A_{n+1} / P_n + \\ C_p (P_n - P_{n-2}) B_{n-1} / P_n & n > k \end{cases} .$$

or in matrix form

$$\phi - \phi_S = \underline{\underline{C}} \underline{\underline{T}} . \quad (B14)$$

The finite difference form of the thermodynamic equation (Eq. 299 in Arakawa and Lamb 1977) in orthogonal curvilinear coordinates is

$$\begin{aligned} & \delta_t [\pi T]_{ij}^k + [\delta_\varepsilon (F \bar{T}^\varepsilon) + \delta_\eta (G \bar{T}^\eta)]_{ij}^k + \frac{1}{\Delta\sigma} p_{ij}^k \delta_\sigma (\dot{S} \hat{\theta})_{ij}^k \\ &= \frac{1}{C_p} [(\pi\sigma\alpha) \frac{\partial \pi}{\partial t} + \frac{\overline{u\Delta\eta}}{\bar{n}} (\overline{\pi\sigma\alpha})^\varepsilon \delta_\varepsilon \pi + \overline{v \frac{\Delta\varepsilon}{m} (\pi\sigma\alpha)^\eta \delta_\eta \pi} + \pi Q]_{ij}^k, \end{aligned} \quad (B15)$$

where $\pi = \pi \frac{\Delta\varepsilon \Delta\eta}{m\eta}$, $F = \pi u \frac{\Delta\eta}{\eta}$, $G = \pi v \frac{\Delta\varepsilon}{m}$, $\dot{S} = \pi \dot{\sigma}$, the overbar is a linear average in the direction of the variable indicated, and δ_x is a difference taken in the direction of the subscript.

To linearize, first subtract

$$T_{ij}^k [\delta_t \pi + \delta_\varepsilon F + \delta_\eta G + \frac{\delta_\sigma (\dot{S})}{\Delta\sigma}]_{ij}^k = 0, \quad (B16)$$

which gives

$$\pi \delta_t T_{ij}^k + \frac{1}{\Delta\sigma} p_{ij}^k \delta_\sigma [\dot{S} \hat{\theta}]_{ij}^k - T \frac{\delta_\sigma [\dot{S}]_{ij}^k}{\Delta\sigma} - \quad (B17)$$

$$\frac{1}{C_p} (\pi\sigma\alpha)_{ij}^k \frac{\partial \pi}{\partial t} = Q_T)_{ij}$$

or

$$\begin{aligned} & \delta_t T_{ij}^k + \left[\frac{\bar{T}_{k+1}}{p_{k+1}} p_k - \bar{T}_k \right] + \frac{\dot{\sigma}_{k+1}}{\Delta\sigma_k} - \left[\frac{\bar{T}_{k-1}}{p_{k-1}} p_k - \bar{T}_k \right] \frac{\dot{\sigma}_{k-1}}{\Delta\sigma_k} - \\ & \frac{(\pi\sigma\alpha)_k}{C_p} \frac{\partial \ln \pi}{\partial t} = Q_T)_{ij} \end{aligned} \quad (B18)$$

where \bar{T}_k is the rest-state temperature.

Substituting the linearized form of the continuity equation (Eqs. 166-167 in Arakawa and Lamb 1972) give

$$\dot{\sigma}_{k+1} = - \sum_{n=1}^k (\nabla \cdot V)_n \Delta\sigma_n + \sigma_{k+1} \sum_{n=1}^K \nabla \cdot (V_n) \Delta\sigma_n + Q_+ \quad (B19)$$

$$\dot{\sigma}_{k-1} = - \sum_{n=1}^{k-1} (\nabla \cdot V)_n \Delta \sigma_n + \sigma_{k-1} \sum_{n=1}^K (\nabla \cdot V)_n \Delta \sigma_n + Q. \quad (B20)$$

$$\delta_t \ln \pi = - \sum_{n=1}^K (\nabla \cdot V)_n \Delta \sigma_n + Q_p \quad (B21)$$

and

$$(\overline{\pi \sigma \alpha})_k = C_p \frac{\bar{T}_k}{P_k} \left(\pi \frac{dP_k}{d\pi} \right) \quad (B22)$$

gives

$$\begin{aligned} \delta_t T_{ij}^k + []_+ \frac{(\sigma_{k-1} - 1) \sum_{n=1}^{k-2} (\nabla \cdot V)_n \Delta \sigma_n + \sigma_{k+1} \sum_{n=k+2}^K (\nabla \cdot V)_n \Delta \sigma_n}{\Delta \sigma_k} \\ - []_- \frac{(\sigma_{k-1} - 1) \sum_{n=1}^{k-2} (\nabla \cdot V)_n \Delta \sigma_n + \sigma_{k-1} \sum_{n=k}^K (\nabla \cdot V)_n \Delta \sigma_n}{\Delta \sigma_k} \\ + \frac{\bar{T}_k}{P_k} \left(\pi \frac{dP_k}{d\pi} \right) \sum_{n=1}^K (\nabla \cdot V)_n \Delta \sigma_n = Q_{T_{ij}} \end{aligned} \quad (B23)$$

In matrix form

$$\delta_t T_{ij} + \tau (\nabla \cdot V)_{ij} = (Q_T)_{ij} \quad (B24)$$

where

$$\tau_{kn} = \begin{cases} \left\{ []_+ \frac{(\sigma_{k+1}-1)}{\Delta \sigma_k} - []_- \frac{(\sigma_{k-1}-1)}{\Delta \sigma_k} + \frac{\bar{T}_k}{P_k} \left(\pi \frac{dP_k}{d\pi} \right) \right\} \Delta \sigma_n & n < k \\ \left\{ []_+ \frac{(\sigma_{k+1}-1)}{\Delta \sigma_k} - []_- \frac{(\sigma_{k-1})}{\Delta \sigma_k} + \frac{\bar{T}_k}{P_k} \left(\pi \frac{dP_k}{d\pi} \right) \right\} \Delta \sigma_n & n = k \\ \left\{ []_+ \frac{(\sigma_{k+1})}{\Delta \sigma_k} - []_- \frac{(\sigma_{k-1})}{\Delta \sigma_k} + \frac{\bar{T}_k}{P_k} \left(\pi \frac{dP_k}{d\pi} \right) \right\} \Delta \sigma_n & n > k \end{cases} \quad (B25)$$

The formula

$$\frac{dP_k}{\pi d\pi} = \begin{cases} \frac{A_{k+1}[\sigma_{k+1}(P_{k+2}-P_k)] + B_{k-1}[\sigma_{k-1}(P_k-P_{k-2})]}{\Delta\sigma_k} & k < K \\ \frac{\hat{P}_S - P_k}{\Delta\sigma_k} & \text{for } k = K \end{cases} \quad (B26)$$

is that derived by Arakawa from the interpolation formulas (B3)-(B10).

Note that the continuity equation may also be written in matrix form by defining

$$\tilde{\Pi} = \begin{bmatrix} \Delta\sigma_1 \\ \Delta\sigma_2 \\ \vdots \\ \vdots \\ \Delta\sigma_K \end{bmatrix}, \quad (B27)$$

so that

$$\delta_t \ln \pi = - \tilde{\Pi}^T \tilde{\delta} + Q_p. \quad (B28)$$

APPENDIX C

EMPIRICAL ORTHOGONAL FUNCTIONS

Holstrom (1963) showed that geopotential, $\phi(x,y,p)$, may be accurately described in terms of a series in orthonormal basis functions, $\phi_k(p)$, derived so that a partial sum,

$$\phi_n(x,y,p) = \sum_{k=1}^n a_k(x,y) \hat{\phi}_k(p) \quad (C1)$$

where

$$a_k(x,y) = \int_{p_1}^{p_2} \phi(x,y,p) \hat{\phi}_k(p) dp, \quad (C2)$$

produces an optimum fit for all choices of n . In these equations, the horizontal coordinates are x and y and the vertical coordinate is p . The values p_1 and p_2 are the vertical boundaries of the domain and the areal mean value of ϕ at each level has been removed.

Obukhov's (1960) method, which is computationally easier to use than Holstrom's (1963), uses the autocovariance as a characteristic measure for determining the empirical orthogonal function, i.e.,

$$B(p,p') = \overline{\phi(x,y,p) \phi(x,y,p')}, \quad (C3)$$

where the overbar operator designates a horizontal average. This function describes the variance of ϕ when p is equal to p' , and it describes the covariance otherwise. The

redundancy of the ϕ -profiles is identifiable by the size of the covariance terms. Consequently, the accuracy of ϕ_n in (C1) depends on the covariance magnitudes. For example, if ϕ is random, then (C1) would not converge rapidly. Holstrom (1963), however, has observed considerable redundancy in the atmosphere for geopotential.

In Obukhov's (1960) method, the eigenfunctions of the integral operator,

$$\int_{p_1}^{p_2} B(p, p') \phi(p') dp' = \mu_k \phi(p), \quad (C4)$$

produce the optimum choice for basis functions, $\hat{\phi}_k(p)$, which produce least mean square error for all values of n in (C1). The eigenvalues of (C4), μ_k , measure the variance that their associated eigenfunctions represent. Therefore, the ordering of the functions is made so that μ_k is in descending order. Also, the averaged normalized variance of ϕ that is represented by ϕ_n is simply

$$\sigma_n = \frac{\sum_{k=1}^n \mu_k}{\sum_{k=1}^{\infty} \mu_k} \quad (C5)$$

To extend Obukhov's (1960) procedure to finite differences, the independent function is represented by

$$\phi_{i,j,k} = \phi(i\Delta x, j\Delta y, k\Delta p), \quad (C6)$$

where Δx , Δy , and Δp are the grid spacings and i, j, k the grid location. Then the autocovariance becomes

$$B_{\ell, m} = \sum_{i=1}^M \sum_{j=1}^N \phi_{i, j, \ell} \phi_{i, j, m} \Delta p / MN \quad (C7)$$

The integral operator (C4) now has the form

$$\sum_{m=\ell}^K B_{\ell, m} \phi_m = \mu_k \phi_{\ell} ,$$

where ℓ and m are vertical indexes. The optimum basis functions are the eigenvectors of $B_{\ell, m}$ arranged so that corresponding eigenvalues are in descending order. There are K modes or eigenvectors in this system, which correspond to the size of the square array $B_{\ell m}$. However, the motivation of this approach is to allow a partial sum to be used that maintains most of the accuracy of the original function $\phi_{i, j, p}$.

LIST OF REFERENCES

- Andersen, J. H., 1977: A routine for normal mode initialization with nonlinear correction for a multilevel spectral model with triangular truncation. ECMWF Internal Rept. No. 15, 41 pp.
- Arakawa, A., and V. R. Lamb, 1977: Computational design of the basic dynamical processes of the UCLA general circulation model. Methods in Computational Physics, Vol. 17, Julius Chang, Ed., Academic Press, 174-264.
- _____, and Y. Mintz, 1975: The UCLA atmospheric general circulation model. Notes distributed at the workshop 25 Mar-4 Apr 1974. Dept. of Meteor., UCLA, CA 90024.
- _____, and W. H. Schubert, 1974: Interaction of a cumulus cloud ensemble with the large-scale environment, Part 1. J. Atmos. Sci., 31, 674-701.
- Baer, F., and J. Tribbia, 1977: On complete filtering of gravity modes through nonlinear initialization. Mon. Wea. Rev., 105, 1536-1539.
- Ballish, B. A., 1981: A simple test of the initialization of gravity modes. Mon. Wea. Rev., 109, 1318-1321.
- Barker, E. H., 1981a: Data impact studies using the U.S. Navy's Operational Global Atmospheric Prediction System. Proceedings of the International Conference on Preliminary FGGE Data Analysis and Results. Bergen, Norway, 23-27 Jun 1980, p. 105-130.
- _____, 1981b: The relationship between analysis of upper tropospheric winds and the mass structure in the tropics. Proceedings of the International Conference on Preliminary FGGE Data Analysis and Results. Bergen, Norway, 23-27 Jun 1980, p. 202-211.
- _____, 1981c: Solving for temperature using unnaturally latticed hydrostatic equations, Mon. Wea. Rev., 108, 1260-1268.
- Barnes, S. L., 1964: A technique for maximizing details in numerical weather map analysis, J. Appl. Meteor., 3, 396-409.

- _____, 1973: Mesoscale objective map analysis using weighted time-series observations. NOAA Tech. Memo. ERL NSSL-62 (NTIS No. COM-73-10781).
- Bengtsson, L., 1981: Data analysis, initialization and data assimilation. Proceedings of the International Conference on Preliminary FGGE Data Analysis and Results. Bergen, Norway, 23-27 Jun 1980, p. 162-185.
- _____, and Gustavsson, N., 1971: An experiment in the assimilation of data in dynamical analysis. Tellus, 23, 328-336.
- _____, and Gustavsson, N., 1972: Assimilation of non-synoptic observations. Tellus, 24, 383-399.
- Bergthorsson, P., and B. R. Doos, 1955: Numerical Weather-Map Analysis. Tellus, 7, 329-340.
- Bourke, W., 1972: An efficient, one-level, primitive-equation spectral model, Mon. Wea. Rev., 100, 683-689.
- Buell, C. E., 1972: Correlation functions for wind and geopotential on isobaric surfaces. J. Appl. Meteor., 11, 51-59.
- Charney, J., 1955: The use of the primitive equations of motion in numerical prediction. Tellus, 7, 22-26.
- _____, R. Fjortoft, and J. von Neumann, 1950: Numerical integration of the barotropic vorticity equation. Tellus, 2, 237-254.
- _____, J., M. Halem, and R. Jastrow, 1969: Use of incomplete historical data to infer the present state of the atmosphere. J. Atmos. Sci., 26, 1160-1163.
- Cressman, G., 1959: An operational objective analysis system. Mon. Wea. Rev., 87, 367-374.
- Daley, R., 1978: Variational nonlinear normal mode initialization. Tellus, 30, 201-218.
- _____, 1979: The application of nonlinear normal mode initialization to an operational forecast model. Atmosphere-Ocean, 17, 97-124.
- _____, 1980: On the optimal specification of the initial state for deterministic forecasting. Mon. Wea. Rev., 108, 1719-1733.

- _____, 1981: Normal mode initialization. Rev. Geophys. Space Phys., 19, 450-468.
- _____, and K. Puri, 1980: Four-dimensional assimilation and the slow manifold. Mon. Wea. Rev., 108, 85-99.
- Dickenson, R. E., and D. L. Williamson, 1972: Free oscillations of a discrete stratified fluid with application to numerical weather prediction. J. Atmos. Sci., 29, 623-640.
- Fleming, R. J., T. M. Kaneshige, and W. E. McGovern, 1979: The Global Weather Experiment, The observational phase through the first special observing period. Bull. Amer. Meteor. Soc., 60, 649-659.
- Gandin, L. S., 1963: Objective Analysis of Meteorological Fields, Translated from Russian by Israel Program for Scientific Translations, 1965, 242 p. (NTIS No. TT 65-50 007).
- Haltiner, G. J., and J. M. McCollough, 1975: Experiments in the initialization of a global primitive equation model. J. Appl. Meteor., 14, 281-288.
- _____, Y. S. Sasaki, E. H. Barker, 1976: An initialization technique for primitive equation models using a balance equation constraint. Proceedings of the GARP Joint Organizing Committee Study Group Conference on Four-Dimensional Data Assimilation, Pon's, France, Nov. 17-21, 1976.
- Hayden, C. M., 1973: Experiments in the four-dimensional assimilation of Nimbus 4 SIRS data. J. Appl. Met., 12, 425-436.
- Hoke, S. E., and R. A. Anthes, 1976: The initialization of numerical models by a dynamic initialization technique. Mon. Wea. Rev., 104, 1551-1556.
- Holl, M. M., and B. R. Mendenhall, 1972: Fields by information blending, sea-level pressure version, Tech. Note No. 72-2, Fleet Numerical Weather Central, Monterey, CA (may be obtained by writing Librarian, Fleet Numerical Oceanography Center, Monterey, CA 93940), 67 p.
- Holstrom, I., 1963: On a method for parametric representation of the state of the atmosphere. Tellus, 15, 127-149.

- Inman, R. L., 1970: Papers on operational objective analysis schemes at the National Severe Storms Forecast Center, NOAA Tech. Memo. ERL NSSL-51, Norman, Oklahoma, 91 pp.
- Johnson, R. H., 1976: The role of convective-scale precipitation downdrafts in cumulus and synoptic-scale interactions. J. Atmos. Sci., 1890-1910.
- Kistler, R. E., and R. D. McPherson, 1975: On the use of a local wind correction technique in four-dimensional data assimilation. Mon. Wea. Rev., 103, 445-449.
- Leith, C. E., 1980: Nonlinear normal mode initialization and quasi-geostrophic theory. J. Atmos. Sci., 37, 958-968.
- Lord, S. J., 1978: Development and observational verification of a cumulus cloud parameterization. Ph.D Dissertation, University of California, Los Angeles, 359 p.
- Lorenc, A. C., 1981: A global three-dimensional multivariate statistical interpolation scheme. Mon. Wea. Rev., 109, 701-721.
- Machenhauer, B., 1977: On the dynamics of gravity oscillations in a shallow water model with applications to normal mode initialization, Beitrag zur Physik der Atmosphere, 50, p. 253-271.
- Miyakoda, K., L. Umscheid, D. H. Lee, J. Sirutis, R. Lusen and F. Pratte, 1976: The near real-time, global, four-dimensional analysis experiment during the GATE period, Part I. J. Atmos. Sci., 33, 561-591.
- Nitta, T., and J. B. Hovermale, 1969: A technique of objective analysis and initialization for the primitive forecast equations. Mon. Wea. Rev., 97, 652-658.
- Obukhov, A. M., 1960: The statistically orthogonal expansion of empirical functions. Bull. (Izvestiya) Acad. Sci., USSR Geophys Ser, 3, 288-291. Translated by Amer. Geophys. Union.
- Otto-Bliesner, B., D. P. Baumhefner, and T. W. Schlatter, 1977: A comparison of several meteorological analysis schemes over a data-rich region. Mon. Wea. Rev., 105, 1083-1091.

- Payne, S. W., 1981: The inclusion of moist downdraft effects in the Arakawa-Schubert cumulus parameterization. Preprint: Fifth Conference on Numerical Weather Prediction, Nov. 2-6, 1981, Monterey, CA, Amer. Meteor Soc.
- Phillips, N., 1977: Variational analysis in pressure coordinates. Office Note 134, U.S. Dept. of Commerce, Nat. Oceanic and Atmos. Admin., National Wea. Serv., National Meteor. Cen., 53 pp.
- _____, 1981: Treatment of normal and abnormal modes. Mon. Wea. Rev., 109, 1117-1119.
- _____, 1982a: Variational analysis and the slow manifold. Mon. Wea. Rev., 110, 2415-2426.
- _____, 1982b: On the completeness of multi-variate optimum interpolation for large-scale meteorological analysis, unpublished manuscript.
- Puri, K., 1981: Local geostrophic wind correction in the assimilation of height data and its relationship to the slow manifold. Mon. Wea. Rev., 109, 52-55.
- Randall, D. A., 1976: The interaction of the planetary boundary layer with large-scale circulations, Ph.D Thesis, Dept. of Meteor., UCLA, 308 pp.
- Rosmond, T. E., and F. D. Faulkner, 1976: Direct solution of elliptic equations by block cyclic reduction and factorization. Mon. Wea. Rev., 104, 641-649.
- Rutherford, I. D., 1976: An operational three-dimensional multi-variate statistical objective analysis scheme. Proc. of the JOC Study Group Conf. on Four-Dimensional Data Assimilation. Paris, 17-21 Nov 1975. Garp Report No. 11.
- Sasaki, Y., 1958: An objective analysis based on the variational method. J. Meteor. Soc. Japan, 36, 77-88.
- _____, 1970: Some basic formalisms in numerical variational analysis. Mon. Wea. Rev., 98, 875-883.
- Schlatter, T. W., 1975: Some experiments with a multi-variate statistical objective analysis scheme. Mon. Wea. Rev., 103, 246-257.

- Stephens, J. J., 1967: Filtering responses of selected distance-dependent weight functions, Mon. Wea. Rev., 95, 45-46.
- _____, 1970: Variational initialization with the balance equation. J. Appl. Meteor., 9, 732-739.
- _____, 1972: Distance distributions for randomly distributed data. Mon. Wea. Rev., 100, 60-61.
- Swarztrauber, P. and R. Sweet, 1975: Efficient FORTRAN subprograms for the solution of elliptic partial differential equations, National Cen. for Atmos. Rsch. Tech. Note NCAR-TN/1A-109, Boulder, CO 80307.
- Tarbell, T. C., T. T. Warner, and R. A. Anthes, 1981: Example of the initialization of the divergent wind component in a mesoscale numerical prediction model. Mon. Wea. Rev., 109, 77-95.
- Temperton, C., 1976: Dynamic initialization for barotropic and multilevel models. Q. J. Roy. Meteor Soc., 102, 297-311.
- _____, and D. L. Williamson, 1979: Normal mode initialization for a multilevel grid-point model. ECMWF Tech. Rept. No. 11, 91 pp.
- _____, and D. L. Williamson, 1981: Normal mode initialization for a multilevel grid-point model. Part I: Linear Aspects, Mon. Wea. Rev., 109, 729-743.
- Tracton, M. S., A. J. Desmarais, R. J. van Haaren, and R. D. McPherson, 1980: The impact of satellite soundings on the National Meteorological Center's analysis and forecast system - The data systems test results. Mon. Wea. Rev., 108, 543-586.
- Tribbia, J. J., 1981: Nonlinear normal-mode balancing and the ellipticity condition. Mon. Wea. Rev., 109, 1751-1761.
- _____, 1982: On variational nonlinear normal mode initialization. Mon. Wea. Rev., 110 pp.
- Williamson, D., and A. Kasahara, 1971: Adaptation of meteorological variables forced by updating. J. Atmos. Sci., 28, 1313-1324.

_____, R. Daley, T. W. Schlatter, 1981: The balance between mass and wind fields resulting from multivariate optimal interpolation. Mon. Wea. Rev., 109, 2357-2376.

_____, and C. Temperton, 1981: Normal mode initialization for a multilevel grid-point model. Part II: Nonlinear aspects. Mon. Wea. Rev., 109, 744-757.

INITIAL DISTRIBUTION LIST

	No. Copies
1. Defense Technical Information Center Cameron Station Alexandria, VA 22314	2
2. Library, Code 0142 Naval Postgraduate School Monterey, CA 93940	2
3. Chairman (Code 68Mr) Department of Oceanography Naval Postgraduate School Monterey, CA 93940	1
4. Chairman (Code 63Rd) Department of Meteorology Naval Postgraduate School Monterey, CA 93940	1
5. Edward H. Barker Naval Environmental Prediction Research Center Monterey, CA 93940	6
6. Professor G. J. Haltiner, Code 63Ha Department of Meteorology Naval Postgraduate School Monterey, CA 93940	1
7. Director Naval Oceanography Division Naval Observatory 34th and Massachusetts Avenue NW Washington, DC 20390	1
8. Commander Naval Oceanography Command NSTL Station Bay St. Louis, MS 39522	1
9. Commanding Officer Naval Oceanographic Office NSTL Station Bay St. Louis, MS 39522	1

	No. Copies
10. Commanding Officer Fleet Numerical Oceanography Center Monterey, CA 93940	1
11. Commanding Officer Naval Ocean Research and Development Activity NSTL Station Bay St. Louis, MS 39522	1
12. Commanding Officer Naval Environmental Prediction Research Facility Monterey, CA 93940	1
13. Chairman, Oceanography Department U.S. Naval Academy Annapolis, MD 21402	1
14. Chief of Naval Research 800 N. Quincy Street Arlington, VA 22217	1
15. Office of Naval Research (Code 480) Naval Ocean Research and Development Activity	1
16. Professor R. T. Williams, Code 63Wu Department of Meteorology Naval Postgraduate School Monterey, CA 93940	1
17. Professor R. L. Elsberry, Code 63Es Department of Meteorology Naval Postgraduate School Monterey, CA 93940	1
18. Professor F. D. Faulkner, Code 53Fa Department of Meteorology Naval Postgraduate School Monterey, CA 93940	1
19. Professor D. Salinas, Code 69Zc Department of Mechanical Engineering Naval Postgraduate School Monterey, CA 93940	1

- | | | |
|-----|--------------------------------|---|
| 20. | Professor Y. K. Sasaki | 1 |
| | CIMMS | |
| | 815 Jenkins | |
| | Norman, OK 73019 | |
| 21. | Dr. A. Weinstein | 1 |
| | Naval Environmental Prediction | |
| | Research Facility | |
| | Monterey, CA 93940 | |
| 22. | Dr. T. Rosmond | 1 |
| | Naval Environmental Prediction | |
| | Research Facility | |
| | Monterey, CA 93940 | |

Thesis
B2178
c.1

Barker

197953

A comparison of two
initialization methods
in data assimilation.

1 JUL 86

9 JUL 87

14 DEC 87

14016
14016
13603

Thesis
B2178
c.1

Barker

197953

A comparison of two
initialization methods
in data assimilation.

thesB2178

A comparison of two initialization metho



3 2768 002 01408 6

DUDLEY KNOX LIBRARY